TRANSFORMATION AND TOUGHNESS OF IRON-9 PERCENT NICKEL ALLOY

SIEW HUAT CHONG

DipTech (TARC, MALAYSIA)
MSc (SUNDERLAND, UK)

A thesis submitted in partial fulfilment of the requirements of
Sheffield Hallam University
for the degree of Doctor of Philosophy

June 1998

Collaboration Organisation: British Steel plc.
Swinden Technology Centre

Preface

This thesis is submitted in partial fulfilment of the requirements of Sheffield Hallam University for the degree of Doctor of Philosophy. It contains an account of research carried out between November 1994 and December 1997 in the School of Engineering, Sheffield Hallam University, under the supervision of Dr. E. A. Wilson, Prof. J. D. Atkinson and Dr. R. P. Stratton. Except where acknowledgements and references are made, this work is, to the best of my knowledge, original and has been carried out independently. No part of this thesis has been, or is being, submitted for any degree or diploma at this, or any other university.

An account of the work in this thesis has been accepted and published in:-
S. H. Chong, A. Sayles, R. Keyse, J. D. Atkinson, E. A. Wilson: "Examination of Microstructure and Microanalysis of an Fe-9%Ni Alloy", Materials Transactions, JIM, Jan 1998, Vol.39, No.1, pp.179-188.

Siew Huat Chong

June 1998

Acknowledgements

First of all, the author would like to thank the School of Engineering, Sheffield Hallam University for providing bursary and facilities to carry out this piece of work. Assistance from the skilled technicians in the School of Engineering are greatly appreciated. Technical support for the electron microscopy was provided by Prof. J. M. Titchmarch, Dr. I. Wadsworth, Mr. P. Slingsby, Mr. G. Gregory, Mr. A. Sheldon, and Mrs C. Show in the MRI, Sheffield Hallam University are acknowledged.

The author also would like to thank Swinden Technology Centre, Rotherham for their generosity in providing experimental materials and carrying out dilatometry work. British Steel Engineering Steels, Stockbridge are thanked for doing forging and the chemical analysis. The School of Materials, Leeds University are thanked for access to their hot roll mill facility. Skilled operation on scanning transmission electron microscopy by Dr. R. Keyse from Materials Department of Liverpool University is greatly appreciated. Kind participation from these parties have made the progress of this work possible.

The author is grateful for the willingness of Mr. H. Everson from British Steel Engineering Steels and Dr. A. A. Howe from Swinden Technology Centre to be the advisors for this piece of work. The participation of Prof. J. D. Atkinson and Dr. R. P. Stratton in joining the supervisory team are acknowledged.

Constructive communication with Prof. H. I. Aaronson of Carnegie Mellon University on the issue of grain corner nucleation is also acknowledged.

Last, but not least, the author would like to thank Dr. E. A. Wilson, for his full support during the course of this research.

Abstract

Phase transformation studies have been carried out on VS2241A, Fe-9.14Ni -0.002C alloy.This alloy was chosen because it was expected that the speed of austenite decomposition would be slow enough to allow continuous cooling transformation and isothermal transformation experiments to be carried out on the same alloy.

Upon furnace cooling, massive ferrite was the predominate phase formed.TEM inspection observed low angle sub-boundaries inside ferrite grains. Pre-polished surface examination showed the presence of Widmanstätten ferrite as evident by tent-shaped surface relief. Martensite-austenite (M-A) constituent was also observed under TEM inspection indicating that partition of carbon had occurred during transformation.

Quantitative analysis of the dilatation curve showed continuous cooling consisted of two portions. One between 575 ± 5^{0}C and 558 ± 3^{0}C corresponding to the formation of grain boundary nucleated massive ferrite while the portion between 558^{0}C to 500^{0}C was thought to correspond to Widmastätten ferrite formation. The observation of an experimental T_0 temperature of 623 ± 5^{0}C and a theorectical T_0 temperature of 614 ± 5^{0}C implied that transformation took place below T_0 in the two phase field.

Microanalysis using a FEG-STEM system with a windowless LINK X-ray detector was carried out at Liverpool University. This showed that the Ni content across a ferrite grain was constant at 8.8 ± 0.2wt%Ni and 12.98 ± 0.43wt%Ni was detected on a grain boundary confirming that the massive transformation was composition invariant, but local partitioning occurred in the interface during transformation.

Thermal arrest experiments observed bainitic ferrite and lath martensite transformed at temperatures ~ 486^{0}C and ~ 384^{0}C respectively.

Incomplete transformation was observed for all the isothermally transformed structures in the Fe-9Ni alloy below T_0. It was suggested that this phenomenon would apply to all transformations occurring in the two phase field below the T_0 temperature.

Separate but overlapping C-curves in a TTT diagram for Fe-9Ni were proposed to account for the co-existence of massive ferrite and Widmanstätten ferrite at the same temperature. The lath formation of Widmastätten ferrite was interpreted as a product of partial coherent interfaces propagated by means of a ledge mechanism, thermally activated by the trans-interphase diffusion of solute atoms.

A thermal arrest at 707 ± 5^{0}C was observed on air cooling an Fe- 3.5Ni alloy,VS2239A. This corresponded to equi-axed ferrite transformation in the single phase region.

In an iced brine quenched Fe-4Cu alloy, massive ferrite and Widmastätten ferrite were observed. A 6^0 misorientation was calculated between two adjacent ferrite grains seperated by a ragged grain boundary.

Charpy impact testing of Fe-9Ni alloy, VS2241A gave a DBTT of -140^{0}C and -100^0 C for massive ferrite and bainitic ferrite respectively. Massive ferrite showed a higher upper shelf energy on the transition curve.

Contents

List of Figures and Tables

Nomenclature and Abbreviations

at.%	Atomic percentage
A_3	Temperature separating the $\alpha+\gamma$ and γ phase fields
A_{C3}	Fully austenitised temperature
B_s	Bainite start transformation
D	Diffusion coefficient
D_0	Pre-exponential diffusion coefficient constant
HV	Vickers hardness
HMV	Vickers microhardness
M_s	Martensitic start transformation
Q	Activation energy
R	Universal gas constant
t	time (in seconds)
T	Temperature
T_0	Temperature at which parent and product phase of the same composition have the same free energy
T_0'	T_0 temperature in the presence of strain energy
T_s	Solidification temperature
W_s	Widmanstätten start transformation
wt.%	Weight percentage
y	Volume fraction of transformation
λ	Diffusion distance
α	Ferrite
α'	Martensite
α_2	Supersaturated ferrite
α_{25}	Temperature for 25% of ferrite transformation
α_f	Ferrite finish transformation temperature
α_m	Massive ferrite
α_q	Quasi-polygonal ferrite
α_s	Ferrite start temperature
α_W	Widmanstätten ferrite
γ	Austenite

γ_{25}	Temperature for 25% of austenite formation
γ_f	Austenite finish transformation temperature
γ_s	Austenite start transformation temperature
θ	Cementite Fe_3C
$\Delta G^{\gamma\rightarrow\alpha}$	Free energy change for transformation without composition change
ΔG_e	Free energy change under equilibrium
ΔG_m	Free energy change by massive transformation
ΔG^*	Activation free energy for nucleation
AC	Air cool
bcc	Body centre cubic
bct	Body centre tetragonal
DBTT	Ductile-brittle transition temperature
EDX	Energy Dispersive X-ray analysis
FC	Furnace cool
fcc	Face centre cubic
fct	Face centre tetragonal
FEG	Field emission gun
hcp	Hexagonal close packed
HAZ	Heat affected zone in weld join
HSLA	High strength low alloy (steels)
IBQ	Iced brine quench
IPS	Invariant plain strain
ISIJ	The Iron and Steel Institute of Japan
M-A	Martensite-austenite constituent
OQ	Oil quench
PTMC	Phenomenological theory of martensite crystallography
SEM	Scanning electron microscope
STEM	Scanning transmission electron microscope
TEM	Transmission electron microscope
TMCP	Thermo-mechanical controlled process
TTT	Time-temperature-transformation (diagram)
WQ	Water quench
ZAF	Atomic number (Z), absorption (A) and fluorescence (F)

1. Introduction

In recent years, there has been a tendency in steel development to keep the carbon content in structural steels as low as possible to promote excellent toughness and weldability, high strength being obtained by transforming to low temperature transformation products. The development of continuously transformed low carbon HSLA steels has largely replaced the traditional heat treated high yield strength (HY) steels, through the advance of microalloying and thermomechanical controlled processing.

Because of the low carbon content and the addition of alloying elements into iron, the transformation of $\gamma \rightarrow \alpha$ becomes very complicated, various kind of microstructures being found from continuously cooled products. Controversial opinions have arisen in determining the transformed products and also the mechanisms involved. With such a low carbon level, the speed of transformation is rapid, thermomechanical processing also enhances the complication of the transformation. The studies of transformation in steels base on carbon diffusion control (in high carbon steels) no longer hold true in such a low carbon level alloys. It is thought that other types of transformation mechanism, for instance massive transformations play an important role in this group of steels.

In view of the problems arising in this new group of steels, it was thought that further studies of low carbon ferrous alloys needed to be carried out in addition to the earlier purely academic studies.

Fe-Ni alloys have been the most extensively used in the study of $\gamma \rightarrow \alpha$ transformation in iron binary alloys. Transformations in Fe-Ni alloys occur by several mechanisms, depending on composition and cooling rate. The transformed microstructures of equiaxed ferrite, massive ferrite, bainitic ferrite, lath (massive) martensite and twinned martensite were reported in Fe-Ni alloys containing ~0.01%C, transformed from high temperature to low temperature range [WILSON 1984, 1994].

Following the first report on massive structure in Fe-4%Ni and Fe-6%Ni alloys by OWEN and WILSON [1965], MASSALSKI et al [1975] has shown the composition invariance of massive ferrite in an Fe-8.74%Ni alloy by microprobe studies. HAYZELDEN and CANTOR [1985] also observed massive ferrite in melt spun Fe-25%Ni alloy. These later two cases clearly demonstrated the massive transformation in the two-phase field ($\alpha+\gamma$), which was regarded as thermodynamically unfeasible [HILLERT 1984]. BEE and HONEYCOMBE [1978] suggested that the observation of ragged boundaries reported in massive ferrite was simply due to the impingement of the Widmanstätten structure.

It has been suggested that solute drag may occur accompanying the transformation. Microanalysis carried out on partially transformed ferrite grain in Fe-7%Cr-2%Ni by RICKS, SOUTHWICK and HOWELL [1981] reported a small statistically significant change in composition within the grain boundaries. Solute drag effect was thought to be responsible for the difference in composition.

While experiments clearly showed that massive transformation would be so rapid that only continuous cooling transformation experiments could be carried out to study the transformation behaviour, theoretical calculation suggested that it might be possible to study it isothermally for Fe-Ni alloy at the vicinity of 10% Ni [WILSON 1991].

Because of outstanding questions concerning transformation in iron-nickel alloys, it was decided to study Fe-Ni alloys with two level of nickel , i.e. 3.5% and 9%. The materials provided by Swinden Technology Centre were vacuum cast Fe-3.5%Ni and Fe-9%Ni with carbon content as low as 0.004 wt.%.

Attention was given to Fe-9Ni alloy as it was expected that the speed of austenite decomposition would be slower in this alloy, allowing continuous cooling as well as isothermal transformation experiments to be carried out on the same alloy. The aim of this work was to carry out a complete metallographic examination on the continuously and isothermally transformed structures.

Thermal arrest experiments were conducted to detect the transformation start temperatures of different structures. Dilatometry experiment was also carried out in order to establish the transformation behaviour in a greater detail to correlate with the observed microstructures.

Investigation on transformed structures in various conditions was carried out by means of optical microscopy, scanning electron microscopy, as well as transmission electron microscopy. Hardness testing was also attempted to aid microstructural identification.

Microanalysis by TEM-EDX and FEG-STEM methods were attempted to establish the solute distribution in the ferrite phase. FEG-STEM machine at Liverpool University facilitates microanalysis using 2 nm probe size provide much higher resolution than the conventional STEM machine. It was hoped to achieve better statistical results than RICKS, SOUTHWICK and HOWELL [1981].

By analysing and comparing the current findings with other work done on similar materials, the literature was revised in view of the current findings in order to reconcile the discrepancy in the results and views of different workers.

An addition of nickel in steels has long been practised to improve toughness. Heat-treated 9% nickel steels show excellent low temperature toughness and are widely used in cryogenic applications. The presence of reverted austenite in the heat-treated conditions was regarded as crucial in scavenging impurities [MARSHALL, HEHEMANN and TROIANO 1962; KIM and SCHWARTZ 1978; KIM and MORRIS 1980]. Vacuum casting minimises the impurities content to a very low level. In addition to that, it was thought that the formation of massive ferrite could improve toughness [ROBERTS 1970; KATSUMATA et al 1994], because the microstructure crosses prior austenite grain boundaries [OWEN and WILSON 1965]. Charpy impact testing was therefore carried out to observe the low temperature toughness for different continuously cooled products in the Fe-9Ni alloy.

2. Literature Survey

2.1. Transformation in Iron

Pure iron exists in two forms, body-centred cubic (bcc), called α-iron or ferrite, stable from the low temperature range up to 912°C, and face-centred cubic (fcc), called γ-iron or austenite, which is stable in the temperature range 912°C - 1394°C. In the temperature range of 1394°C - 1538°C, γ-iron reverts to the bcc form, which is called δ-iron, before the temperature reaches the melting point of 1538°C [OKAMOTO 1992].

For pure iron, the γ→α reaction is so rapid that isothermal transformation studies are practically impossible. The study of the γ→α transformation were all carried out by rapid quenching. Transformation experiments on iron began when SAUVEUR and CHOU [1929] examined a polished sample of electrolytic iron in evacuated quartz tube, heated to 1000°C for 2 hours and quenched in mercury. Surface relief of Widmanstätten / martensitic structures was observed, i.e. the normal ferrite transformation was suppressed. ENTWISLE [1956] reproduced this surface relief effect and worked out the habit plane to be close to $\{111\}_\gamma$, implying martensitic transformation.

It was DUWEZ [1951] who first studied the effect of cooling rate on the transformation in pure iron. Despite the scatter in his results, the transformation was suppressed from 900°C at 10 $K.s^{-1}$ to 750°C at 10^4 $K.s^{-1}$. GILBERT and OWEN [1962] found that more than one transformation was possible, i.e. a plateau temperature at 816°C with cooling rate up to 1000 $K.s^{-1}$ and a thermal arrest at 545°C with cooling rate as high as 5,500 $K.s^{-1}$ in iron containing 0.01% C and 0.002% N. The later figure is in agreement with GRENINGER's [1942] M_s values in Fe-C alloys extrapolated to pure iron, see figure 2.1. BIBBY and PARR [1964] also presented the characteristic of temperature-transformation plateaux in iron, with two plateaux at 742°C and 694°C in Fe-0.0017 %C alloy.

The γ→α transformation for iron became more complicated when WILSON [1970, 1984] reported 4 and later 5 plateaux in iron containing 0.011% C at different cooling rate and temperature range. Each plateau represents different transformation behaviour forming different microstructures, viz. equiaxed ferrite, massive ferrite, bainitic ferrite, lath

martensite and twinned martensite, figure 2.2. MOROZOV et al [1971, 1972] found similar results at cooling rates up to 340,000 $K.s^{-1}$. WILSON [1991, 1994] believed that the plateaux temperature corresponded to the maximum rate of transformation or nose temperature of TTT curves. Evidence for this was provided by the agreement between the plateaux temperature of Fe-Cr and the nose of the C-curve in a TTT diagram for an Fe-8.5%Cr-0.05%C alloy [ENTIN 1962]. The presence of 0.05% C in Entin's alloy was thought to provide sufficient hardenability to enable a TTT diagram to be obtained whereas cooling rates greater than 5,500 $K.s^{-1}$ were required to suppress the transformation in Fe-Cr alloys [WILSON 1984].

Further evidence for such correlation was presented by WILSON [1994], which showed that the plateau temperature in an Fe-0.343%C alloy corresponded to the nose of a TTT diagram for Fe-0.35%C-0.37%Mn. In this case, 0.37% Mn only lowered the Ac_3 transformation temperature by 10.5K (30 x 0.37 = 10.5K ANDREWS [1965]), and provided sufficient hardenability to enable a TTT diagram to be obtained in the ternary alloy.

However, it should be noted that HILLERT [1975] considered that the transformation temperature was obtained when the rate of heat evolution due to the latent heat of transformation was balanced by the rate of heat extraction of the cooling gases. This basis of analysis also gives plateaux temperature with increasing cooling rate.

In view of the rapid $\gamma \rightarrow \alpha$ transformation in pure iron, there is little hard evidence on the results obtained from rapid quenching method to deduce the transformation start temperature for different transformations. In addition to that, the materials used by many researchers were not genuine "pure iron", contained a certain amount of impurities. The zone refined iron used by MOROZOV et al [1972] contained 10^{-6} - 10^{-7} % interstitial impurities was the purest material used to date. When these results are brought into comparison and discussion, dispute arises. Having said that, most of the researchers were aware of the significance of impurities in pure iron in terms of affecting the transformation start temperature in relation to different transformations, especially carbon and nitrogen. A critical review on this topic can be found in [WILSON 1994],

[SCHASTLIVTSEV et al 1995], [ZHAO and NOTIS 1995], [BORGENSTAM and HILLERT 1996].

The dispute over the M_s temperature for iron had led to the suggestion of studying onto iron binary alloys, such as Fe-C, Fe-Cr, Fe-Si, Fe-Mn, Fe-Ni etc. By adding alloying elements into iron, the speed of transformation is slowed down, lower temperature range transformations are therefore more easily achieved. Fe-Ni binary system, has been the most widely studied materials in understanding the $\gamma \rightarrow \alpha$ transformation of iron-substitutional binary alloys.

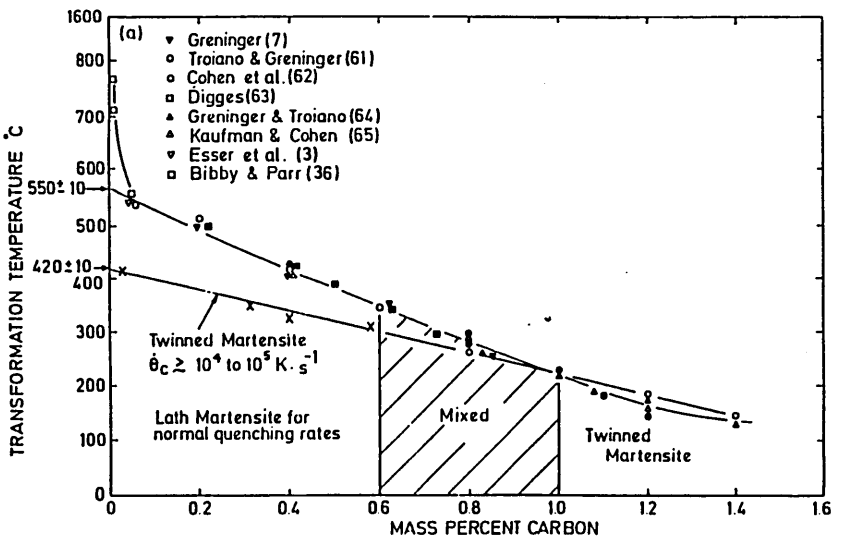

Fig. 2.1. Martensite start temperatures for Fe-C alloys. From WILSON [1994].

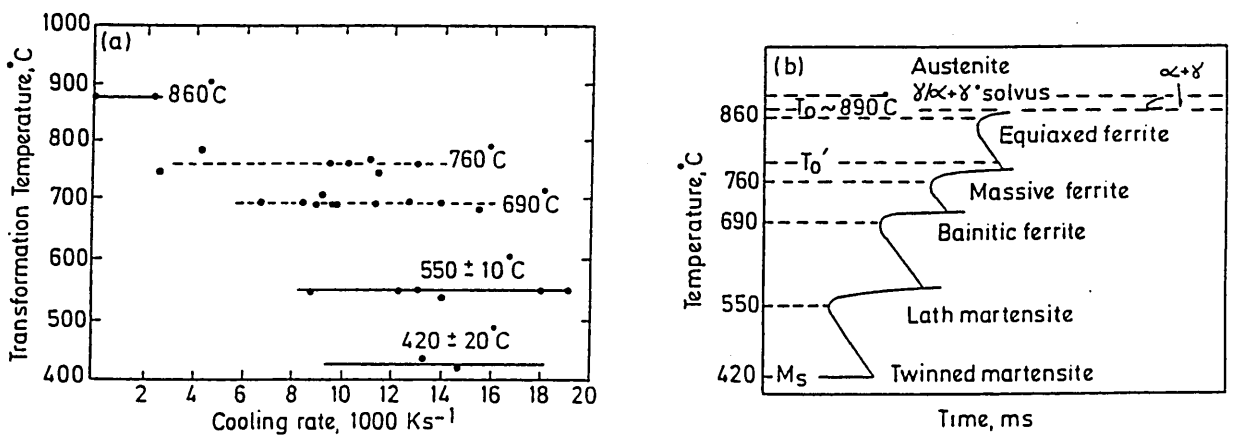

Fig. 2.2. (a) Variation of transformation temperatures with cooling rate in iron containing 0.011% C; (b) Schematic TTT curve for iron. After WILSON [1984]. Note T_0' was added as an asymptote for massive ferrite transformation by WILSON [1995].

2.2. Transformation in Iron-Nickel Alloys

When an Fe-Ni alloy is cooled in the laboratory from the γ region into the $\alpha+\gamma$ field, the nickel atoms diffusion is so sluggish that the equilibrium α phase will not nucleate. In fact, the $\gamma \rightarrow \alpha+\gamma$ transformation is only found in meteorites occurs because of the presence of phosphorous and, with cooling rate as low as a few degree Kelvin per million years, in which the Widmanstätten pattern is observed, formed by the precipitation and growth of α ferrite in γ austenite [GOLDSTEIN 1983].

To construct the Fe-Ni phase diagram in the laboratory, the Fe-Ni alloys are cooled from γ region to form a supersaturated bcc phase α_2; α_2 is normally formed as martensite. Since diffusion in bcc (α_2) is much faster than in fcc (γ) due to less atom packing in bcc, tempering in the two-phase field allows the γ phase to nucleate and grow. As the Ni-rich γ grows it will deplete the α_2 phase of Ni until the α phase attains its equilibrium composition.

The Fe-Ni binary phase diagram in figure 2.3 constructed by ROMIG and GOLDSTEIN [1980], shows the retrograde solubility for the $\alpha/(\alpha+\gamma)$ solvus line with the maximum solubility of Ni in α at 6.1 $\pm$ 0.5 wt.% at 475°C. A complete Fe-Ni phase diagram is shown in figure 2.4.

Nickel is an austenite stabiliser of the $\gamma \rightarrow \alpha$ transformation in irons and steels. The addition of nickel into iron suppresses the transformation into a lower temperature range with a lower cooling rate. By varying the percentage of nickel addition or cooling rate, the transformation experiments can be carried out in an accessible way to obtain different microstructures. Nickel has therefore been the most favourable additive alloying element to iron / steels to study the transformation mechanisms.

Early studies of Fe-Ni transformation were focused on martensite formation (see PETTY [1970] and NISHIYAMA [1978]). A high percentage of nickel addition into iron allows martensitic transformation at very low cooling rate, even allowing martensite to be isothermally transformed [YEO 1964; LEE et al 1977].

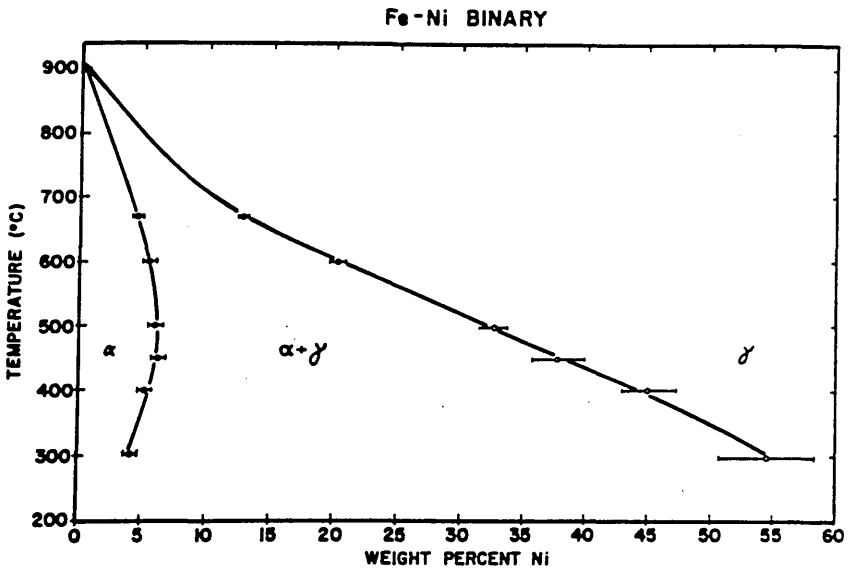

Fig. 2.3. The equilibrium phase diagram of Fe-Ni in Fe-rich region. After ROMIG and GOLDSTEIN [1980].

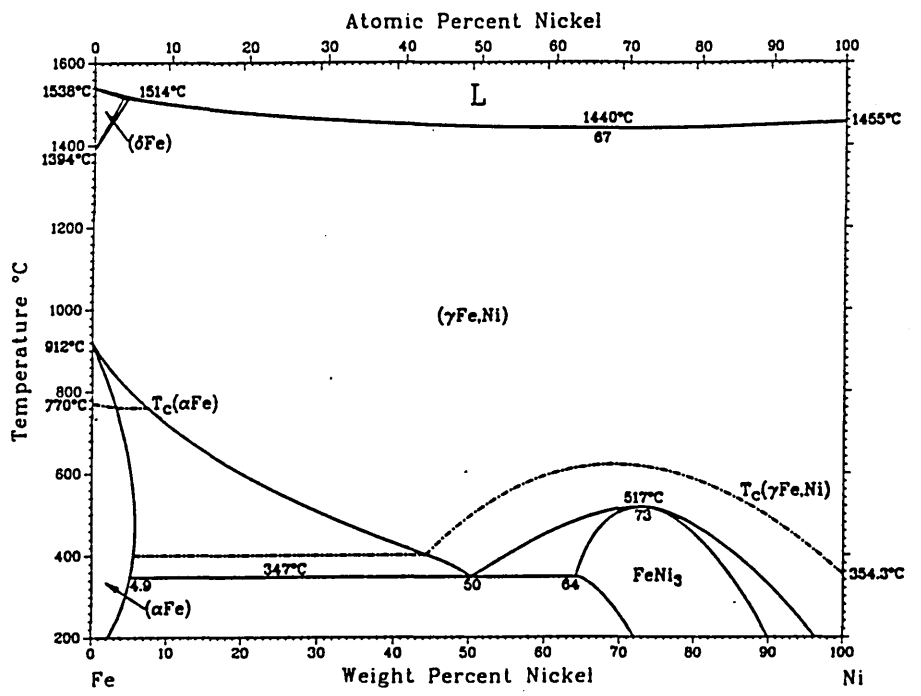

Fig. 2.4. Equilibrium phase diagram of Fe-Ni system. After SWARTZENDRUBER [1991]

KAUFMAN and COHEN [1956] determined the martensitic transformation for a range of nickel contents, high M_s values obtained at low nickel level were later shown to be other "diffusionless" transformation rather than martensite [GILBERT and OWEN 1962; WILSON 1965].

As mentioned previously, high cooling rate experiments were carried out for iron and various iron binary alloys, initiated by GILBERT and OWEN [1962] and then followed by others. The term "massive ferrite" was first applied to the transformed product that had the same composition as the parent austenite, similar to that observed in non-ferrous alloys subjected to massive transformation. The term "equiaxed ferrite" was then added to distinguish the different microstructures that could also transform massively. ROBERTS [1970] made a clear distinction between massive ferrite and equiaxed ferrite based on Fe-2Mn alloy.

Due to the rapid transformation of dilute iron binary alloys, the transformation studies were mainly carried out by continuous cooling experiment. The higher percentage of substitutional alloying elements, however, leads to transformation at lower temperatures, e.g. martensitic transformation. Therefore it is only possible to study the high temperature range transformation in certain alloys. The alloying addition slows down the speed of high temperature transformation, allowing it to be studied in reasonable times, but suppressed on quenching.

The transformation of Fe-Ni alloys around 9% Ni addition have been studied by a few researchers. KAUFMAN and COHEN [1956] first defined M_s and M_f of 9.5 at.%Ni as 525°C and 477°C at a cooling rate of 5 $K.min^{-1}$. GILBERT and OWEN [1962] reported the transformation plateau at 510°C for 9.57 at.%Ni. SWANSON and PARR [1964] obtained a transformation plateau at 360°C, defined as M_s for Fe-10 at.%Ni alloy. GOODENOW and HEHEMANN [1965] worked on Fe-9Ni alloys with varying carbon content, found that acicular structure formed at 546°C for carbon content less than 0.006 wt.% and 470°C for 0.007 wt.%C. They regarded this structure as bainitic ferrite, and concluded that B_s could vary significantly with small variation in carbon content. However, TSUZAKI et al [1990] worked on the isothermal transformation of Fe-9Ni-C, found the B_s was relatively insensitive to the change in carbon content.

The nature of the massive transformation in Fe-Ni alloys is still unclear, especially whether the massive transformation for Fe-Ni alloy occurs beyond the retrograde solvus line (i.e. in two-phase field, ($\alpha+\gamma$) in the Fe-Ni equilibrium diagram). Initially, SWANSON and PARR's [1964] work showed 2 plateaux for Fe-Ni alloys up to 7 at.%Ni only. The disappearance of first (upper) plateau in Fe-10 at.%Ni, figure 2.5, suggesting the absence of the massive transformation outside the one-phase field. However, MASSALSKI et al [1975] and HAYZELDEN and CANTOR [1985] observed the massive ferrite formation in Fe-9Ni and Fe-25Ni respectively, as did WILSON [1984] for the multiple thermal arrest results in Fe-9.57 at.%Ni. These observations are of course in the ($\alpha+\gamma$) two-phase field.

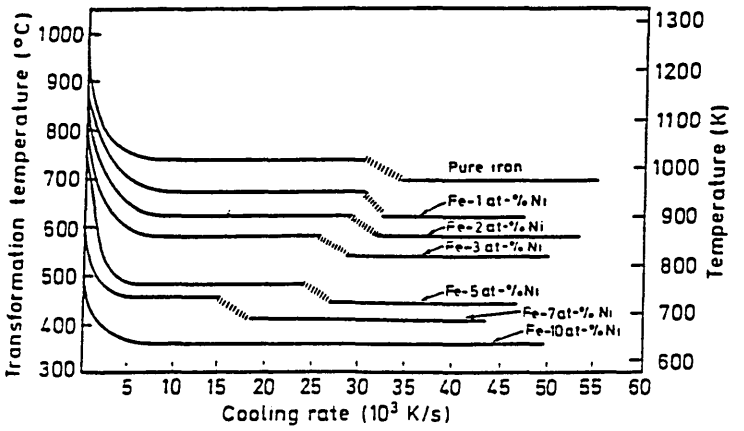

Fig. 2.5. The effect of cooling rate on the $\gamma \rightarrow \alpha$ transformation in Fe-Ni alloys. After SWANSON and PARR [1964].

On the other hand, BEE and HONEYCOMBE [1978], by studying isothermal transformation of Fe-10Cr alloy, discounted the existence of the massive ferrite transformation, viewing it merely as fully transformed Widmanstätten ferrite. They concluded that the transformation of iron binary alloys are essentially the same as Fe-C and the morphologies of the microstructures are agreed with the Dubé classification [DUBÉ 1948; AARONSON 1962].

MOISEYEV et al [1981] studied the isothermal transformation of Fe-Ni alloys. They found that the transformation kinetics in Fe-9Ni are not a "normal" type of

transformation in the sense that the maximum rate of isothermal transformation is observed at an early stage and does not go to completion, figure 2.6. The percentage of transformation being asymptotic to values less than 100%. This phenomenon is called *transformation stasis* or *incomplete transformation*, which is often appeared in bainite transformation in steels. Apparently, this transformation behaviour is different from Fe-Cr where transformation occurs in the equilibrium α phase.

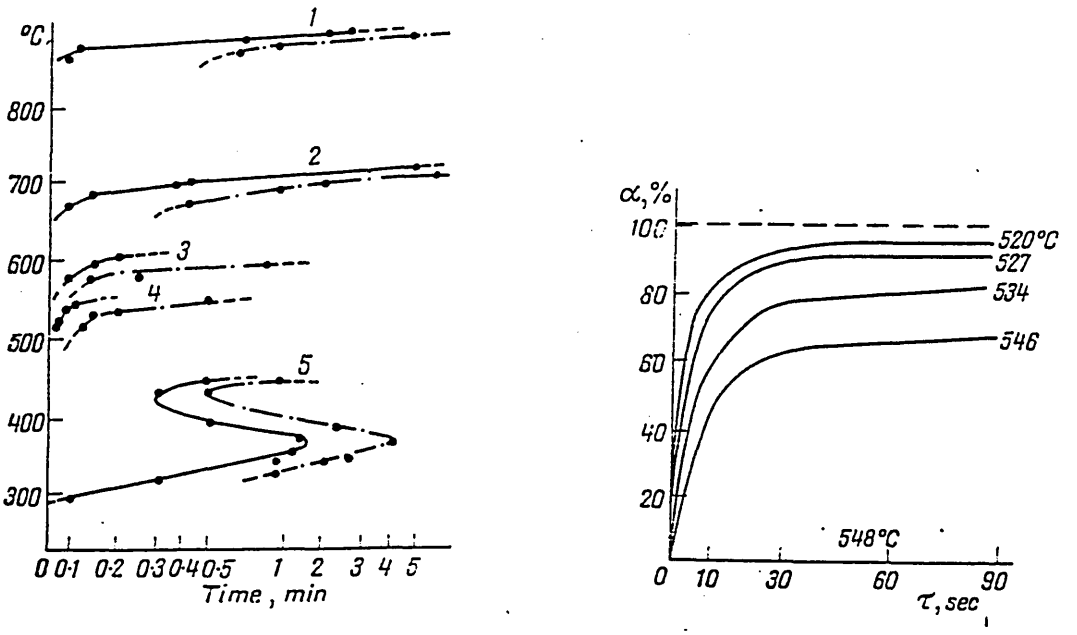

(a) (b)

Fig.2.6. γ→α isothermal transformation of Fe-Ni alloys. (a) TTT curves of (1) Fe, (2) Fe-3Ni, (3) Fe-6Ni, (4) Fe-9Ni, and (5) Fe-12Ni. (b) Percentage α transformation of Fe-9Ni at different temperatures [MOISEYEV et al 1981].

In spite of the dispute and discrepancy of the results, efforts have been made periodically to compile, collect and rationalise all the data in terms of transformation mechanism [WILSON 1984, 1994; ZHAO and JIN 1990; ZHAO 1992; BORGENSTAM and HILLERT 1996, 1997]. Figure 2.7 shows the tentative diagram drawn by WILSON [1994] to describe the possible transformation in Fe-Ni alloys.

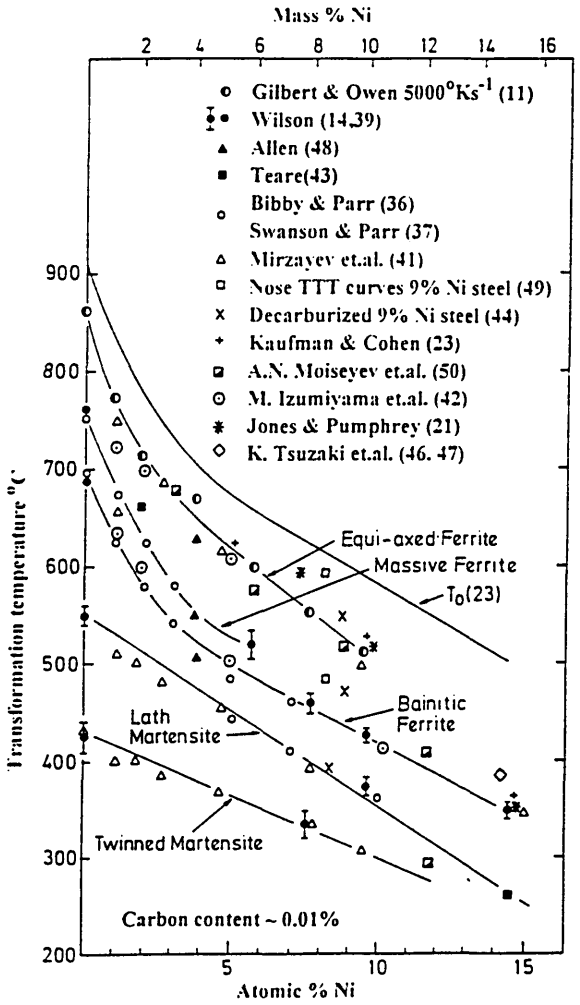

Fig 2.7. Variation of transformation with nickel content in Fe-Ni alloy. After WILSON [1984, 1994].

2.3. Transformation in Low Carbon Steels

Steels exhibit various types of transformation from austenite, depending on the chemical composition and cooling rate. In carbon steels, the major structures of ferrite, pearlite, bainite and martensite are generally found. In fact, after isothermal transformation in various steels undergoing decomposition of austenite, more than ten different microstructures are found.

For hypoeutectoid steels, or low carbon steels, ferrite would be the dominant microstructure in the matrix. Dubé [DUBÉ 1948; AARONSON 1962] observed various shapes of ferrite, and classified them as few distinctive morphologies, figure 2.8.

1. Grain boundary allotriomorphs, Fig. 2.8a.
2. Widmanstätten sideplates.
   - Primary sideplates, Fig. 2.8b(1).
   - Secondary sideplates, Fig. 2.8b(2).
3. Widmanstätten sawteeth.
   - Primary sawteeth, Fig. 2.8c(1).
   - Secondary sawteeth, Fig. 2.8c(2).
4. Idiomorphs equiaxed crystal.
   - Intragranular, Fig. 2.8d(1).
   - Grain boundary, Fig. 2.8d(2).
5. Intragranular Widmanstätten plates (or needles), Fig. 2.8e.
6. Massive structure*, Fig. 2.8f.

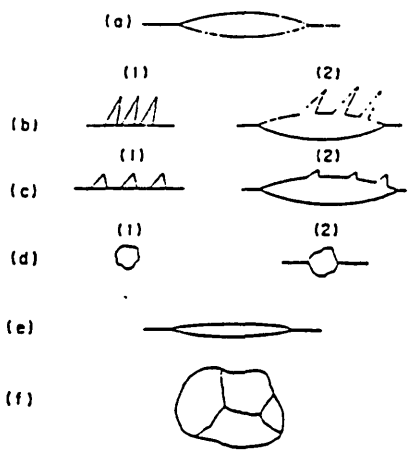

Fig. 2.8. The Dubé morphological classification system. From AARONSON [1962].

* This "massive structure" was a term used by Dubé before the massive transformation in ferrous alloys was discovered.

Carbon is the most important element in steels. The size of carbon atom (0.8Å) is much smaller than iron (1.28Å). Carbon atoms therefore enter the interstices of the α-iron There are tetrahedral voids and octahedral voids in fcc and bcc arrangement available for carbon atoms to be accommodated interstitially, figure 2.9. Carbon atoms in ferrite phase (α-iron) fit in octahedral voids rather than tetrahedral voids because a carbon

atom only has to displace two iron atoms to fit in rather than four iron atoms in a tetrahedral void [BARRETT and MASSALSKI 1966]. Under equilibrium condition, the maximum solubility of carbon in α-iron would be 0.022 wt.% at 727°C [OKAMOTO 1992].

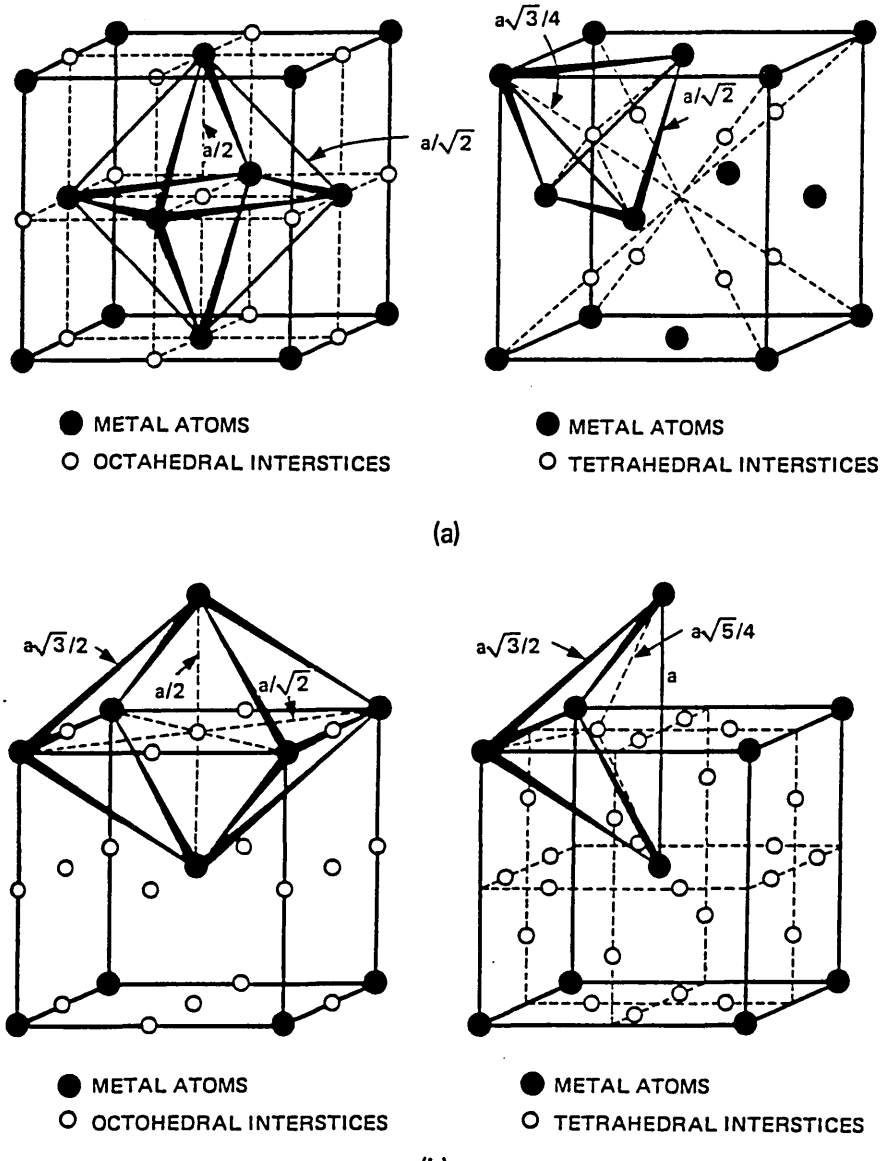

Fig. 2.9. Interstitial voids in iron. (a) Interstitial voids in fcc austenite, (b) interstitial voids in bcc ferrite. After BARRETT and MASSALSKI [1966].

Beyond the solubility limit of α ferrite, carbon precipitates as carbide such as cementite (Fe_3C, θ). Because of the high diffusion rate of carbon in steels, the γ→α transformation

in steels would be largely governed by the diffusion of this element. Very often, the determination of the transformed product depends on the presence of carbide (or cementite, θ) in the matrix, typically for the pearlite and bainite. For example, figure 2.10 shows four different temperature-composition-product diagrams constructed by different researchers.

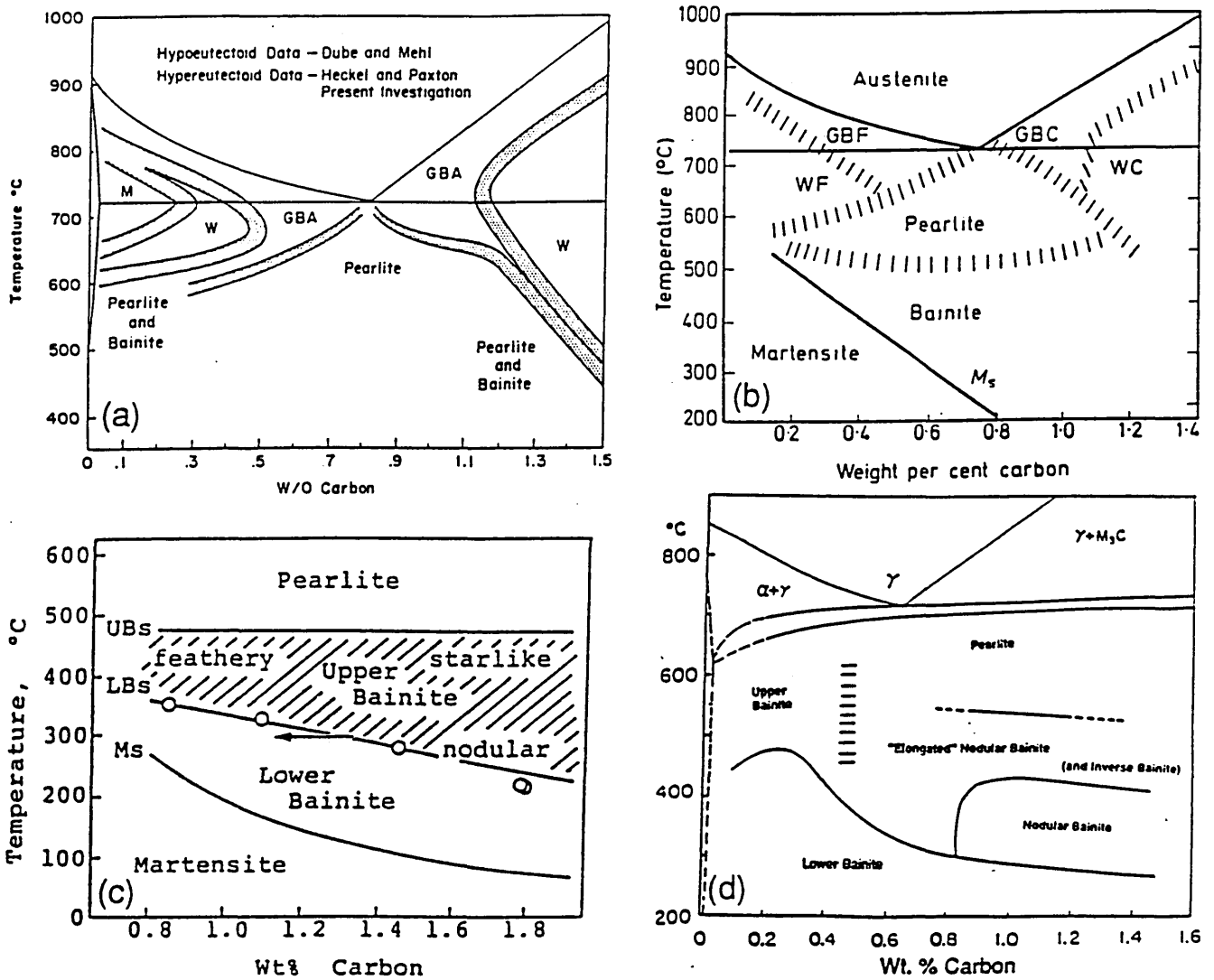

Fig. 2.10. Various kinds of (metastable) product (phase) diagram for the isothermal decomposition of austenite: (a) from AARONSON [1962], GBA = grain boundary allotriomorphs, W = Widmanstätten sideplates and / or intragranular plates, M = massive ferrite; (b) from CHADWICK [1972], GBF = grain boundary ferrite, GBC = grain boundary cementite, WF = Widmanstätten ferrite, WC = Widmanstätten cementite; (c) from OKAMOTO and OKA [1990]; and, (d) from SPANOS et al [1990] for Fe-2Mn-C steels. From ZHAO and NOTIS [1995].

In recent years, the modern steels with very low carbon content so called ultralow carbon steels, IF (interstitial free) steels and TMCP (thermo-mechanical controlled process) HSLA steels have been developed to improve the formability, weldability, toughness, while maintaining the strength at acceptable values. The matrix of these steels is predominant by ferrite phase (with various morphologies) and the present of minor secondary phases occasionally. It is difficult to identify the transformed products of ferrite grains with irregular shapes, and the acicular structure that could be either Widmanstätten ferrite, bainitic ferrite or lath martensite. The Dubé classification of ferrite morphologies, under this circumstances is difficult to apply.

In fact, the carbon content of these steels can be so low (less than 0.02 wt.%C) that the austenite can transformed directly into α single phase region with no carbon partitioning, as illustrated by composition C_1 in figure 2.11. Under this circumstances, the understanding of transformation mechanism in general carbon steels can not be applied. Instead, the composition invariance of the massive transformation is thought to play an important role.

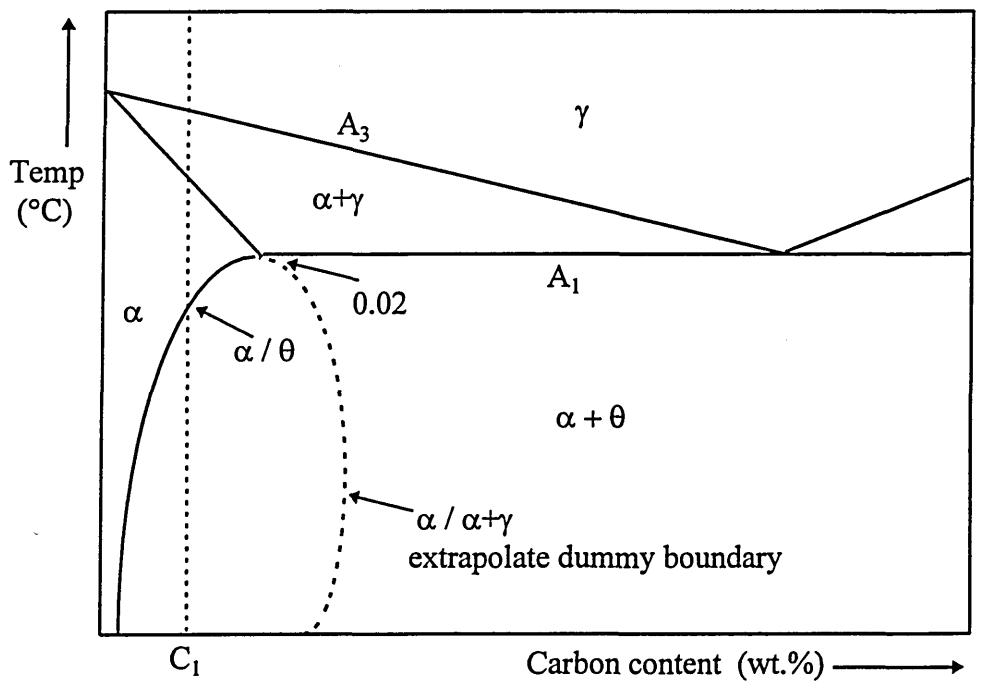

Fig. 2.11. Schematic illustration of phase diagram of Fe-C binary alloy. After MAKI [1994]. $\theta = Fe_3C$.

In view of the development of low carbon and ultralow carbon steels, the phase transformation on low carbon irons and steels have been critically reviewed in recent years [WILSON 1994; MAKI 1994; KRAUSS and THOMPSON 1995; SCHASTLIVTSEV et al 1995].

As far as industrial HSLA low or ultralow carbon steels are concerned, various types of transformations can occur, resulting in complicated microstructures in the finished product. ARAKI et al [1991, 1994] proposed the classification and terminology, shown in table 2.1, to identify the microstructures and possible transformation mechanisms in low carbon steels. Table 2.1 is taken from the published atlas by ISIJ Bainite Committee [ARAKI et al 1992].

Table 2.1. Symbols and nomenclature for ferritic microstructures in continuously-cooled very low carbon HSLA steels. From ARAKI et al [1992].

I_0	Major matrix-phase	II_0	Minor secondary phases
α_p	Polygonal ferrite	γ_r	Retained austenite
α_q	Quasi-polygonal α	MA	Martensite-austenite constituent
α_W	Widmanstätten α	α'M	Martensite
α_B	(Granular bainitic) α	aTM	Auto-tempered martensite
α°_B	Bainitic ferrite	B	BII, B2 : upper bainite
α'_m	Dislocated cubic martensite		B_U : upper bainite
			B_L : lower bainite
		P'	Degenerated pearlite
		P	Pearlite
		θ	Cementite particle

2.4. Massive Transformation

When an alloy is undergoing continuous cooling from high temperature, for example X_i in figure 2.12(a), the parent phase (γ) can transform massively into α_m provided that the free energy of the new phase is lower than the parent phase. As can be noticed from the free energy diagram of figure 2.12(b), when the system is undercooled to a certain degree, the precipitation process, indicated by ΔG_e, will lead to the equilibrium thermodynamic, represented by the reaction:-

$$\gamma (X_i) \rightarrow \alpha (X_1) + \gamma (X_2) \qquad (2.1)$$

This equilibrium state $\alpha+\gamma$, has the lowest possible free energy and require very long transformation time if the diffusivity of the solute atom is very low.

Alternatively, decrease in free energy upon transformation, indicated by ΔG_m will also be possible, as represented by:-

$$\gamma (X_i) \rightarrow \alpha (X_i) \qquad (2.2)$$

This is called a composition invariant phase transformation in which the transformed product inherits the composition of the parent phase. If the transformation is of nucleation and growth type, it will be regarded as "massive transformation", or it will be regarded as "martensitic transformation" if the transformation takes place by shear. Under these circumstances, the final product is in metastable form and can only take place below T_0.

The word "massive" was first used by GRENINGER [1939] to describe an α constituent found in quenched Cu-9.3%Al alloy from 1020°C, β phase, figure 2.13. The α phase appeared as shapeless area with very jagged and irregular boundaries, termed it as "massive α". Slow cooling from β phase would produce the mixture of $\alpha+\beta$ by long range diffusion process. This specific solid→solid phase transformation behaviour without a change in chemical composition is now referred to as a "massive transformation".

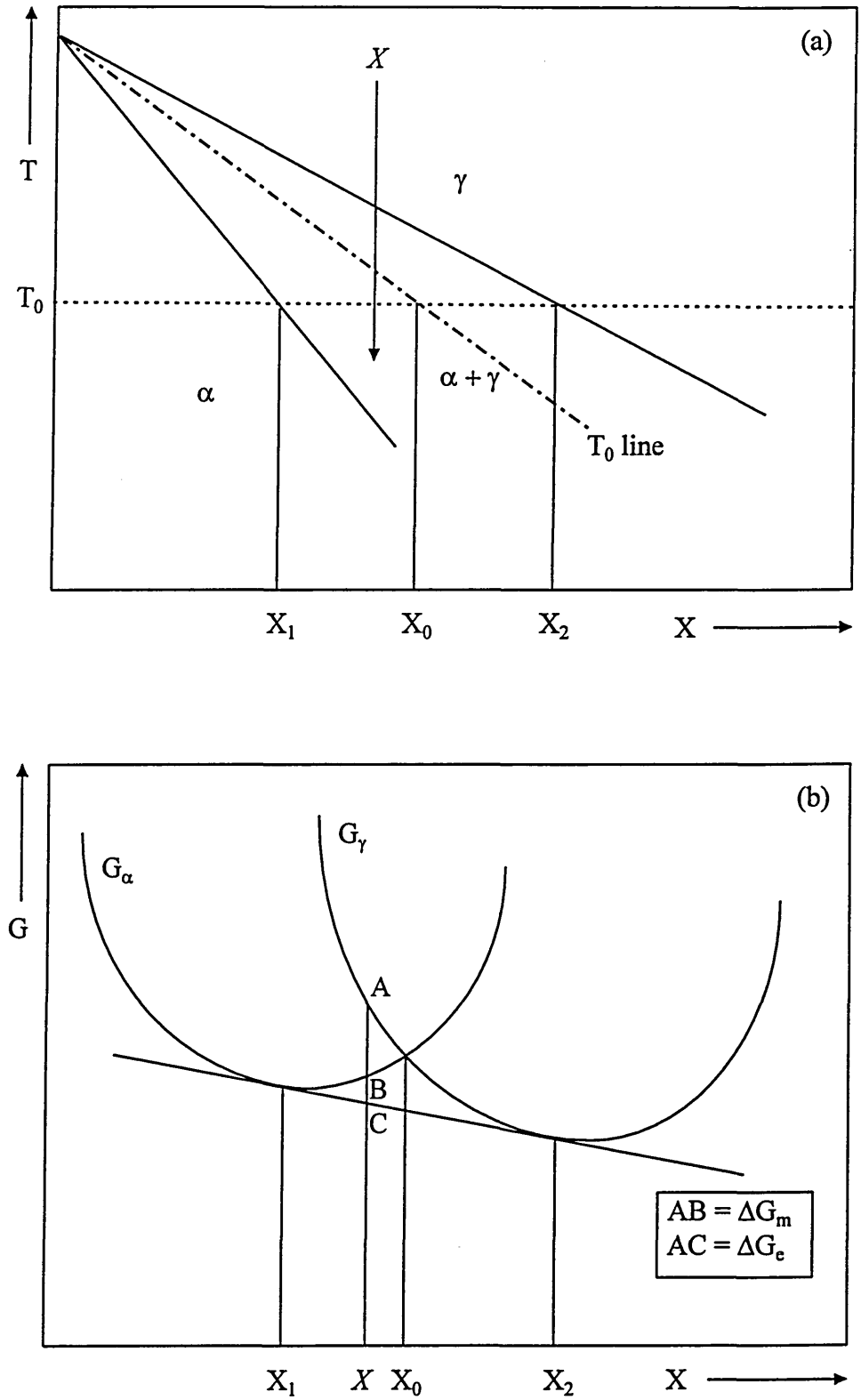

Fig. 2.12. (a) Schematic equilibrium phase diagram showing decomposition of γ upon continuous cooling system into two-phase field, and (b) a schematic representation of the free energy-composition curve showing the possibility of composition invariance transformation in two-phase field.

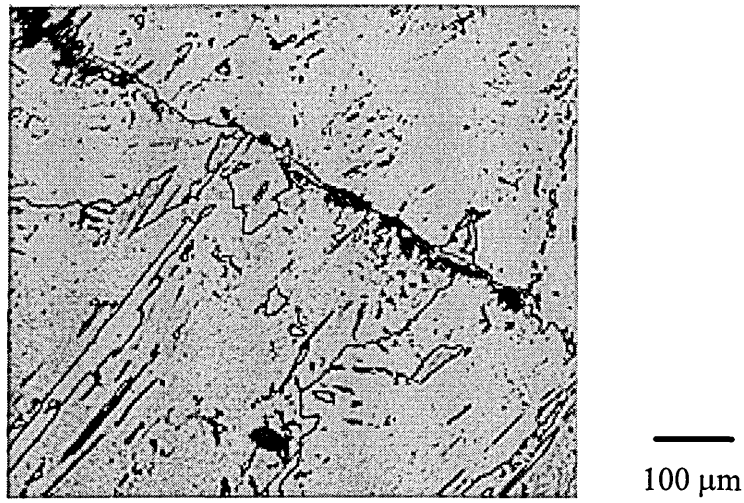

Fig. 2.13. Greninger's massive α; Cu-9.3%Al quenched from 1020°C into 10% NaOH, etched with $NH_4OH + H_2O_2$ [GRENINGER 1939].

Since Greninger's work, massive transformations have been found in other alloys. MASSALSKI's [1958] work showed that massive transformations occur at specific composition range in a number of copper, zinc, gallium binary or ternary alloys system.

The possibility of massive transformation occurring in iron was first proposed by MASSALSKI [1958] and was confirmed by OWEN and GILBERT [1962]. After 1962, on rapid quenching, massive transformation was also found in Fe-C [ACKERT and PARR 1971; MIRZAYEV et al 1987] and Fe-N [OWEN et al 1964; BELL and OWEN 1967], and iron substitutional alloys such as Fe-Ni [GILBERT and OWEN 1962; SWANSON and PARR 1964; WILSON 1965, 1984; DUBROV 1966; MIRZAYEV et al 1973], Fe-Cr [GILBERT and OWEN 1962; WILSON 1965; WALLBRIDGE and PARR 1966; PASCOVER and RADCLIFFE 1968], Fe-Mn [GOMERSALL and PARR 1965; ROBERTS 1970; HOLDEN et al 1971], Fe-Cu [WILSON 1968; RÄSÄNEN 1969].

Figure 2.14(a) shows the morphology of massive ferrite with jagged boundaries, formed by iced brine quenching an Fe-0.002%C alloy [MASSALSKI 1985], and 2.14(b) the massive ferrite grain boundaries growing across prior austenite grain boundaries [WILSON and OWEN 1965]. These are the characteristic of ferrite grains that subjected to transformation with no carbon partitioned by the massive reaction, forming from low

carbon austenite, as to distinguish from the formation of carbon-depleted grain boundary allotriomorphs α ferrite that form at high temperatures and low supersaturations by diffusion process.

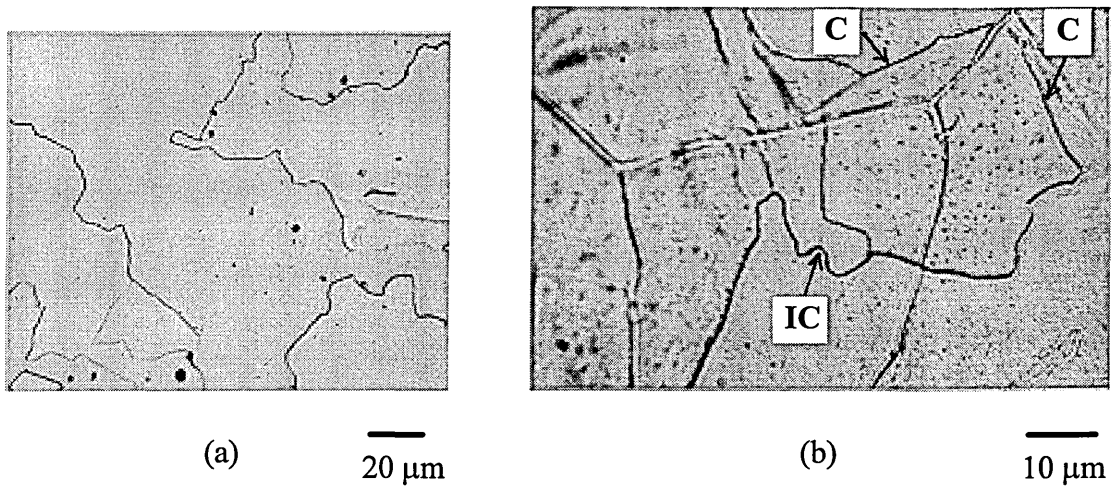

Fig. 2.14. (a) Microstructures of massive ferrite when an Fe-0.002%C alloy was iced brine quenched. After MASSALSKI [1985]. (b) Ferrite grain of Fe-4%Ni, thermally etched to revealed prior austenite grain boundaries, quenched and nital etched to reveal ferrite boundaries. After OWEN and WILSON [1965]. The indication of incoherent (**IC**) and possible coherent (**C**) ferrite boundaries are added in figure 2.14(b) by WILSON [private communication 1998].

2.4.1. Massive Transformation Mechanism

It is now generally accepted that massive transformation is a composition invariant transformation involving short range diffusion process. The new phase grows via thermally activated processes that exhibit diffusional and growth characteristics, controlled mainly by interfacial diffusion rather than volume diffusion. It is nonmartensitic in nature which does not produce invariant plane strain (IPS) surface relief effects [MASSALSKI 1970]. Therefore it is considered as a transformation that occurs at intermediate temperature range, in between the diffusional process that occurs at high temperature and diffusionless, martensitic transformation at low temperature range. Figure 2.15 presents a schematic TTT diagram illustrating the position of the C-curve for the massive transformation.

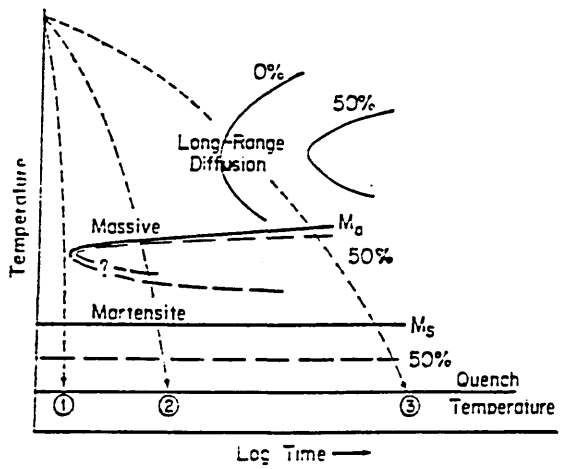

Fig. 2.15. Schematic diagram illustrating the region of massive C-curve in between diffusional and martensitic transformations. After MASSALSKI [1970].

According to Massalski's school, nucleation of massive grains most likely occurs at heterogeneous sites without any low index orientation relationship between the parent and the product phases. Such grain would grow at relatively high speed and across several parent grain boundaries, with the propagation of incoherent interfaces. As soon as the nuclei form, growth will complete within a very short period, with growth rates as high as 10^{-4} to 10^{-2} m.s^{-1}. The thermal arrest data can be interpreted as the nucleation temperatures for massive transformation under continuous cooling conditions. As a result, it is believed that the controlling process is the nucleation event [BHATTACHARYYA, PEREPEZKO and MASSALSKI 1974].

Aaronson school [AARONSON et al 1968; PLICHTA and AARONSON 1980; PLICHTA et al 1984; MOU and AARONSON 1994] viewed that massive transformation must always involve special crystallographic orientation relationships which arise during the nucleation stage, to lower the activation energy ΔG^* for massive grains formation in much the same way as they do in numerous precipitation reactions from solid solutions. The nuclei enclosed by low energy interfaces are usually present during growth as partially coherent boundaries which can migrate by ledge mechanism. A growing massive crystal was envisaged as being bounded by ledged partially coherent interfaces. This is especially proven by the studies of interfaces structure bcc β : hcp ζ_m with high-

resolution TEM on massively transformed Ag-26 at.%Al alloy [MOU and AARONSON 1994].

On the other hand, WILSON [1984, 1994] worked on the massive transformation in ferrous alloys, perceived two types of structure upon massive transformation, viz. equiaxed ferrite and massive ferrite. Equiaxed ferrite is thought to nucleate at grain corner in austenite with one or more coherent interfaces. Because the volume change is thought to be accommodated by austenite grain boundaries and the dislocation density is low. Theoretical calculations indicate that the equiaxed ferrite transformation is controlled by growth [WILSON 1991]. This concept was supported by the studies of transformation behaviour in ultra-low carbon steels [SHIBATA and ASAKURA 1995].

According to WILSON [1984, 1991, 1994], massive ferrite is thought to nucleate as a semi-coherent cap on grain face with a planar surface on the boundary and an upper curved incoherent boundary. In this case, the volume change is not thought to be accommodated by the grain boundary resulting in a high dislocation density. Growth occurs by movement of the incoherent boundary with rapid atom transfer across the incoherent boundary, and the coherent boundary is keeping pace with the incoherent interface by lateral movement of ledges. The ragged structure could be as a result of solute drag, the movement of incoherent boundary being pinned by solutes at various point along it's length. According to local equilibrium concept, HILLERT [1975, 1984] suggested that there might be a composition spike in the γ / α interface during growth.

2.4.2. Massive Transformation Below T_0 in The Two-Phase Field

The composition invariance of massive transformation in Fe-8.7 at.% Ni [MASSALSKI et al 1975], and Cu-Zn system [MASSALSKI et al 1972] proven by microprobe studies raised the interesting question on whether massive transformation can occur in the two-phase field.

KARYLN, CAHN and COHEN [1969] have criticised the evidence on this point and provided theoretical reasons why a massive transformation should occur only in the one-

phase region. HILLERT [1984] viewed the solvus line rather than the T_0 line as the natural limit for the massive transformation. The observations of massive transformation inside two-phase field is due to the effect of coherency strains in the composition spike formed in front of the interface, otherwise the composition invariance would be impossible in the two-phase field if local equilibrium is required.

MENON et al [1983, 1985], initially, regarded massive transformation in two-phase field as impossible from a thermodynamic point of view. However, in the later, these workers [MENON et al 1988] developed an approach to explain the presence of the massive transformation below T_0 in the two-phase region. According to them, massive transformation in a two-phase field is viable if the volume diffusivity in the matrix is too low relative to the trans-interphase boundary diffusivity to allow solute partition during growth. The main factor controlling the ability of equilibrium precipitation to compete with the massive transformation is the operative volume diffusivity, which tends to scale with homologous temperature T_0/T_s (where s = solidus) [MENON et al 1988; AARONSON et al 1994].

In attempt to explain the massive transformation in two-phase field, ÅGREN and JÖNSSON [ÅGREN 1989; JÖNSSON and ÅGREN 1990; JÖNSSON 1990] adopted the solute drag model and developed two solutions for massive transformation. In single-phase region, massive transformation takes part with high growth rate and weak solute drag effect, and becoming low in growth rate with strong solute drag effect if occurring in the two-phase region. In the two-phase field, transformation will only start when the temperature has fallen below the T_0 line.

To date, in most of the research on massive transformation, the examination on massive structures were carried out only after the transformation was completed. The development of modern electron microscopy has certainly contributed in proving the assumption that massive grains growth by ledge mechanism via partial coherent boundaries movement. [MOU and AARONSON 1994]. However, there is still insufficient evidence to prove the mechanism of trans-interphase diffusion of solute atoms involved in the massive transformation. The occurrence of a compositional spike, suggested by HILLERT [1975, 1984] awaited confirmation.

2.5. Bainitic Transformation

In the isothermal transformation TTT curve for Fe-C alloys, the product at temperature range below the "nose" of pearlite reaction is called bainite. This product is a mixture of ferrite (in the form of laths or plates) and carbides (precipitate as cementite Fe_3C or ε-carbide $Fe_{2.4}C$).

With the additions of other alloying element into Fe-C system, the bainite transformation can be separated from the pearlite C-curve, establishing a distinctive C-curve at intermediate temperature range below the pearlite reaction and above martensitic transformation, for example, the TTT diagram for 9% nickel steel as shown in figure 2.16.

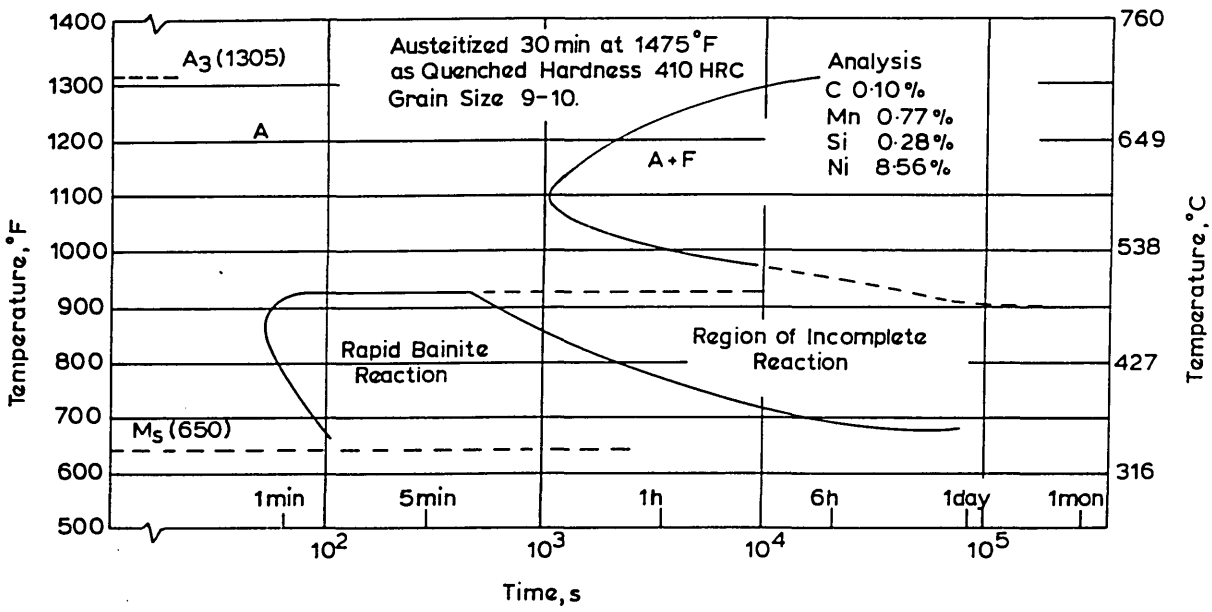

Fig. 2.16. Isothermal transformation diagram for 9%Ni steel. After MARSHALL et al [1962].

As the research on bainite transformation in steels progresses, the understanding on bainite transformation is not becoming clearer, but more complicated. Bainite is found to appear in many different morphologies in different alloyed steels, and various

theories have been proposed to explain the findings of such peculiar behaviour that take place at the intermediate temperature range in steels.

Table 2.2 shows the bainite morphologies listed by OTHANI et al [1990]. There are others which regarded as "nonclassical bainite" such as granular bainite [HABRAKEN and ECONOMOPOULOS 1967; THOMPSON et al 1988], columnar bainite [SPANOS et al 1990; NILAN 1967] or inverse bainite [KINSMAN and AARONSON 1970; HILLERT 1962] also found in certain alloyed steels.

Table 2.2. Morphology of bainite in isothermal transformation. After OTHANI [1990].

Microconstituent	Criteria	
	Ferrite Morphology	Carbide distribution
Ferrite	Lath-like	Acicular ferrite (carbide free)
Upper bainite	BI BII BIII	Lath interface
Lower bainite	Plate-like	Within grain

At present, there are three different definitions on bainite transformation:

I Microstructural definition

This, in general, describes bainite as two-phase nonlamellar product of eutectoid decomposition. The transformation takes place by diffusional, non-co-operative, competitive ledgewise growth. This definition is supported by Aaronson school [HEHEMANN, KINSMAN and AARONSON 1972; AARONSON et al 1990].

II Overall reaction kinetics definition

This definition assumes that bainite transformation is having a separate C-curve on a TTT diagram whose maximum temperature, the kinetic-B_s (bainite start), in analogy with the M_s temperature for the martensitic reaction, lies below the eutectoid temperature. The kinetic-B_s is defined as the temperature above which austenite will not transform to bainite [HEHEMANN and TROIANO 1956; HEHEMANN 1970; HEHEMANN, KINSMAN and AARONSON 1972].

Below B_s, as in many nucleation and growth process, transformation proceeds first to a maximum rate and then gradually slows down. The transformation does not go to completion and the remaining austenite in these bainitic structures is sluggish to transform. This has become known as the *incomplete transformation phenomenon* or *transformation stasis*. With prolong isothermal holding, the residual austenite could transform into pearlite [BHADESHIA and EDMONDS 1979].

III Surface relief definition

The surface relief definition terms bainite the plate-shaped product of a shear mode of phase transformation, usually takes place above the M_s, as evidence by an invariant plane strain (IPS) relief effect when plate forms at a free surface. The laths or plates formation is simultaneous or highly co-ordinated, non-thermally activated glide of atoms across the advancing interphase boundary, as evidence by an invariant plane strain (IPS) relief effect at free surface. The formation of IPS is usually explained by Phenomenological Theory of Martensite Crystallography (PTMC).

The arguments in supporting this definition have been presented by CHRISTIAN and EDMONDS [1984], OLSON et al [1988] and CHRISTIAN [1990].

2.5.1. Bainitic Ferrite Formation

When the carbon content in alloyed steels has fallen to such a low level that the carbide precipitation does not take place in phase transformation, the bainitic transformation defined above, with a certain degree, would be irrelevant under these circumstances.

The term "bainitic ferrite" was first proposed by WILSON [1965, 1970] to distinguish the transformed product at temperature range in between the massive ferrite and lath martensite. For example, from the transformation studies of Fe-15%Ni [WILSON et al 1982], bainitic ferrite was found to transform at 350 ± 5°C, whilst lath martensite at 260 ± 20°C, with tentative habit plane of $\{112\}_\alpha$ and $\{110\}_\alpha$ respectively, figure 2.17.

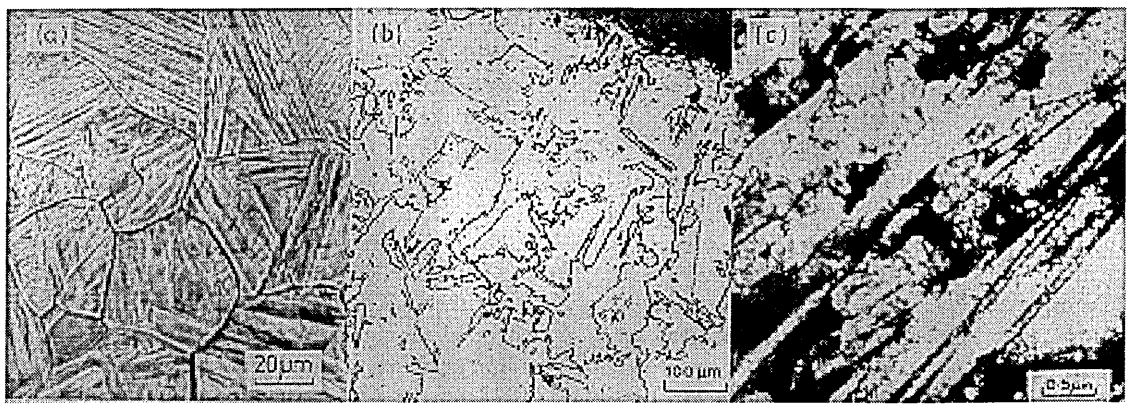

Fig. 2.17. Bainitic ferrite in Fe-15 %Ni. (a) Surface tilt on prepolished sample, (b) nital etched optical micrograph, and (c) electron micrograph. From WILSON [1994].

By studying the isothermal transformation of Fe-10Cr [BEE and HONEYCOMBE 1978], broad and heavily dislocated laths were found at the temperature above M_s and below the ferrite C-curve, identified as bainitic ferrite transformation. Carbide-free bainitic ferrite transformation was also reported by GOODENOW and HEHEMANN [1965], RÄSÄNEN [1969], MCEVILY [MCEVILY et al 1967; MCEVILY and MAGEE 1968], HOLDEN et al [1971]. However, there are also scholars who regarded the existence of carbide-free bainitic ferrite as unjustifiable [MENON et al 1988; BHADESHIA 1992].

Due to the development of ultralow carbon steels, the studies on carbide-free bainitic transformation have nevertheless received increasing attention. In the transformation studies on these steels [JUNG et al 1994,1995; OHMORI et al 1994], these authors suggested bainite nucleates via diffusional mechanism and grows in the longitudinal direction via a displacive mechanism. These workers also suggested that the classification of bainite should be based on ferrite morphology only.

Apparently, with the development of modern low carbon bainitic steels, further research on bainitic transformation in ferrous materials would appear to be necessary in order to revise the current definitions of bainite.

2.6. Martensitic Transformation

Martensitic transformation is a diffusionless process, involving lattice distortion shear displacements where the atoms rearranging themselves in co-ordinated way. Therefore, it is also called as "military transformation" as oppose to "civilian transformation" which take place by diffusion process [CHRISTIAN 1965]. This mode of transformation kinetics is athermal, required high undercooling at a well-defined temperature, M_s (i.e. martensitic start transformation temperature).

When martensitic transformation takes place, a shape change is observed which results in surface upheavals called surface relief on a polished flat, indicating a transformation occurs by a displacive movement of parallel plates with crystallographic characteristics, and with a defined habit plane, figure 2.18. Since the habit plane or martensite/matrix interface is observed to be linear under the optical microscope for all angles of section, habit plane is thought to remain planar, undistorted and unrotated during transformation. Hence the strain accompanying the martensite is regarded as invariant plane strain (IPS).

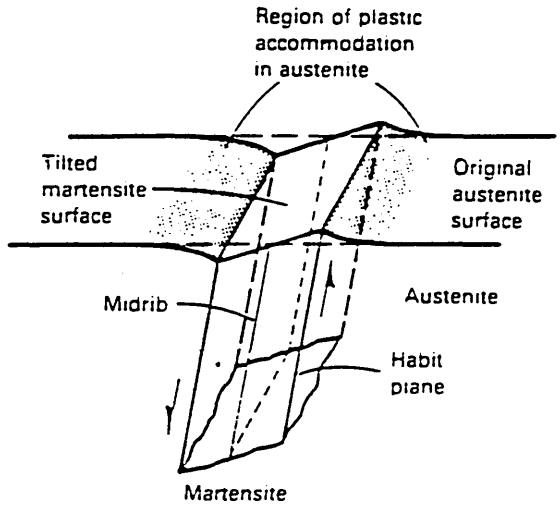

Fig. 2.18. Schematic shape deformation produced during the formation of a martensite plate. The arrows indicate the directions of shear. From SPEICH [1985]. Originally BILBY and CHRISTIAN [1961].

In order to explain the martensitic transformation and crystal structure, BAIN [1924] proposed a simple model to describe how a fcc→bcc/bct transformation could take place by lattice distortion . This is known as "Bain strain", figure 2.19. However, the Bain strain although producing the correct crystal structure, does not produce an invariant plane strain.

Later, WECHSLER, LIEBERMAN and READ [1953] and BOWLES and MACKENZIE [1954] showed that crystallographic features of martensitic transformation can be completely explained by multiple steps involving the Bain strain, shear deformation and rotation. This is then referred to as Phenomenological Theory of Martensite Crystallography (PTMC).

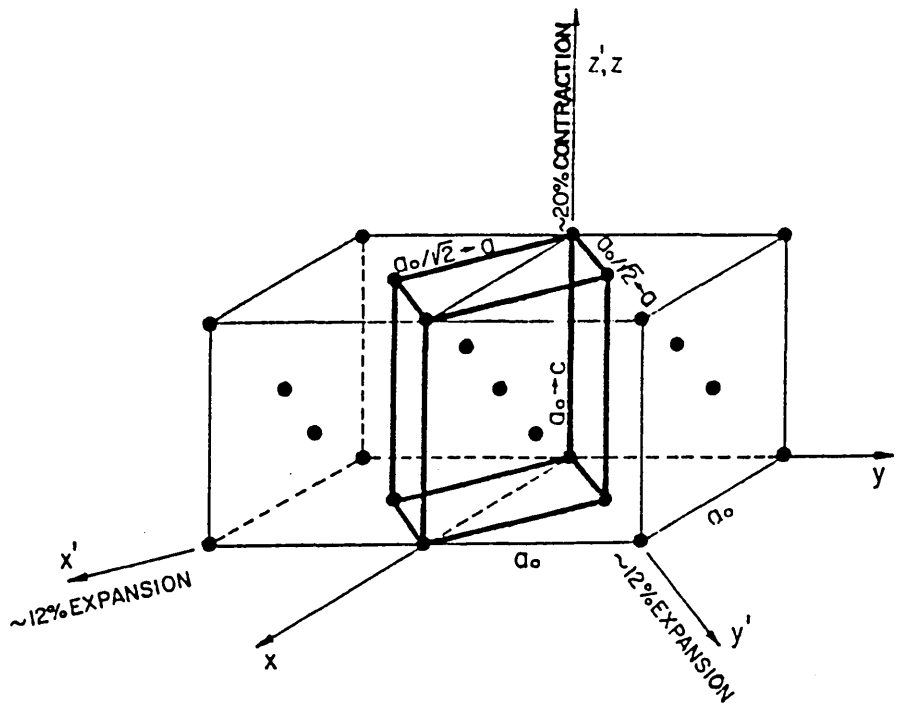

Fig. 2.19. Lattice distortion and correspondence by BAIN [1924] for the fcc→bcc (bct) martensitic transformation in iron alloys. The correspondence related cell in the parent phase (bold lines) becomes a unit cell in the martensite as a consequence of a homogeneous lattice deformation, involves an expansion of about 12% along the x $[100]_\gamma$ and y $[010]_\gamma$ directions, and 20% contraction along the z $[011]_\gamma$ direction. From WAYMAN and BHADESHIA [1996].

2.6.1. Martensite in Ferrous Alloys

In ferrous alloys, 3 kinds of martensite with different crystal structure can form, depending on alloying elements and compositions :-

(a) bcc / bct martensite - α′ martensite,

(b) hcp martensite - ε martensite [SATO et al 1982; OTSUKA et al 1990], and

(c) fct martensite [SOMURA et al 1980; OSHIMA et al 1985].

The α′ martensite presents in different morphologies, table 2.3.

Lath martensite is the most prevalent structure. It's structure is characterised by packet and blocks of parallel laths within a prior austenite grain. A packet consists of two components:-

(a) a matrix of laths with the same orientation and separated by low angle boundaries,

(b) sets of other laths that have a different orientation from that of the matrix and separated from the matrix by high angle boundaries [MARDER and MARDER 1969].

Lath widths are generally less than 1 μm. For low carbon (< 0.01%) and / or low substitutional ferrous alloys, there could be no trace of retained austenite. Single surface trace analysis found the habit plane of lath martensite as $(110)_{\alpha'}$ [RICKS et al 1979; WILSON et al 1982]. The growth rate of lath martensite was found to be about 0.072 - 4 $mm.s^{-1}$ in an Fe-24.5Ni alloy [MARDER and MARDER 1969].

Twinned martensite can only form when the cooling rate is extremely high, or with high percentage addition of carbon or others substitutional alloys. Twinned martensite is the transformed product that is known to occur at lowest temperature range. Twinned martensite can grow at the speed of sound [BUNSHAH and MEHL 1953; YU and CLAPP 1989].

Since the name "martensite" was first used in honour of the German metallurgist Adolf Martens in 1895 on the structure found in quenched steels, there have been enormous number of articles published to date on the findings of various martensitic structures in ferrous alloys. The characteristic of various martensites in ferrous alloys is briefly summarised in table 2.3.

Table 2.3. Morphology, substructure, habit plane, orientation relationship of 5 types of α' martensites. Adapted from MAKI [1990].

Morphology	Substructure	Habit plane	Orientation relationship	M_s	Example
Lath	Dislocations	$(111)_\gamma$ or $(557)_\gamma$	K-S	High ↑	Fe-20Ni-5Mn [WAKASA and WAYMAN 1981] Fe-17.3Cr-7Ni-0.097C [SANDVIK et al 1984]
Butterfly	Dislocations + Twins	$(225)_\gamma$	K-S		Fe-18Ni-1Cr-0.5C [UMEMOTO et al 1984]
(225) type plate	Dislocations + Twins	$(225)_\gamma$	K-S		Fe-6Mn-0.9C [DAUTOVICH and BOWLES 1972] Fe-3Mn-3Cr-1C [JANA and WAYMAN 1970]
Lenticular	Dislocations + Twins (Mid-rib)	$(259)_\gamma$ or $(3\ 10\ 15)_\gamma$	N G-T		Fe-31.1Ni [BREEDIS and WAYMAN 1962] Fe-29.8Ni [PATTERSON and WAYMAN 1966]
Thin-plate	Twins	$(3\ 10\ 15)_\gamma$	G-T	↓ Low	Fe-31Ni-0.23C [MAKI et al 1971] Fe-7Al-2C [WATANABE and WAYMAN 1971] Fe-24.5Pt [EFSIC and WAYMAN 1967]

K-S : Kurdjumov-Sachs relationship [KURDJUMOV and SACHS 1930]:

$(1\,1\,1)_\gamma // (0\,1\,1)_{\alpha'}$ $\quad [\bar{1}\,0\,1]_\gamma // [\bar{1}\,\bar{1}\,1]_{\alpha'}$

N : Nishiyama relationship [NISHIYAMA 1934]:

$(1\,1\,1)_\gamma // (0\,1\,1)_{\alpha'}$ $\quad [1\,1\,\bar{2}]_\gamma // [0\,\bar{1}\,1]_{\alpha'}$

G-T : Greninger-Troiano relationship [GRENINGER and TROIANO 1940]:

$(1\,1\,1)_\gamma \sim (0\,1\,1)_{\alpha'}$ $\quad [\bar{1}\,0\,1]_\gamma \sim [\bar{1}\,\bar{1}\,1]_{\alpha'}$ - within approximately 1° and 2.5° respectively.

2.7. Development of Lean Carbon Steels

Carbon addition into steels promote strength, figure 2.20. With the absence of carbon, the austenite decomposed products are generally low in strength, even in the martensitic condition. However, the increase in strength associated with carbon addition often suffer the disadvantages such as poor weldability and low toughness.

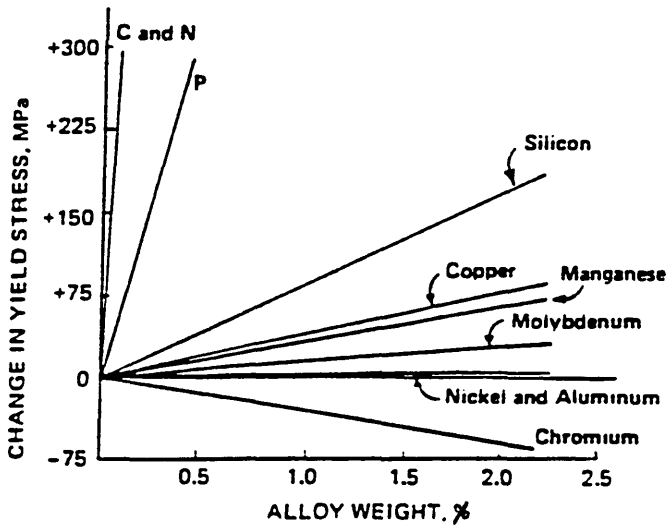

Fig. 2.20. Degree of strengthening low carbon ferritic steels with different alloying element. After PICKERING [1978].

Low carbon steels (0.01%C) could not be used until the development of controlled rolling and microalloying. In this case, the strength and toughness were improved due to grain refinement. Weldability was also improved due to elimination of brittle high carbon martensite in the HAZ. These developments were particularly significant for oil and gas as well as automobile industries.

Strength has always been the main consideration in the development of structural steels. It is now recognised that the strengthening mechanism in steels is governed by the factors below [PICKERING 1978]:-

(a) Solid solution;

(b) Grain size;

(c) Second-phase particle;

(d) Dislocations; and

(e) Transformation.

Above all, strengthening by grain refinement is most desirable as it also improves the toughness as well as the strength because grain boundaries act as barrier to dislocation movement and propagation of brittle crack.

The understanding of the strengthening mechanism is best described by the ultra-high strength maraging nickel steels [PETTY 1970; PICKERING 1978]. This steel is a high strength, high toughness but low carbon steel. The microstructure of this steel consists of fine grain and lath martensite, with high dislocation density. But because of the low carbon content, the martensitic structure is relatively soft and can easily be cold worked. The strength can be improved by age hardening due to the precipitation of intermetallic compound such as Ni_3Mo. However, grain refinement by high nickel addition is not desirable due to its high cost.

The development of controlled rolling technique which produces strong and tough steels by grain refining was began in 1960's [TAMURA et al 1988]. Microalloying elements such as niobium, titanium and vanadium are added to minimise grain growth and also contributed to precipitation hardening [SAGE 1989].

The performance of ferrite-pearlite structures of pipe-line steels met its limitation when higher strength with reduced cost was required. In the 70's, the development of FAMA steels [MÅRTENSSON 1972] for instance, was an example in which the traditional ferrite-pearlite steels started to be displaced by ferrite-bainite steels. Manganese was added to promote bainite transformation, and niobium was added to for grain refinement and precipitation hardening purposes, while the carbon content was kept below 0.04 wt% to avoid embrittlement. For ferrite+pearlite steels, high precipitation hardening is required to achieve yield strength greater than 480 MPa, with unfortunately a deterioration in toughness. Bainitic structure with low carbon provides transformation strengthening by dislocation substructure, and at the same time affects toughness to a lesser degree [EDMONDS and COCHRANE 1990].

A HSLA steel of 0.05% C with attainable yield strength of 700 MPa and highly weldable has been developed for U.S. Navy ship plate application [KRAUSS and THOMPSON 1995]. HSLA-100 steel was developed for surface ship and submarine construction to replace HY-100 steel. Compared with HY-100 (with carbon content 0.2%), HSLA-100 consisted of 0.036C, 0.91Mn, 0.59Cr, 1Cu, 0.6Mo, 3.59Ni gave better weldability and reduce or eliminate cold cracking [DEARDO 1995].

In recent years, the development of low-temperature transformation products in ultralow carbon - low alloyed steels led to the production of non-heat-treated steels in as-rolled or as-forged condition. Very low carbon steels with unique microstructures offer potential and satisfying sheet and plate applications which require excellent combinations of strength, ductility and toughness. ARAKI et al [1994] reported the potential usage of such steels in pipeline, automobile, ship and carriers.

Mild steel with ~0.1%C was used in sheet steel form for car body. Features such as the ability for extensive cold-forming and production of defect-free surface are desirable. Nowadays, ultra-low carbon steels were developed for better deep drawability. This type of steels contain very little carbon (0.0026%) with added Nb and Ti to enhance deep drawability [DEARDO 1995].

In mass production under continuous cooling conditions, the products usually contain mixed microstructures. It has been reported that for the very low carbon steels, the toughness of the mainly massive ferrite (or so called quasi-polygonal ferrite) was superior to that of the bainitic ferrite [KATSUMATA et al 1994]. Excellent toughness of massive ferrite (as compare with martensite) was also reported by ROBERTS [1970] in Fe-5Mn alloy, figure 2.21.

In a steel with low carbon content (0.01C, 1Mn, 0.2Si, 0.1Nb), a nickel addition was found to improved the tensile property significantly due to the high dislocation density and fine ferritic substructure, while ductility remained over 20%, and providing excellent toughness value at low temperatures [LEE et al 1995].

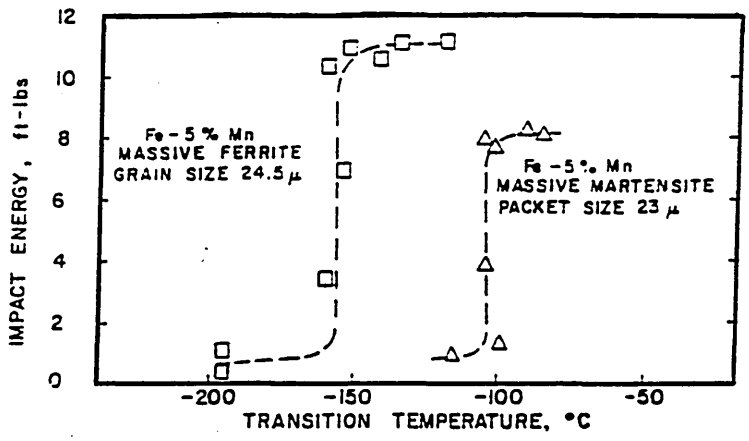

Fig. 2.21. Impact transition curves of massive ferrite and lath martensite in Fe-5Mn alloy [ROBERTS 1970].

2.7.1. Nickel in Steels

In fact, the addition of nickel to steels to improve toughness has long been practised. Nickel as an austenite stabiliser, suppresses the transformation to lower temperatures, grain growth is minimised, and as a consequence, fine ferrite grains or small sized packets lath martensite can be produced. Toughness is then improved and DBTT lowered.

For iron-nickel alloy with low nickel addition, FLOREEN et al [1971] discovered that the nickel addition increases the cleavage strength of ferrite lattice. Similar to JOLLEY [1968], it was believed that nickel addition changes the slip characteristic by increasing the ability of cross slip of dislocation at low temperatures in Fe-Ni alloys.

GERBERICH et al [1980] also found that Ni addition (up to 4 at.%) increased the cleavage fracture stress and the effective fracture surface energy of iron, whereas Si addition showed reverse effect. The fracture surfaces showed greater amount of twinned related cleavage and intergranular fracture in the Fe-Ni alloys whilst {100} cleavage predominant in Fe-Si alloys by impact testing at 77K.

9% Nickel -lean carbon steels are widely used for cryogenic applications. The toughness property of commercial nickel steels have been studied extensively, particularly in a series of articles published by MORRIS , KIM and co-workers [JIN et al 1975a, 1975b; HWANG et al 1975; SYN et al 1976; KIM and MORRIS 1980, 1981; KIM et al 1983, 1984]. The heat-treated nickel steels consist of tempered martensite, martensite and reverted austenite. The presence of reverted austenite is an important element in achieving excellent toughness. This led to a conclusion that the excellent toughness of nickel steels is due to grain refinement and the composite effect of such complex structure [KIM et al 1984].

Fe-Mn shows similar transformation behaviour as Fe-Ni alloys. This has led to the attempt in replacing Ni with Mn in steels for low temperature application so that toughness is preserved while cost of production is reduced. However, results show that Mn-bearing steels can not achieve as excellent toughness property as nickel steels, mainly because Fe-Mn alloys are susceptible to intergranular fracture [BOLTON 1970; BOLTON et al 1971; HWANG and MORRIS 1979, 1980] due to the segregation of Mn, N and P to prior austenite grain boundaries [NASIM 1979; BRAMHALL 1989].

Until recently, nickel remains as a superior additive to steels in order to improve toughness.

3. Experimental Procedures

3.1. Materials Preparation

Iron-nickel and iron-nickel-carbon alloys were made by British Steel plc., Swinden Technology Centre, Rotherham. These alloys were vacuum cast into 26 kg ingots of size 75 x 100 x ~350 mm, using Japanese electrolytic iron, INCO nickel shot, pure graphite, Fison's ferrosulphur and Chinese electrolytic manganese. Pipes on top of each ingot were cut off. These ingots were then upset forged into flat bar with dimension of 28 x 60 mm in cross section with different length for each bar (about 500 mm) at British Steel Engineering Steels, Stockbridge.

The basic chemical composition (weight %) analysis and the code for each cast is listed in table 3.1 below, given by Swinden Technology Centre.

Table 3.1. Chemical analysis of each ingot in as-cast condition.

Code	Weight %			
	Ni	C	S	Mn
VS2239A	3.40	0.002	0.002	0.02
VS2240B	3.49	0.120	0.003	0.03
VS2241A	8.88	0.004	0.001	0.02
VS2241B	8.85	0.085	0.002	0.02

3.1.1. Homogenisation Treatment

Before these materials were used for experiments, they had to be homogenised first to eliminate the segregation of alloying element distribution and to anneal the microstructural deformation caused by metal forming. An excessive high austenitisation temperature and long times holding are essential on account of the sluggish rate of nickel atom diffusion in austenite. MASSALSKI et al [1975] reported times of 20 days at 1100°C were required for complete homogenisation. Arrhenius calculation (below)

shows that 4 days at 1200°C would give equivalent homogenisation and this treatment was used in the present work.

The following calculation is based on Smithells' data [BRANDES and BROOK 1992] for diffusion of Ni^{63} in Fe-9.7 wt% Ni :

Diffusion coefficient, D,

$$D = D_0 \exp(-Q/RT) \qquad \text{where } D_0 = 1.32 \times 10^{-5}\ m^2.s^{-1}$$

$$Q = 267.5\ kJ.mol^{-1}$$

$$R = 8.314\ J.mol^{-1}.K^{-1}$$

and diffusion distance, λ, is given by:-

$$\lambda \sim \sqrt{Dt} \qquad \text{where } t = \text{time (seconds)}$$

From Massalski's work ;

$$T_1 = 1100°C\ (1373K) \qquad t_1 = 20\ \text{days}$$

so, $$D_1 = 1.32 \times 10^{-5} \exp(-267.5 \times 10^3 / 8.314 \times 1373)$$

$$= 8.778 \times 10^{-16}\ m^2.s^{-1}$$

and $$\lambda = 38.9\ \mu m$$

For austenitisation temperature of 1200°C.;

$$T_2 = 1200°C\ (1473K) \qquad t_2 = ?$$

so, $$D_2 = 1.32 \times 10^{-5} \exp(-267.5 \times 10^3 / 8.314 \times 1473)$$

$$= 4.308 \times 10^{-15}\ m^2.s^{-1}$$

as; $$\sqrt{D_1 t_1} = \sqrt{D_2 t_2} \qquad \text{i.e.} \quad D_1 t_1 = D_2 t_2$$

therefore, $$t_2 = 8.778 \times 10^{-16} \times 20 / 4.038 \times 10^{-15}$$

$$= 4.07\ \text{days.}$$

∴ Homogenise at 1200°C for 4 days.

For homogenisation treatment, a block about 60 mm in length was cut from each bar. The oxide layer of the block was removed by surface grinding, and then put into a cast iron box. A piece of fire brick was laid beneath the bottom of the block to avoid direct contact with the box. It was then covered up and sealed with fire clay, and inserted into a preheated furnace. Before sealing, titanium chips were spread in the box to absorb the residual oxygen and nitrogen.

After 4 days at 1200°C, the cast iron box was taken out from the furnace. Although 1200°C was rather high for cast iron, the box was still intact. The cast iron box was uncovered while still red hot, and allowed to cool in free air.

After being homogenised, a small section was cut out for chemical analysis, tested by British Steel Engineering Steels, Stockbridge. The result obtained, table 3.2, showed that this method of homogenisation process causes severe decarburisation, as can be seen from alloy VS2240B and VS2241B. Analyses of VS2241B1 and VS2241B2 were obtained from different sections in the same piece, showing different carbon content.

For the extremely low carbon content alloys, VS2239A and VS2241A, this homogenisation method seems to be satisfactory. The chemical analysis in the as-cast and homogenised condition were consistent in these alloys. Hence the homogenised alloy of Fe-3.5Ni (VS2239A) and Fe-9Ni (VS2241A) were then used to carry out the continuous cooling transformation experiments.

Following the decarburisation problems encountered in homogenisation treatment, a different method was thought to be necessary to improve the homogenisation treatment. For the materials used in subsequent experiments, another block was cut out from the upset forged bar, sectioned into the dimension of 25 x 35 x 55 mm, with the scaled layer removed, enabling the homogenisation work to be carried out in a tube furnace. The parameters of 1200°C austenitising temperature for 4 days were again selected. Argon gas was allowed to flow through the tube continuously to create a protective atmosphere during heat-treatment. Homogenised block was then taken out from the furnace and air-cooled. Judging from the oxide layer of the homogenised block, this later method provided a better protective environment than the sealed cast iron box.

Table 3.2. Full scale chemical analysis after homogenisation. Figures in brackets give the values before homogenisation.

	Weight %								
Alloy	Ni	C	Si	Mn	P	S	Cr	N	O
VS2239A	3.47 (3.40)	0.002 (0.002)	0.020	0.03	0.002	0.002	0.02	0.018	0.0070
VS2240B	3.46 (3.49)	0.016 (0.120)	0.020	0.03	0.002	0.002	0.02	0.017	0.0043
VS2241A	9.14 (8.88)	0.002 (0.004)	0.020	0.03	0.002	0.002	0.02	0.008	0.0065
Vs2241B1	9.20 (8.85)	0.012 (0.085)	0.020	0.03	0.002	0.002	0.02	0.014	0.0045
VS2241B2	9.00 (8.85)	0.006 (0.085)	<0.02	<0.03	0.002	0.003	<0.02	0.015	0.0053

3.2. Continuous Cooling Transformation Experiment

3.2.1. Specimen Preparation

Specimens with size of 6 x 12 x 24 mm were prepared. K-type NiCr-NiAl thermocouples of size 1mm and 1.5 mm diameter were used. Thermocouples were attached to each of the specimen by drilling a hole of 5 mm deep from the thin section, as shown by figure 3.1. One half was to be cut and machined into 3 mm diameter rod for TEM inspection, and the other half reserved for metallography purposes. The thermocouples were reused by exposing the end junctions and welding them back.

These specimens were coated with Berkatekt*, held in furnace at 1000°C for 20 minutes followed by ice brine quenched (IBQ), water quenched (WQ), oil quenched (OQ), air cooled (AC) or furnace cooled (FC).

*Berkatekt is a proprietary refractory coating for resisting oxidation and decarburisation available from Acheson Colloids Co., Prince Rock, Plymouth PL4 0SP.

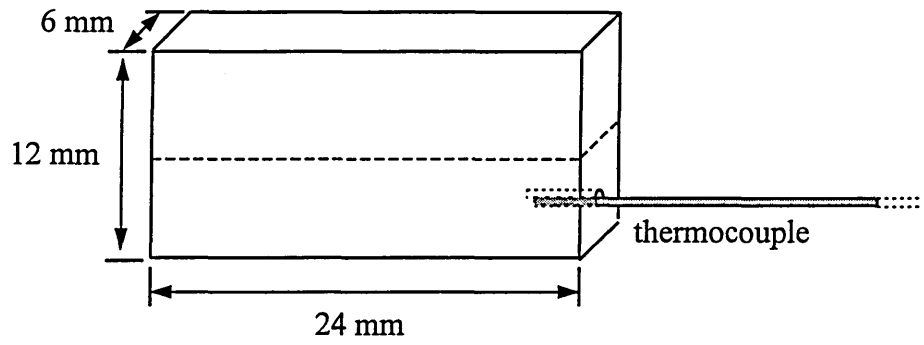

Fig. 3.1. Specimen used for continuous cooling experiment.

3.2.2. Thermal Arrest and Cooling Rate Determination

Thermocouples were connected to a chart recorder to monitor the heating and cooling transformation of $\alpha \rightarrow \gamma$ and $\gamma \rightarrow \alpha$ respectively. Transition points from the heating and cooling curves (thermal arrest) corresponding to transformation start temperatures were detected. It was thought the thermal arrest results at different temperatures with different cooling condition meant that different types of transformation mechanism had taken place.

For high cooling rates (WQ and IBQ), the maximum travel speed of chart recorder was not fast enough to plot the cooling curve, nor was the response time of the recorded full scale deflection (f.s.d.) sufficiently fast to record the thermal arrest. A transition point was not detected from every test. Subsequently, an oscilloscope was installed to replace the chart recorder.

Neither the chart recorder nor oscilloscope were ideal in terms of arresting transformation start temperature for the fast quenching experiments. Nevertheless, a few successful cases were obtained and careful analyses was carried out on these graphs to find out if the arrested points were fruitful and reasonable in relation to previous work (GOODENOW and HEHEMANN [1965] and WILSON [1984]).

3.3. Isothermal Transformation Experiment

Specimens with size 5 x 5 x 35 mm were cut out from the bar for this experiment. A hole of about 5 mm deep was drilled at one end of each specimen, a high temperature resistance chromel-nickel wire was attached for handling purposes. For some of the specimens, a thermocouple was attached instead.

Initially, the specimens were coated with Berkatekt, austenitised at 1000°C for 20 minutes, and then transferring into salt bath for isothermal transformation at set temperatures and times, followed by an iced brine quenched. The transformed microstructures were found to be too fine to be inspected under the optical microscope.

Subsequently, it was decided to choose the austenitisation parameters of 20 minutes at 1150°C, producing a lager austenite grain size, and hence facilitate the transformed microstructures to be distinguished under optical microscope. With such a high austenitising temperature, Berkatekt failed to prevent the specimens from oxidation. Therefore, Berkatekt coating method was abandoned, replaced by blowing of argon gas into the furnace during austenitising period to minimise specimens oxidation.

The isothermal transformation took place using two types of salts:-

1. Durferrit GS 430 with the working temperature range from 495°C to 700°C, and
2. Durferrit AS 140 with the working temperature range from 160°C to 550°C.

The salt bath temperature could be controlled with an accuracy of ±5°C. The cooling curves of some of the isothermal transformations were recorded by using the specimens attached to thermocouples. The resulting graphs allowed the effectiveness of the quenching to be observed as well as allowing the stability of the isothermal holding temperature to be monitored.

3.4. Dilatometry Experiment

Dilatometry was carried out using MMC Quenching Dilatometer at British Steel plc., Swinden Technology Centre.

10 mm x 5 mm diameter cylinders were prepared. The specimen was heated in vacuum condition by induction heating. The temperature of the specimen was monitored by spot welding a platinum-platinum/10% rhodium thermocouple to the surface. Change in length upon transformation was monitored by push rod connected to linear variable differential transducer (LVDT).

3.5. Metallographic Work

3.5.1. Polished and Etched Surface

Heat treated specimens were ground by emery paper up to 1200 grid, and fine-polished with diamond paste down to 1μm, followed by etching in nital. Optical microscopy inspection allows magnification up to 1000X. Higher magnification were obtained using the scanning electron microscopy (SEM JEOL 840A). The SEM is useful not only in terms of higher magnification, but also the greater depth of field, so that the etched surface is revealed clearer. The advantages of SEM as compared with the optical microscope is particularly significant in this work due to the fact that only ferrite phase (with different morphologies) is found, in iron-nickel alloys.

3.5.2. Surface Relief Inspection

Specimen of size 6 x 12 x 20 mm was prepared with one side fine-polished down to 1μm. Sample was placed in a silica tube, sealed off under vacuum condition (< 20 torr). Before sealing, gas argon was pumped into silica tubes followed by evacuation at least twice in order to keep the residual oxygen at minimum level.

Sealed sample was placed into furnace at 1000°C for 20 minutes followed by furnace cooling. The capsule was broken only when the heat treated sample had cooled down to room temperature. Any change on the fine-polished surface was inspected by optical microscope or SEM.

3.5.3. Thin Foil Transmission Electron Microscopy

Discs were cut out from 3 mm diameter cylinders using silicon carbide disc wheel. The discs were ground by emery paper up to 1200 grid, gave final thickness of 80 - 100 μm. Electropolishing using twinned jet polisher was conducted for further thinning with 5 % perchloric acid in methanol. Electropolishing was carried out with the conditions of 30 - 35 V, 100 - 200 mA with the solution temperature maintained at subzero temperatures around -40°C.

Transmission electron microscopy (TEM) was performed using Philips CM20 instrument operated at 200 kV. This machine was equipped with both a scanning transmission and transmission facility with energy dispersive X-Ray (EDX) analysis system attached.

3.6. Microanalysis by Electron Microscopy

3.6.1. TEM-EDX Semi-Quantitative Analysis

PHILIPS CM20 TEM machine is equipped with EDAX PV 9900 System, PMTHIN software allowing semi-quantitative analysis to be carried out on nanometer scale. The foil in the specimen holder needs to be tilted 25° - 30° to the EDX detector when performing the microanalysis with TEM mode.

TEM-EDX mode of operation enabled the X-Ray analysis of a spot on an area of interest without switching to STEM mode. Thus once an area of interest is located by TEM imaging, X-Ray analysis can be carried out simply by reducing the spot size.

A small spot size with small current means only a small number of X-rays can be generated, and the collected X-rays would be meaningless for analysis. Eventually, nominal probe size of 20 nm was selected to carry out the spot analysis, with a counting time of 50 seconds.

The initial emphasis of the work was to monitor the relative change in nickel content across the grains. Therefore no correction was made to calculate the actual composition. The foil thickness, which was unknown, is required to calculate the actual composition.

3.6.2. Microanalysis by FEG-STEM

In order to achieve a better resolution with a smaller spot size, analysis is best carried out by using the dedicated field emission gunned scanning transmission electron microscopy (FEG-STEM). It produces high brightness, with high current in small probes, provides the best spatial resolution for analysis in the EM family [GOODHEW and HUMPHREYS 1988; BISCHOFF and RÜHLE 1990; BENTLEY et al 1991].

A Vacuum Generators VG HB601 scanning transmission electron microscopy equipped with field emission gun (FEG-STEM) was used to carry out microanalysis. This part of the work was carried out at Liverpool University.

This instrument is attached with a windowless LINK X-Ray detector. Microanalysis work was based on a probe size of 2 nm with an applied voltage of 100 kV. Results were analysed using a ZAF (atomic number(Z), absorption (A) and fluorescence(F)) corrected programme package.

3.7. Hardness Measurement

Vickers hardness measurements were carried out using 20 kg load. Specimens were cut in cross-sectional, allowing the hardness measurement on the centre and the surface of the specimens. For microhardness testing, 50 g load was used.

3.8. Charpy Impact Testing

To prepare Charpy specimens, an homogenised block was reheated to 1100°C and hot rolled to 7 mm plate at Leeds University. The scaled layer was then removed, coated with Berkatekt and heat-treated to produce the required microstructures. Heat-treated plates were subsequently machined into sub-size (10 x 5 x 55 mm) V-notch Charpy specimens. Charpy specimens were prepared in such a way that the longitudinal section was parallel with the rolling direction, and V-notch perpendicular to the rolling plane.

Impact testing was carried out using Avery-Denison Impact Testing Machine, with an impact velocity of 5.24 $m.s^{-1}$, according to EN 10 045-1 : 1990 specification. For low temperature testing, specimens were immersed in the cooling medium for at least 10 minutes and broken within 10 seconds of the time of removal from the medium. Cooling medium was prepared from mixed solutions as listed below:

0°C to -10°C	ice + NaCl solution
-10°C to -50°C	solid CO_2 + methanol
-50°C to -78°C	solid CO_2 + acetone
-78°C to -129°C	liquid nitrogen + low boiling point petroleum ether
-129°C to -159°C	liquid nitrogen + iso-pentane
-196°C	liquid nitrogen

Broken specimens were warmed in alcohol, dried and stored in desiccator for subsequent examination of fracture surface in the SEM.

4. Experimental Results

4.1. Continuous Cooling Transformation of Fe-9Ni Alloy

4.1.1. Determination of Cooling Rate and Thermal Arrest Temperatures

Several experiments were repeated for each of the cooling methods. The average cooling rate was calculated from the cooling curves with temperature range between 900°C - 300°C. Thermal arrest results, i.e. the transition points of the cooling curves, enabled the transformation start temperatures to be identified. After careful calculation, arrested temperatures measured from the graphs are thought to be accurate within ±5°C.

Only those graphs obtained at slow cooling rates were able to give consistent thermal arrest results. Most of the time, cooling curves plotted from water quenching and iced brine quenching experiments did not show thermal arrest, neither by using a chart recorder nor an oscilloscope. Thermal arrest results are shown in table 4.1, question marks for the WQ and IBQ indicate that these results are difficult to reproduce with current equipment. The cooling curves for different cooling methods are shown in figure 4.1(a) - (e).

Table 4.1. Continuous cooling transformation results for VS2241A, Fe-9Ni alloy.

Cooling Medium	Cooling Rate	Transformation Start Temp.
Furnace cool (FC)	0.25 $K.s^{-1}$	~555°C
Air cool (AC)	4 $K.s^{-1}$	~536°C
Oil quench (OQ)	70 $K.s^{-1}$	~482°C
Water quench (WQ)	210 $K.s^{-1}$	~486°C (?)
Iced brine quench (IBQ)	420 $K.s^{-1}$	~384°C (?)

Although for most of the thermal analysis specimens were austenitised for 20 minutes at 1000°C, the result for iced brine quenching in table 4.1 (shown in figure 4.1(e)) was obtained by austenitising for 20 minutes at 1150°C.

4.1.2. Morphology of Slow Cooled Structures

The products of FC and AC experiments showed similar structure. The specimens were predominated by irregular ferrite grains with a wide range of sizes. The determination of grain size was difficult as grain boundaries often showed uneven etching and were somewhat discontinuous. The existence of substructures and sub-boundaries inside ferrite grains were observed in certain grains. Optical micrograph of figure 4.2 was taken from the centre of the cross-sectional of a FC specimen. The chaotic region as indicated by arrow , α_W, might probably be the recovered Widmanstätten ferrite.

A specimen was put in a sealed evacuated silica capsule and allowed to undergo furnace cooling. Ferrite grains boundaries were often found to grow across the γ grains - a typical feature of massive ferrite transformation. These ferrite grains do not produce surface relief but surface rumpling. However, in certain area, laths were found as evident by surface relief. Figure 4.3 shows a series of optical micrographs taken from this area. SEM picture of figure 4.4(a) and 4.4(b), taken from different specimens with the same treatment, shows a clearer view of the surface relief. These laths were found only in particular γ grains significantly larger than the average grain size. Ferrite grains formed at the prior γ grain boundaries and grew towards the centre of the γ grain. As the cooling continued, grain boundary ferrite transformation stopped and was replaced by Widmanstätten ferrite. Widmanstätten laths appeared to be nucleated from ferrite on the austenite grain boundaries, and continue to grow towards the centre of the austenite grain until they impinged with the ferrite grain or laths that grew from the opposite side. In the case of figure 4.4(b), the growth of Widmanstätten laths were terminated by the prior austenite grain boundaries. Note the surface relief of Widmanstätten laths are in "tent" shape, similar to that reported in Fe-0.003C alloy by KINSMAN, RICHMAN and VERHOEVEN [1976] and Fe-0.5C alloy by HALL and AARONSON [1994] .

Ferrite grain formation at austenite grain corner was also found as presented in figure 4.5. Note the planar (rather than curved) type of boundaries surrounding the ferrite grain - a feature of equiaxed / massive ferrite formation observed by OWEN and WILSON [1965] in figure 2.14(b).

A TEM montage of ferrite grains is presented in figure 4.6. The dislocation density in ferrite grains is generally high but unevenly distributed. Grain boundaries are of planar or undulating type.

Figure 4.7 presents a particular ferrite grain which clearly shows the presence of sub-boundaries form inside the grain. Such an irregular ferrite grain shows the features of ragged grain boundaries and contains substructures or sub-boundaries, often refers as massive ferrite [ROBERTS 1970] or quasi-polygonal ferrite (α_q) [ARAKI et al 1992; SHIBATA and ASAKURA 1995].

The laths structure, when revealed under TEM, consisted of a group of broad, and uneven sizes of individual lath, figure 4.8. The lath boundaries are somewhat discontinuous and "steps" can be identified. This group of laths, however, only gave a single electron diffraction pattern, implying that they were in fact separated by low angle boundaries.

In addition to the ferrite morphologies, M-A constituent was also identified in both FC and AC specimens, figure 4.9.

BODNER and HANSEN [1994] worked on Fe-0.2C-1.1Mn steel and found that as the austenite grain size increases, the volume fraction of Widmanstätten ferrite formation increases. Inspired by their observation, one specimen was finely polished on one surface, kept in an evacuated silica capsule and subjected to air cooling after austenitised for 4 days at 1200°C to produce excessive large grains. As a result, large ferrite grains and very long laths were observed with larger area fraction for the laths structure. These packets of laths remained identifiable even after polished and etched, some of the laths were observed to cross prior austenite grain boundaries, figure 4.10. In this case, it was not sure if the thermal grooving as shown on the prepolished surface represented the real prior austenite grain boundaries. It could be that thermal grooving formed at the initial stage of austenitisation and remained while the austenite grains were still growing. Nevertheless, we can see that the ferrite grains are much more irregular due to the interaction with the laths structure, resembling the mix structures found by MASSALKSI et al [1975].

4.1.3. Morphology of Quenched Structures

Oil quenched and water quenched specimens produced quite similar microstructure, except few massive ferrite grains were found in oil quenched specimen. Planar boundaries of ferrite packets are clearly revealed by nital etched, as shown in figures 4.11(a) and 4.12(a). Nital attacks the boundaries of the laths packets, and also possibly cross-section of the individual lath, showing as holes on the etched surface. Picral etched is better in revealing prior austenite grains boundaries as well as the laths that lie parallel with the surface, figures 4.11(b) and 4.12(b).

TEM pictures, shows the different lath formed in oil quenched and water quenched specimens. Perfect lath structure is formed in the water quench specimen, figure 4.12(c). Laths structure that found in oil quenched specimen are comparatively irregular and contain sub-units that break down the laths into segments, figure 4.11(c).

Packets and blocks of parallel laths within a prior austenite grain were produced by iced brine quenching. Such features are typified by lath martensite structure, see figure 4.13.

4.1.4. Slow Cooled Bainitic Ferrite

MIRZAYEV et al [1973] reported that critical cooling rate for martensitic transformation could be lowered by producing larger austenite grain size. Since the current equipment performed satisfactory on slow cooling, martensitic transformation by air cooled was therefore attempted. A specimen was austenitised at 1200°C for 24 hours in tube furnace (in gas argon atmosphere), followed by air-cooled. A thermal arrest at 471°C was identified, figure 4.14. Under optical microscopy, the transformed product resembled bainitic structure.

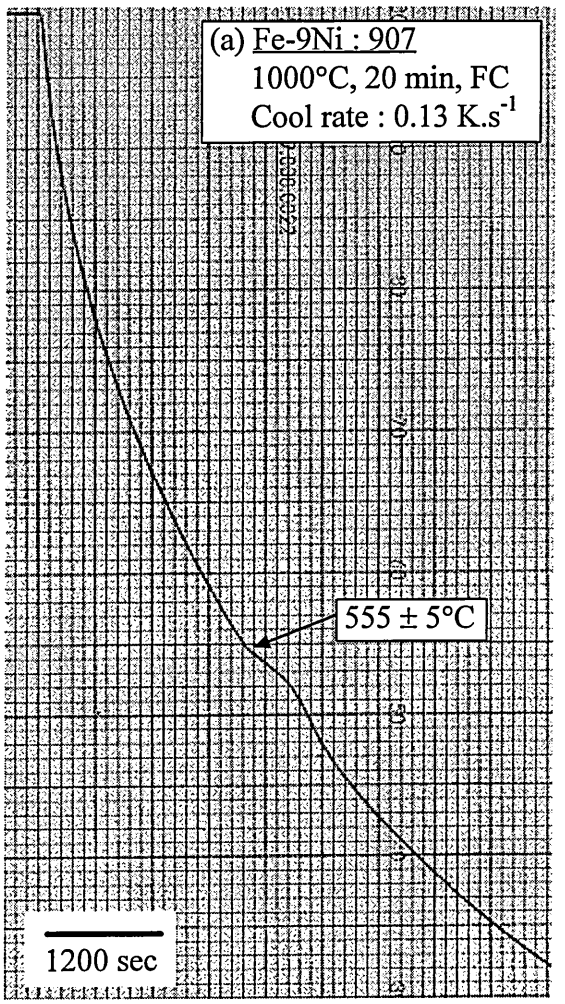

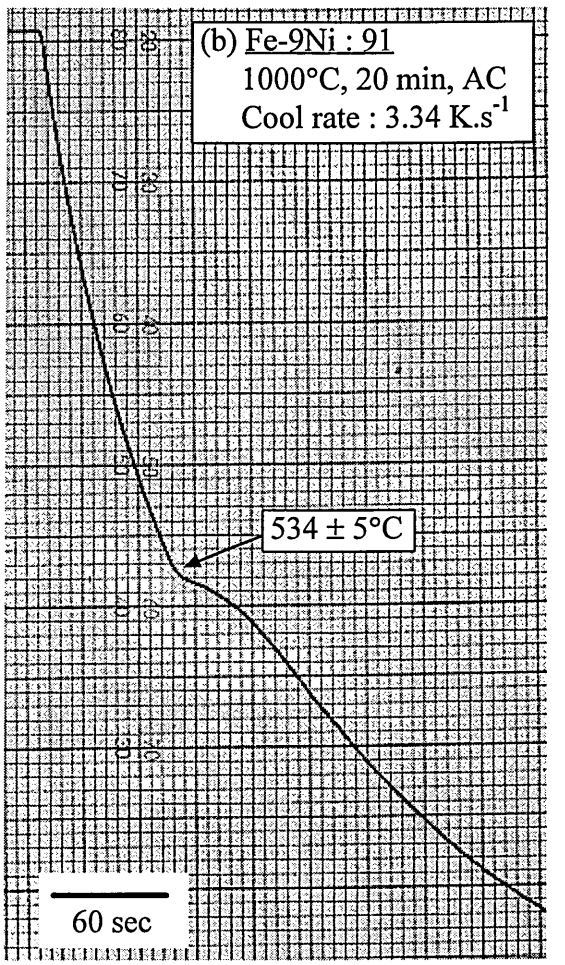

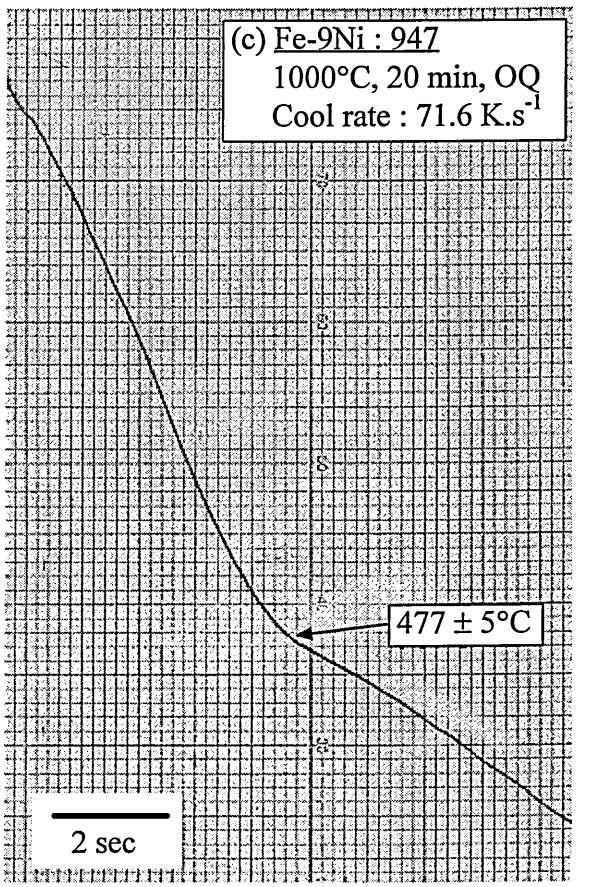

Fig. 4.1. Thermal arrest diagrams of VS2241A, Fe-9Ni alloy subjected to different cooling rates;
(a) furnace cool (FC),
(b) air cool (AC), and
(c) oil quench (OQ).

Continue:

Fig. 4.1. Thermal arrest diagrams of VS2241A, Fe-9Ni alloy subjected to different cooling rates;
(d) water quench (WQ), and
(e) iced brine quench (IBQ).

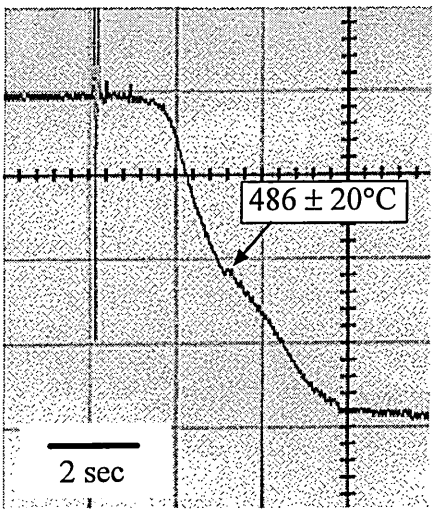

(d) Fe-9Ni : 967
1000°C, 20 min, WQ
Cool rate : 260 $K.s^{-1}$

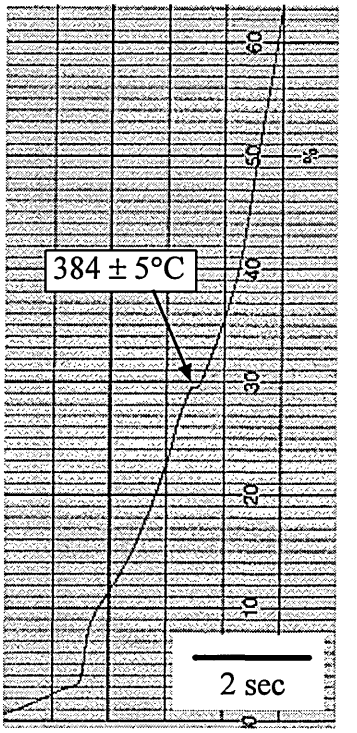

(e) Fe-9Ni : 12
1150°C, 20 min, IBQ
Cool rate : 607 $K. s^{-1}$

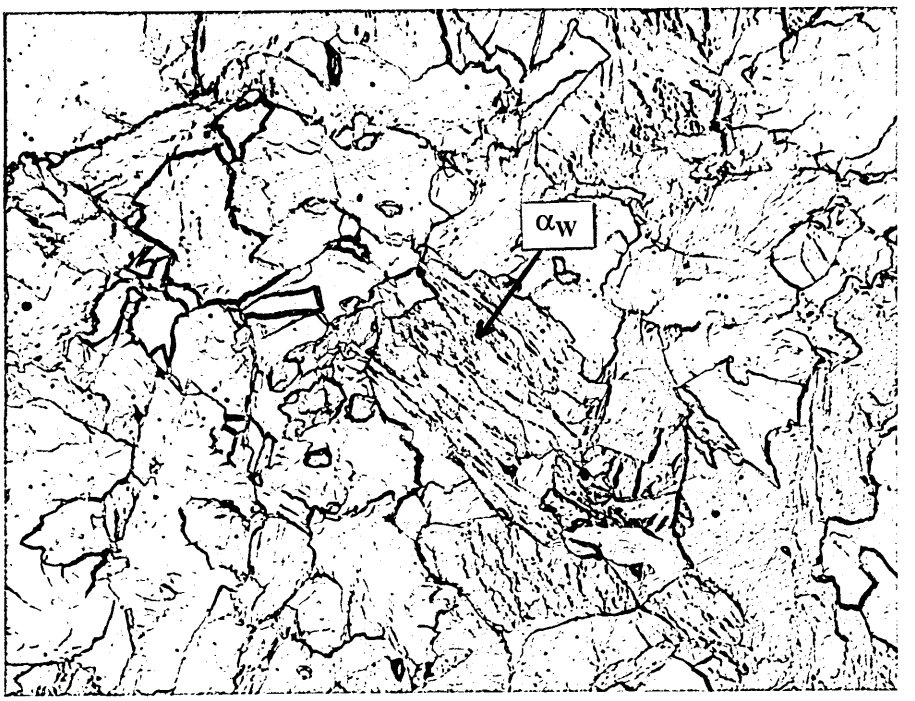

Fig. 4.2. Optical micrograph of furnace cooled microstructures in Fe-9Ni alloy.

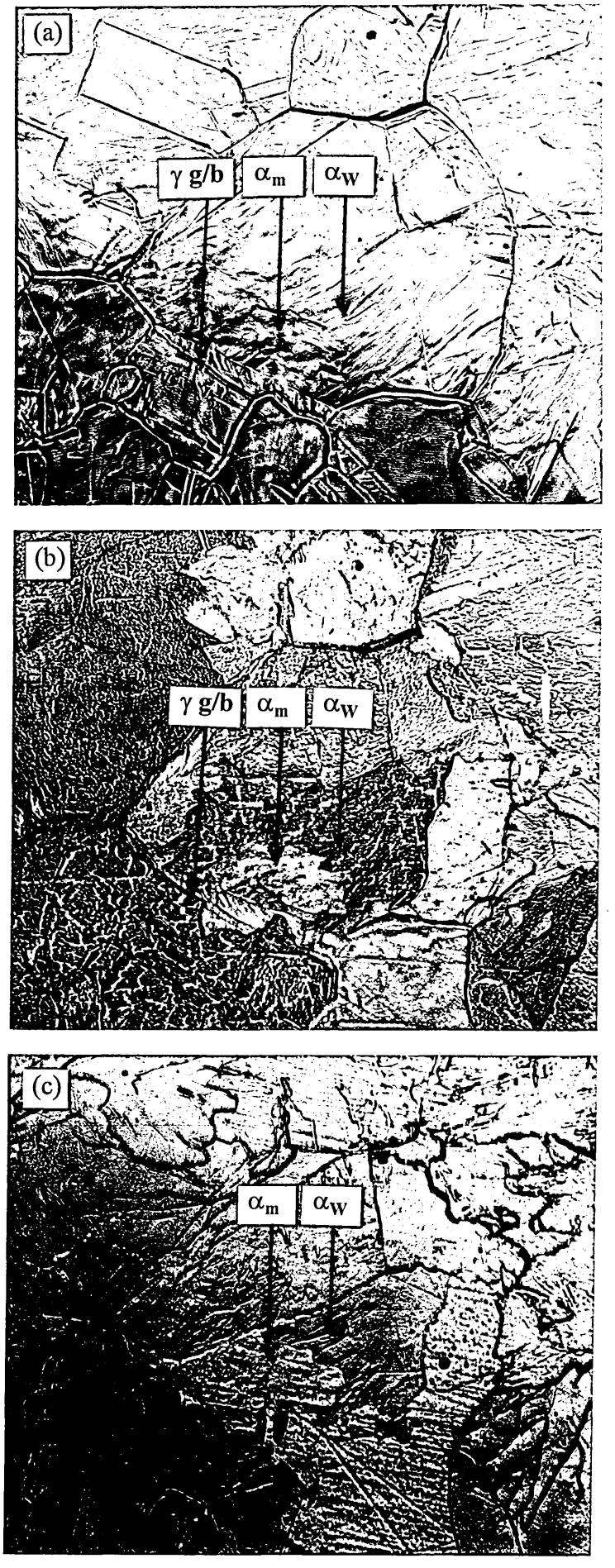

Fig. 4.3. Optical micrographs of Fe-9Ni alloy, showing the transformed structures on a fine polished, evacuated silica capsule sealed specimen, austenitised at 1000°C for 20 minutes followed by furnace cooled;

(a) prepolished,
(b) prepolised and 1/2 % nital etched,
(c) polished and 2 % nital etched.

γ g/b = austenite grain boundary
α_m = massive ferrite
α_W = Widmanstätten ferrite

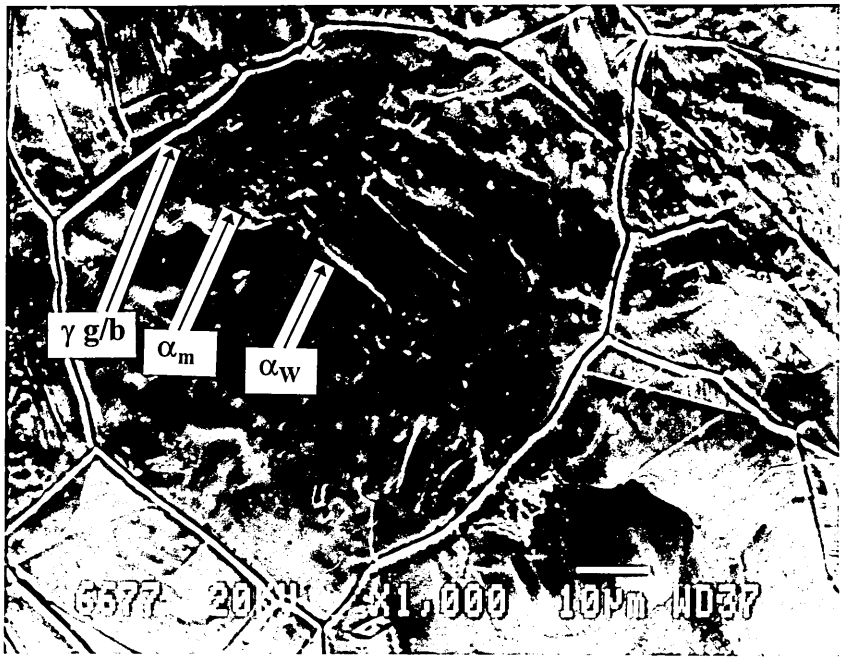

(a)

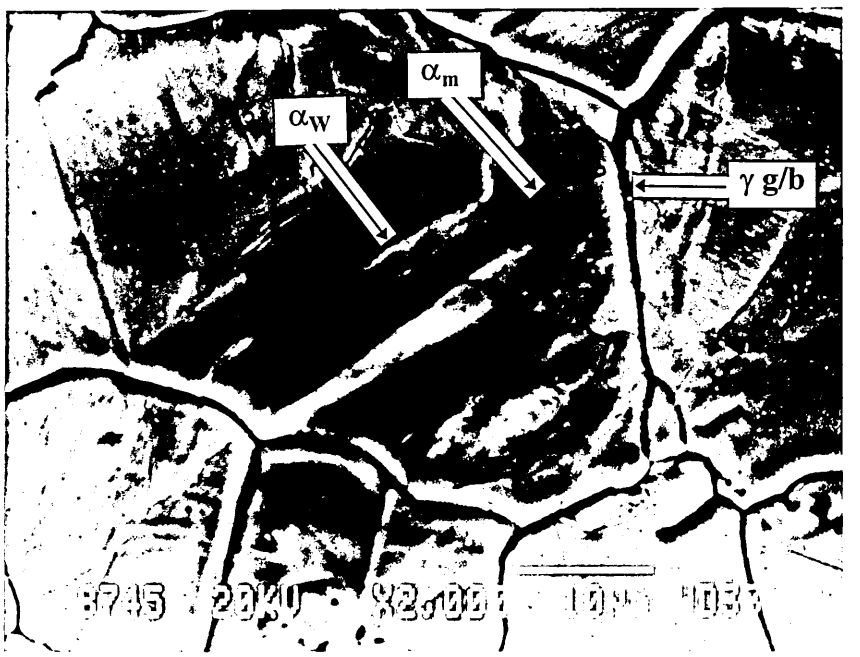

(b)

Fig. 4.4. SEM pictures showing the surface relief of Widmanstätten laths formation in furnace cooled Fe-9Ni alloy. Laths formed at the ferrite grain boundaries and grew towards the centre of the austenite grain (a), and (b) terminated by the austenite grain boundary.

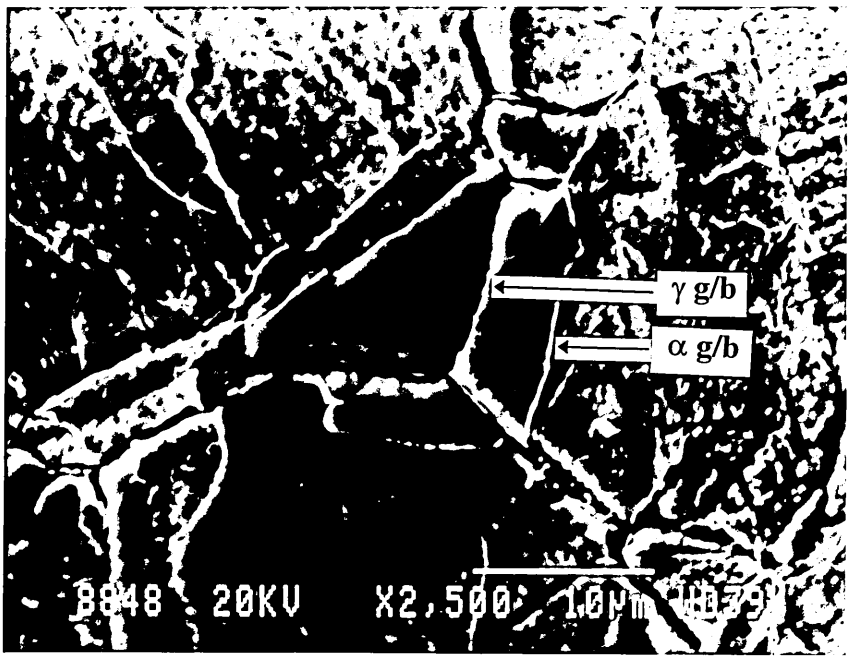

Fig. 4.5. Ferrite grain formation at the austenite grain corner on the surface of a furnace cooled Fe-9Ni alloy. Austenite grain boundaries (γ g/b) revealed by thermal grooving , ferrite grain boundaries (α g/b) revealed by nital etching.

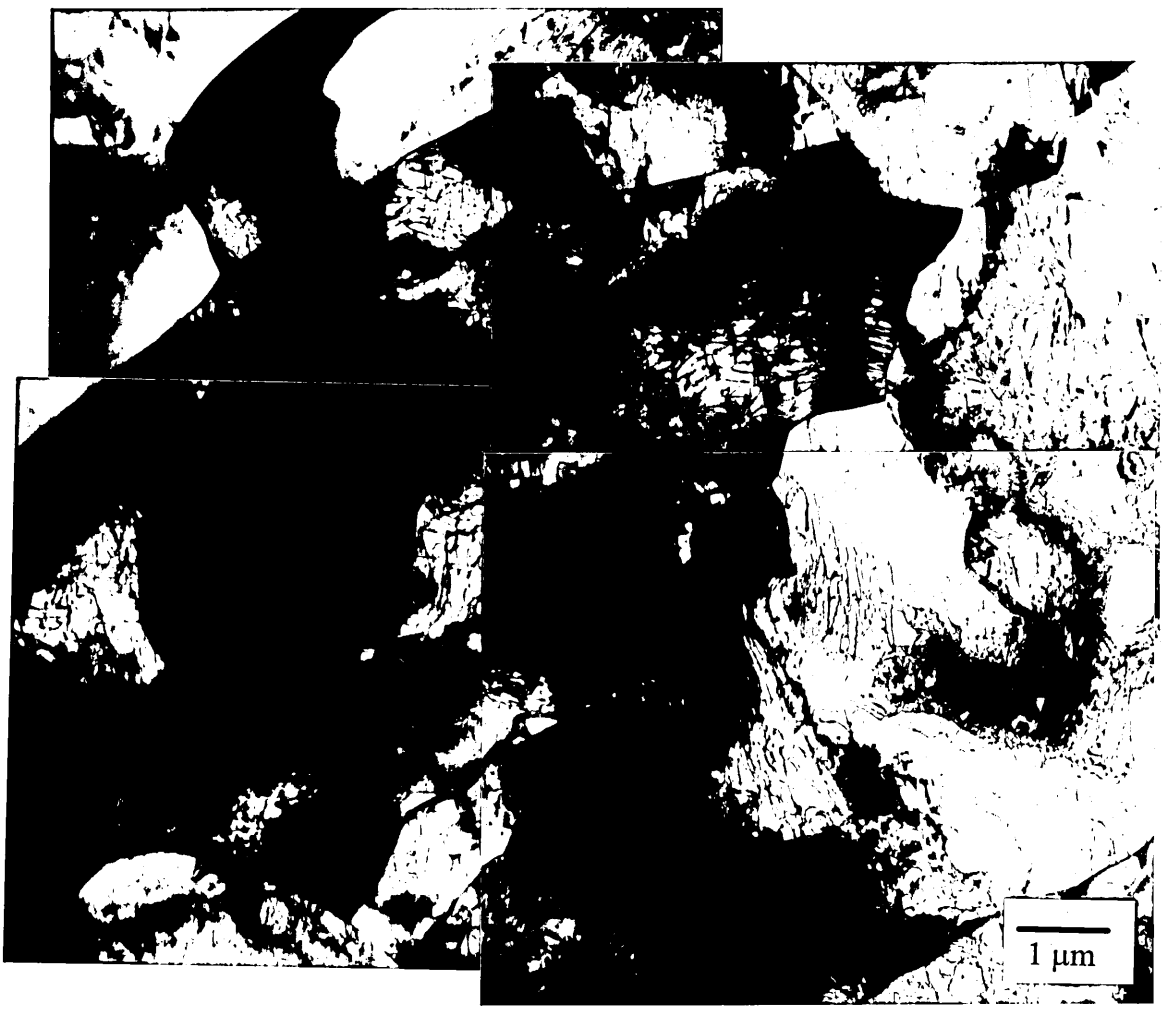

Fig. 4.6. TEM montage of ferrite grains formed in a furnace cooled Fe-9Ni alloy.

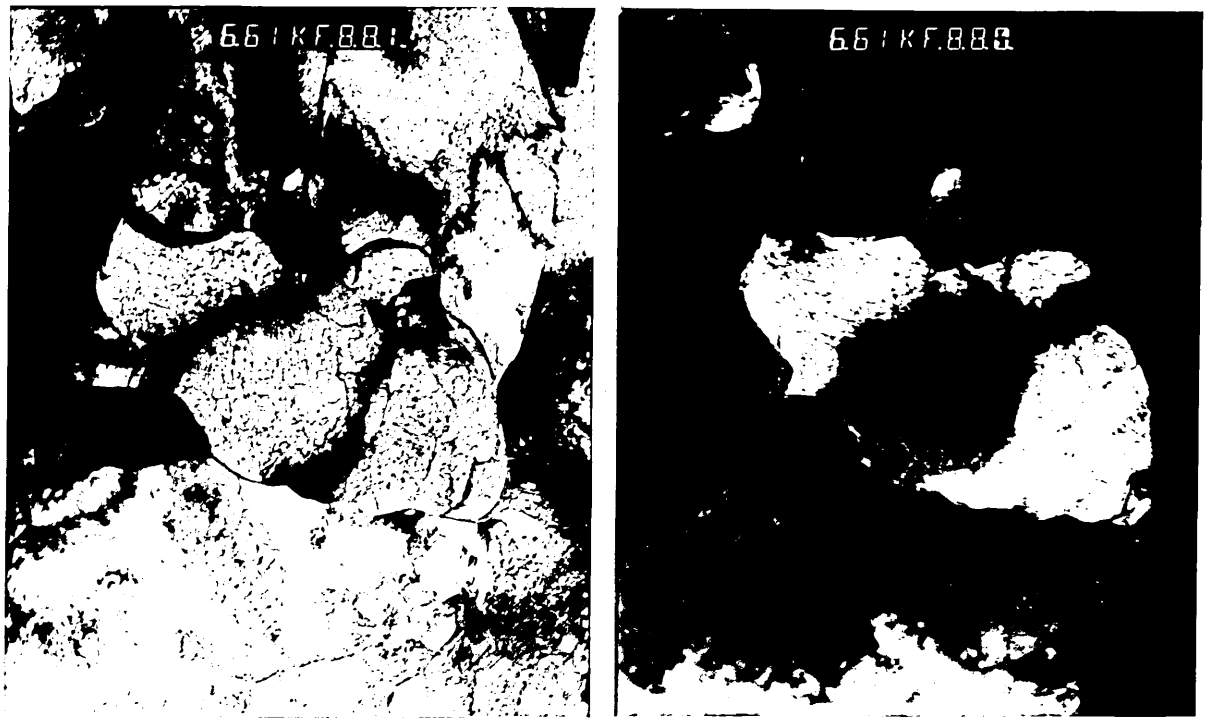

Fig. 4.7. TEM picture of a massive ferrite grain from furnace cooled Fe-9Ni alloy, shows irregular grain boundaries and contains sub-boundaries / substructures inside grain;
(a) bright field,
(b) dark field, and
(c) electron diffraction pattern.

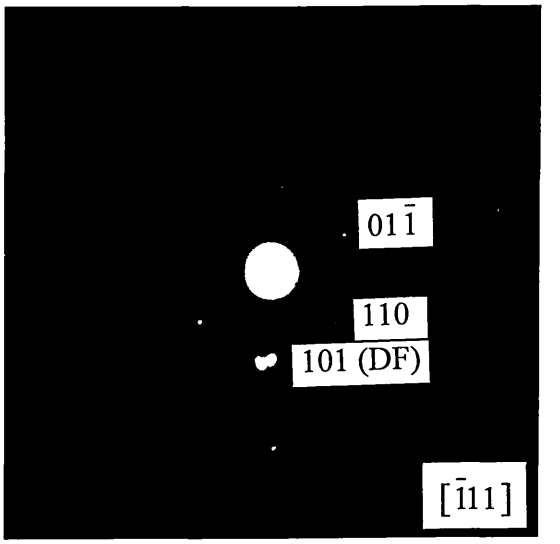

(c)

(a)

2μm

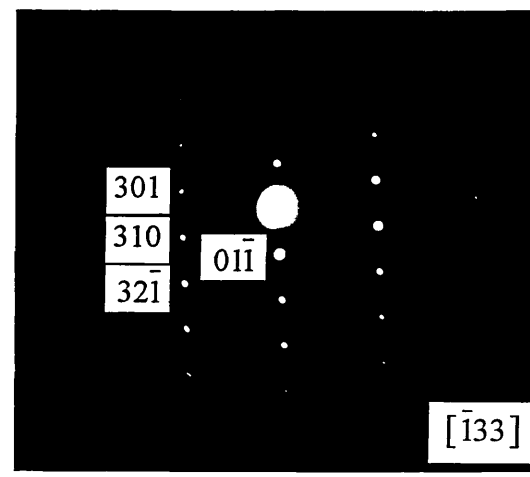

(b)

Fig. 4.8. TEM picture of Widmanstätten laths (a), and electron diffraction pattern (b), from furnace cooled Fe-9Ni alloy.

Fig. 4.9. M-A constituent in furnace cooled Fe-9Ni alloy.

(a)

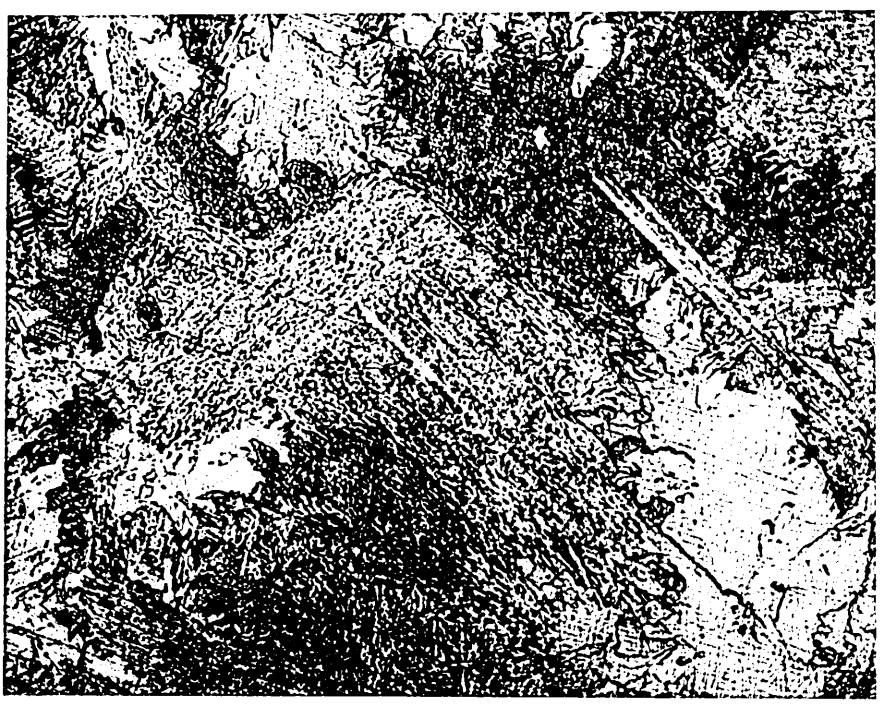

(b)

100 μm

Fig. 4.10. Optical micrographs of the microstructure from Fe-9Ni alloy, austenitised at 1200°C for 4 days followed by air cooled (in evacuated silica capsule); (a) prepolished surface, (b) polished and 2 % nital etched for the same location.

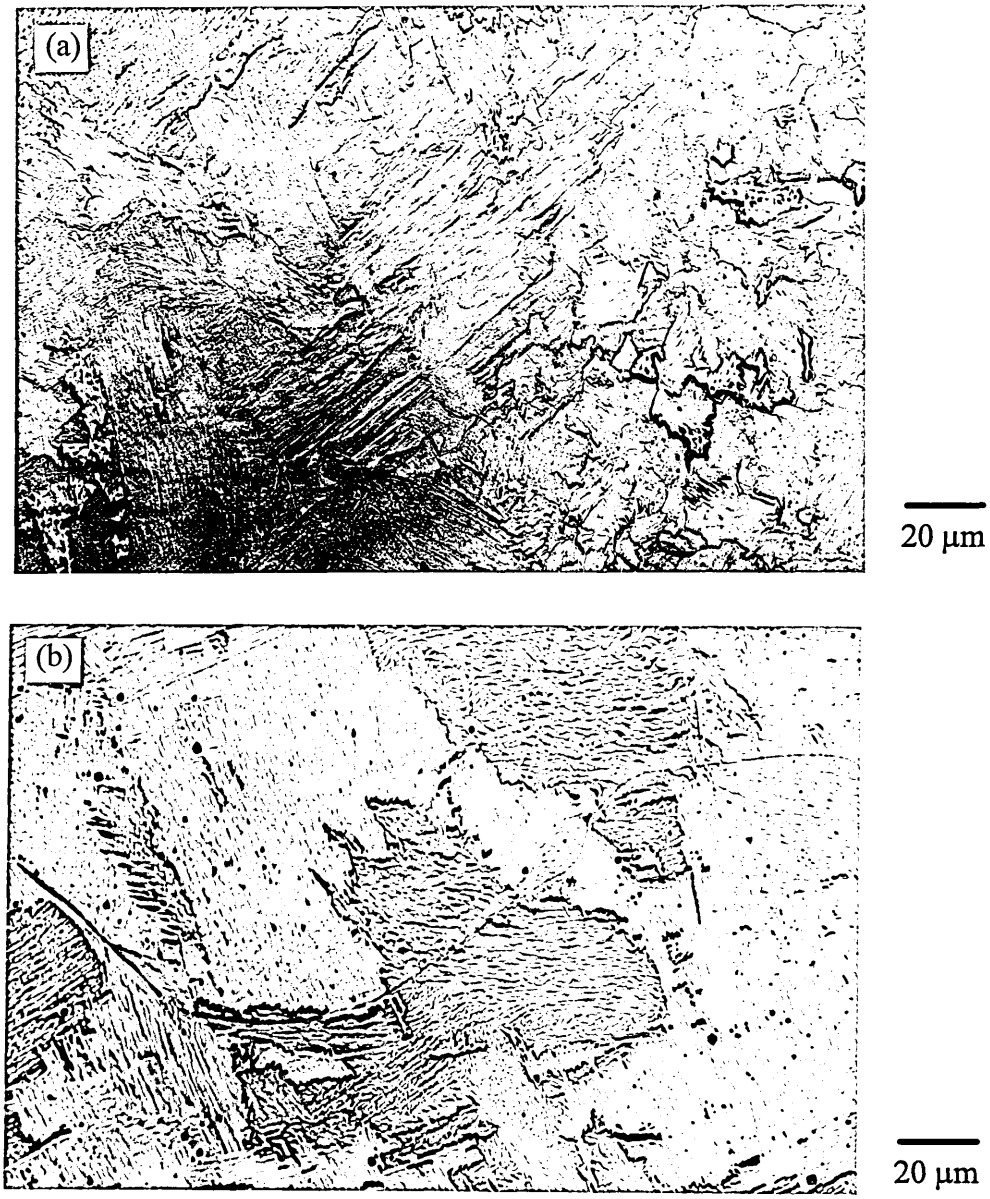

Fig. 4.11. Microstructure of oil quenched Fe-9Ni alloy; (a) optical micrograph by 2 % nital etched, (b) 4 % picral etched, and (c) TEM picture.

Fig. 4.12. Microstructure of water quenched Fe-9Ni alloy; (a) optical micrograph by 2 % nital etched, (b) 4 % picral etched, and (c) TEM picture.

(a) 50 μm

(b) 1 μm

Fig. 4.13. Microstructure of iced brine quenched Fe-9Ni alloy; (a) optical micrograph by 2 % nital etched, and (b) TEM picture.

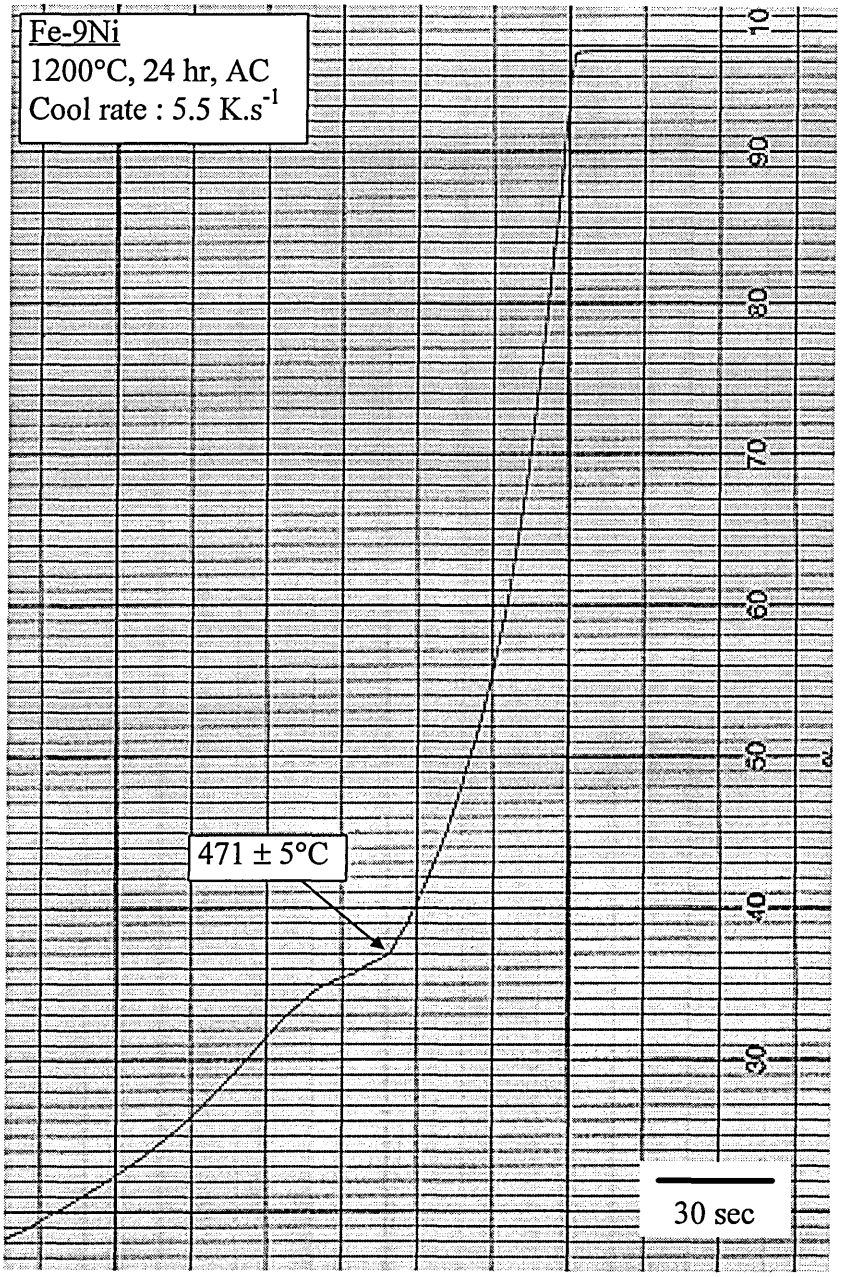

Fig. 4.14. Thermal arrest of bainitic transformation for Fe-9Ni alloy, VS2241A, austenitised at 1200°C for 24 hours followed by air cooled.

4.2. Isothermal Transformation of Fe-9Ni Alloy

4.2.1. Transformation Behaviour

The percentage transformation as a function of time and temperature was determined by point counting method. It was hoped to establish the TTT diagram by this method.

Isothermal transformation was carried out from 575°C down to 495°C using salt bath containing Durferritt GS 430. Transformation was detected by microstructural inspection. At 575°C, no transformed structures were found, even after being isothermally held for 24 hours.

Transformation was first detected at 565°C. The percentage of transformed structures increased with the decreased of isothermal holding temperature, but it never reached to completion, at least within the maximum holding time of 24 hours, figure 4.16.

While trying to monitor the effectiveness of salt bath quenching with a thermocouple inserted into a specimen, it was found that the transformation already started at ~557°C, as identified by the cooling curve shown in figure 4.15. The cooling rate of salt bath quenching was about 80 $K.s^{-1}$.

With short holding periods, the boundaries of the transformed structures could not be clearly revealed by nital etching. The percentage of transformation shown in figure 4.16 was determined by performing point counting on specimens that were isothermal held for 20 minutes or longer, because it was difficult to identify the transformed phases under the optical microscope. The shorter the transformation time, the more ambiguous was the phase boundary revealed by nital etching.

Fraction of transformation was determined by areal analysis on the projection screen of the microscope, by superimposing a square grid. The percentage transformation at 565 - 545°C was determined by counting the areal fraction of transformed phase, and that of the quenched phase for 535 - 495°C. The area was chosen randomly wherever the

boundaries of the phases could be identified, which were sometimes found to be indistinguishable.

For each specimen, 20 different locations were chosen covering total area of 0.72 mm^2, with 1800 points all together. Base on the formula in reference [PICKERING 1976], the maximum counting error would be ±2.3%. Nonetheless, the error bar is not presented in figure 4.16. It is thought that the error must be larger than the calculated value due to the reasons mentioned above.

Despite of the problems arose in attempting TTT curve establishment, the data collected in figure 4.16, are similar to the transformation curves in figure 2.6(b) which was determined by dilatation measurement [MOISEYEV et al 1981].

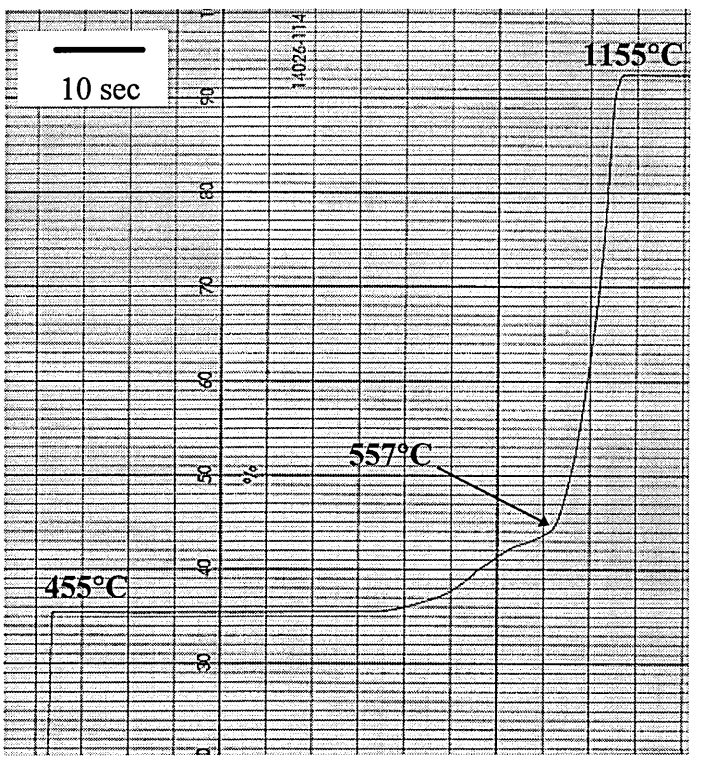

Fig. 4.15. Cooling curve of a specimen subjected to austenitising temperature of 1150°C for 20 minutes, quenched into salt bath at 450°C and soaked for 1 minute, followed by iced brine quenched.

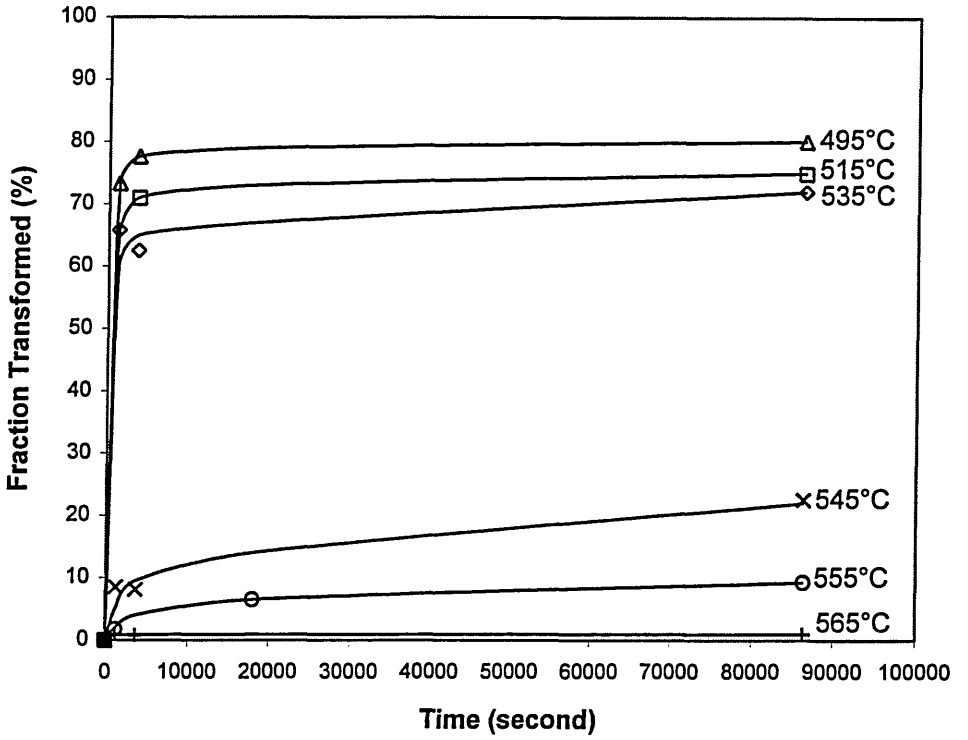

Fig. 4.16. Percentage transformation of Fe-9Ni alloy, VS2241A subjected to austenitising temperature at 1150°C for 20 minutes, soaked into salt bath at various temperatures and for different period, followed by iced brine quenched.

4.2.2. Transformed Structures

The identification of transformation at the initial stage was found to be difficult as mentioned in the previous section. After extensive studies from a wide range of transformation at various times and temperatures, it was observed that the morphologies of the transformed structures essentially followed the Dubé classification.

Equiaxed (Massive) Ferrite / Grain Boundary Allotriomorph

Transformation was first detected at 565°C. Few small grains were identified as the isothermally transformed phase. Figure 4.17 presents a ferrite grain nucleated at the austenite grain corner. It is interesting to observe that the prior austenite grain boundaries are revealed in the isothermal transformed region after polish and etch. It

suggests that the grain boundaries dividing up the corner-nucleated ferrite allotriomorph are delineated by a carbide or segregated impurities. Alternatively, it is not a single grain, but composed of three ferrite grains nucleated at the same point (grain corner) and grow independently in different direction.

The most commonly found transformed structure was at the austenite grain boundary. In quite a few transformed regions, the grain boundary allotriomorph was found to grow into both side of the austenite grain boundary, figure 4.18. This phenomenon had been particularly mentioned by RICKS et al [1981]. The ferrite is thought to be rationally oriented with respect to both adjacent austenite grains. However, again, the presence of (prior austenite) grain boundaries is puzzling.

As the fraction of transformation was so small and the transformed ferrite grains were minute, it was difficult to find the transformed structure even from the bulk sample. A ferrite grain was detected under TEM, which is believed to be the ferrite transformation at the austenite grain corner, figure 4.19. Note the partially annihilated grain boundary inside the grain.

Figure 4.19 does not show particles precipitating on the internal boundaries subjected to 24 hours of holding at 555°C. Similarly, with short isothermal holding, TEM inspection of such boundary for the grain boundary allotriomorph, figure 4.20, again, shows the absence of particles precipitation.

Nonetheless, grain boundary allotriomorphs without trace of prior austenite grain boundary inside ferrite grains were also observed, as shown in figure 4.21.

After long hours of holding (24 hours maximum), ferrite grains did not grow further to occupy the rest of the untransformed region. Apparently, the transformation stopped (or stasis) after a short period of holding. Extended isothermal holding allowed the recovery process to take place in the transformed structure, leading to low dislocation density of the isothermally transformed structure and the annihilation of the two adjacent grains, as evident by grain boundary network presented in figure 4.22.

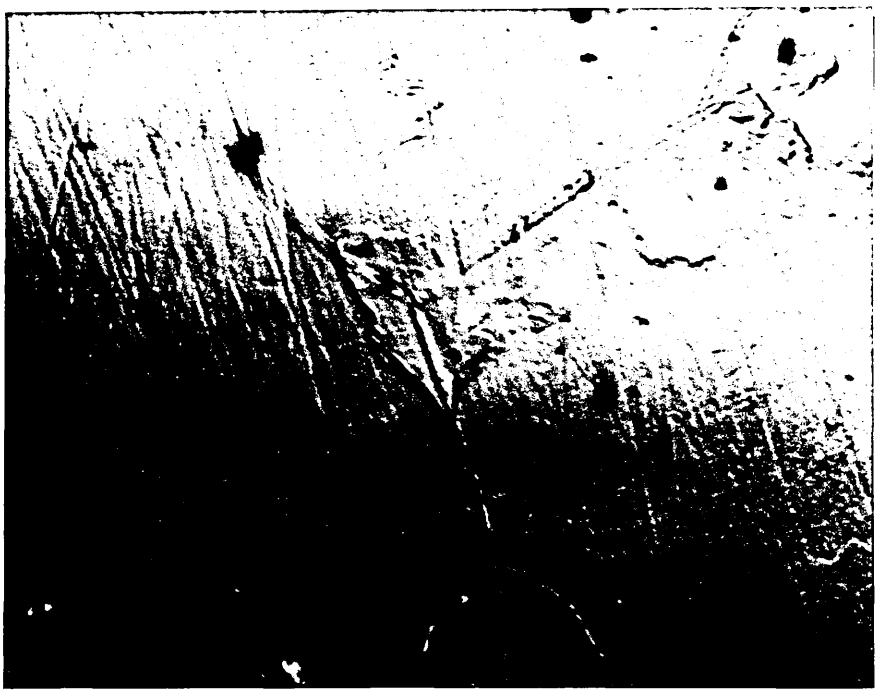

Fig. 4.17. Ferrite grain(s) transformed at the austenite grain corner, austenitised 20 min at 1150°C, isothermally held 1 hr at 565°C. 2 % nital etched.

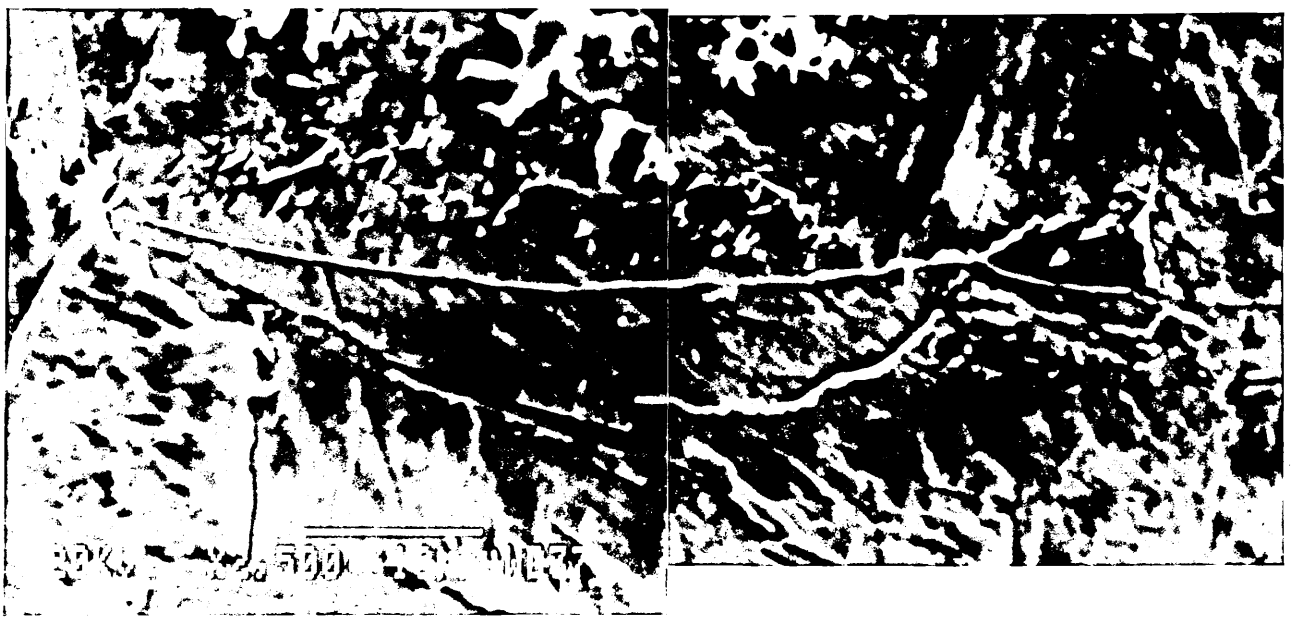

Fig. 4.18. Grain boundary allotriomorph formation at the austenite grain boundary, austenitised 20 min at 1150°C, isothermally held 2 min at 565°C. 2 % nital etched.

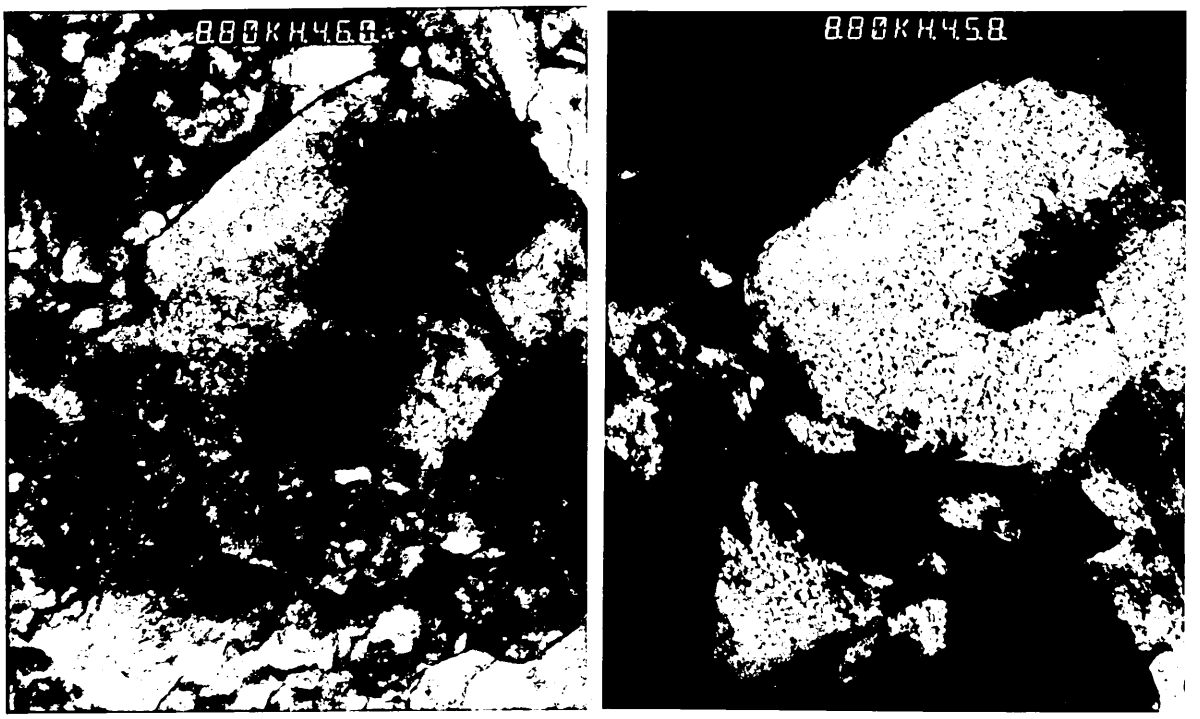

(a) (b)

2 μm

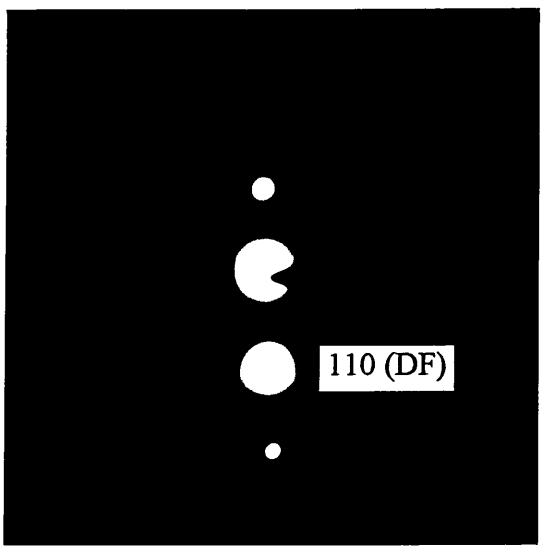

(c)

Fig. 4.19. TEM micrograph of a ferrite grain formed at the austenite grain corner, austenitised 20 min at 1150°C, isothermally held 24 hr at 555°C; (a) bright field, (b) dark field, (c) the corresponding electron diffraction pattern.

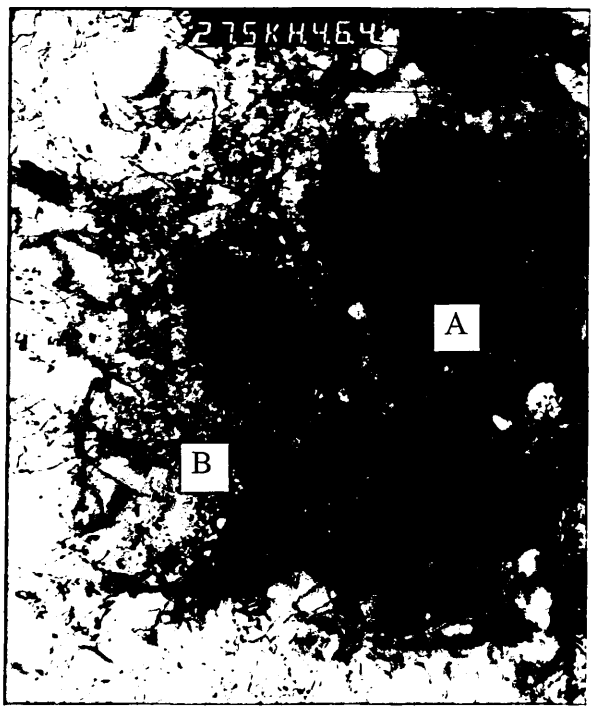

(d) 0.4 μm

(e) 0.1 μm

(f) 0.1 μm

Continue:

Fig. 4.19. TEM micrograph of a ferrite grain formed at the austenite grain corner, austenitised 20 min at 1150°C, isothermally held 24 hr at 555°C; (d) the boundaries inside the grain, (e) magnified boundary A, (f) magnified boundary B.

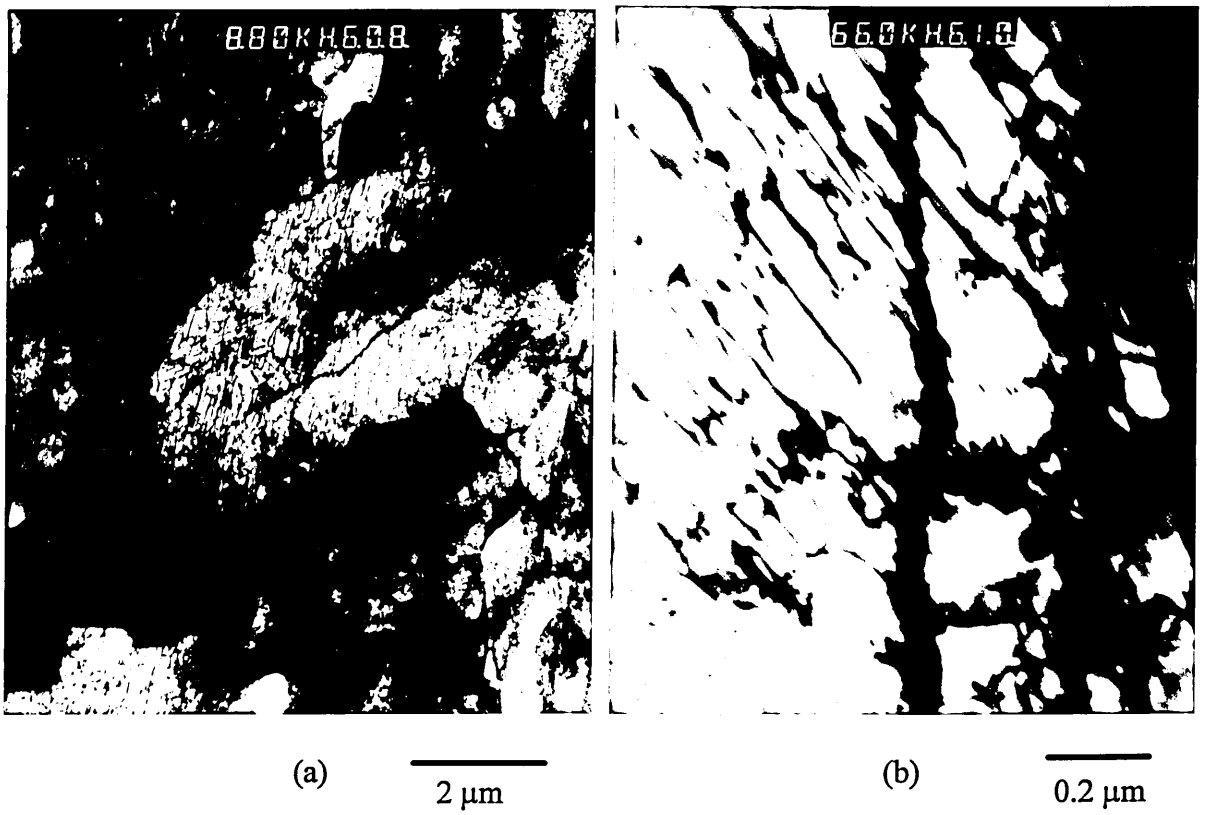

Fig. 4.20. (a) Grain boundary allotriomorph with a dividing boundary inside the grain, (b) magnified internal boundary to show the absence of particle (carbide) precipitation on the boundary. Specimen austenitised at 1150°C for 20 min, and isothermally held at 555°C for 2 min.

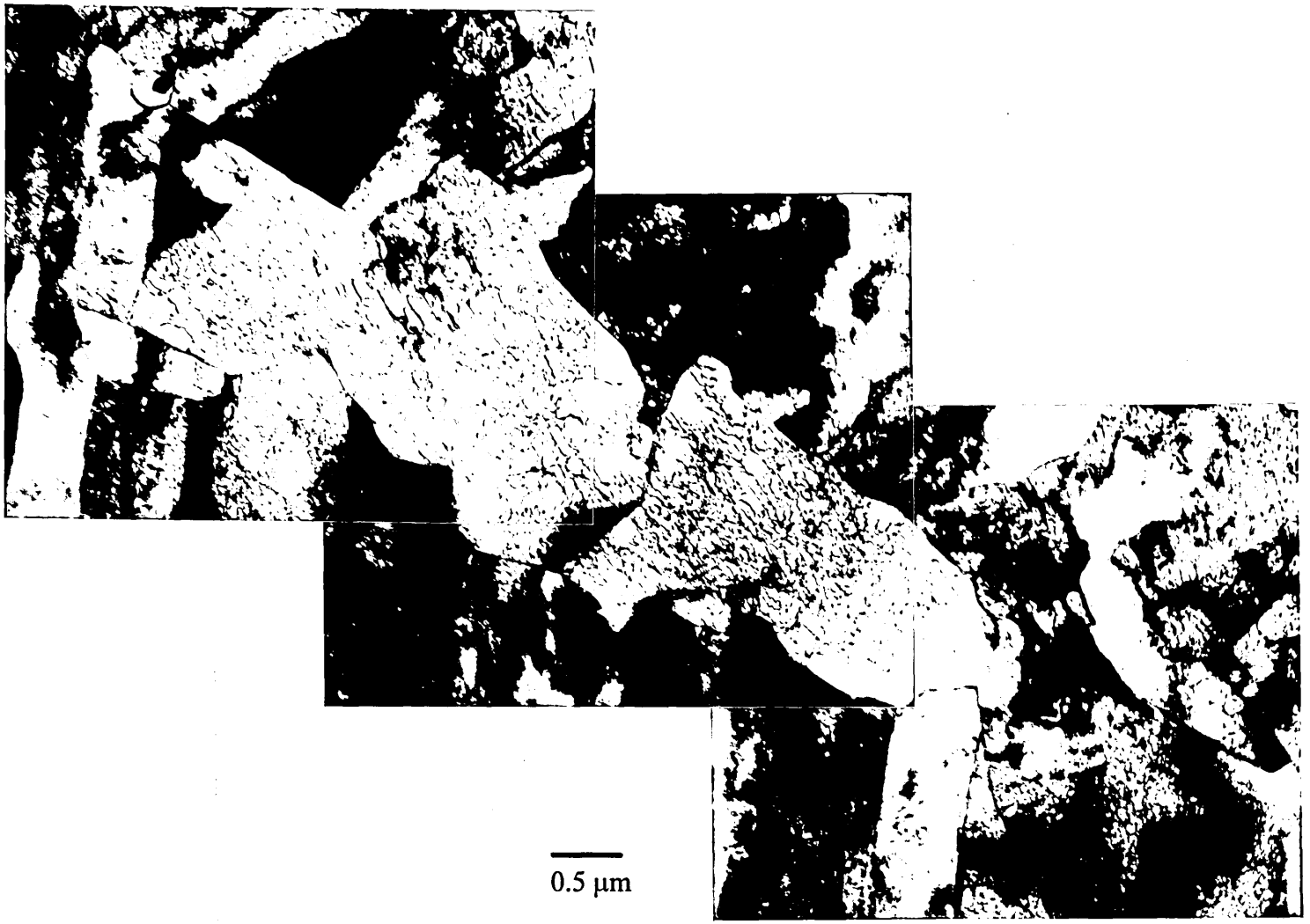

Fig. 4.21. Grain boundary alltriomorphs without showing trace of prior austenite grain boundary inside the grains, austenitised 20 min at 1150°C, isothermally held 2 min at 555°C.

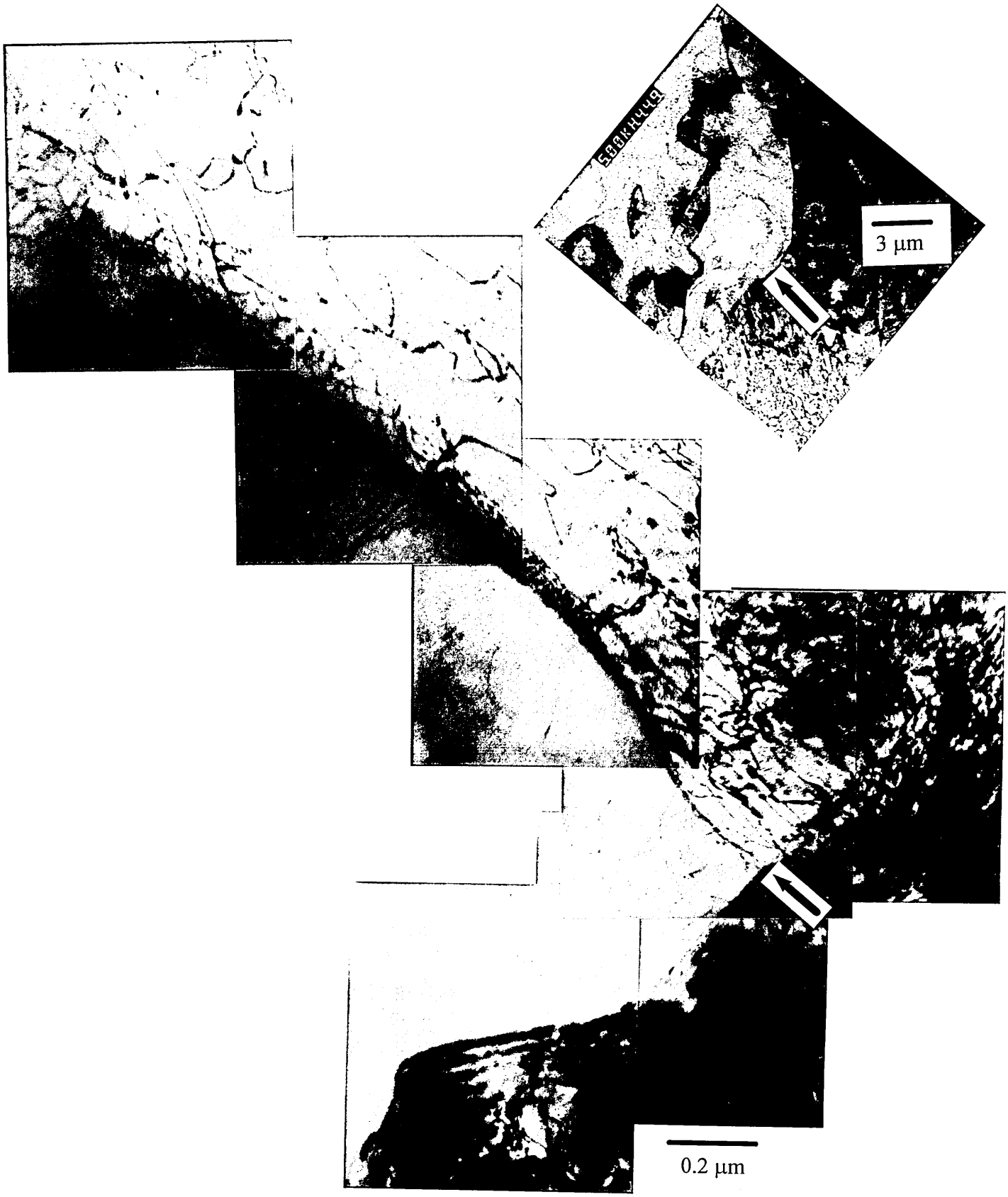

Fig. 4.22. Dislocation network showing grain boundary annihilation between two adjacent grain boundary ferrites in Fe-9Ni alloy, VS2241A. Specimen austenitised 20 min at 1150°C, isothermally held 24 hr at 555°C.

Widmanstätten Sawteeth / Comb

Because of the high degree of undercooling, the formation of grain boundary ferrite was found in a narrow range of temperature only, and was immediately replaced by Widmanstätten structure.

Grain boundary allotriomorphs with a larger size started to show the protuberance growing continuously from the grain boundary ferrite into the austenite grains, figure 4.23. With such a high degree of undercooling, the migration of transformed phase by the movement of incoherent high angle boundary would be difficult, and was therefore replaced by another mode of grain boundary movement - i.e. by ledge mechanism, to allow further growth of the isothermally transformed phase. Growth by the ledge mechanism was anisotropic with sideways growth less preferable than growth in the forward or longitudinal direction. As a consequence, the transformed structure became sawteeth-like. Note also in figure 4.23, the trace of prior austenite grain boundary can still be seen inside the transformed phase.

As mentioned in the previous section, the identification of the transformed structures for the short isothermal holding would be rather difficult as the phase boundaries could not be clearly revealed by etching. Widmanstätten structure with comb-shaped / sawteeth was identified in a specimen subjected to 2 minutes holding, figure 4.24. The boundary between the "comb" and quenched structure might be partially coherent with low angle of misorientation, therefore not able to be revealed by etching. The Widmanstätten structure became more apparent in specimens with longer period of isothermal holding, as shown in optical micrograph, figure 4.25(a) and TEM picture, figure 4.25(b). Growth of Widmanstätten sawteeth into both sides of the austenite grain boundary was commonly found.

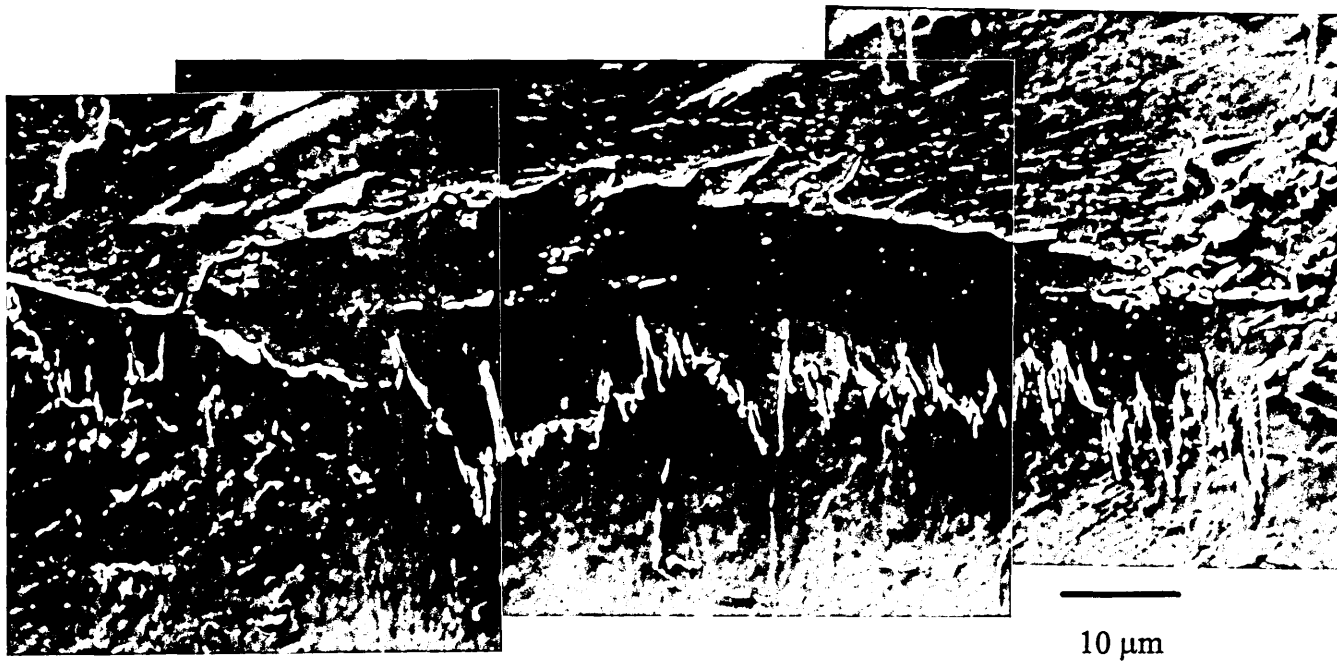

Fig. 4.23. Growth of grain boundary allotriomorph with sawteeth type protuberance, austenitised 20 min at 1150°C, isothermally held 24 hr at 555°C. 2 % nital etched.

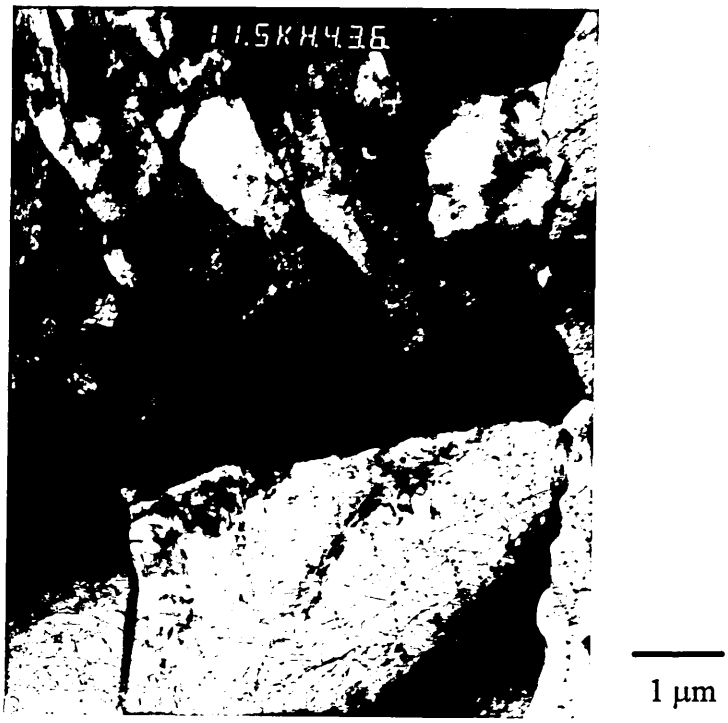

Fig. 4.24. Comb-shape of Widmanstätten structure, austenitised 20 min at 1150°C, isothermally held 2 min at 555°C.

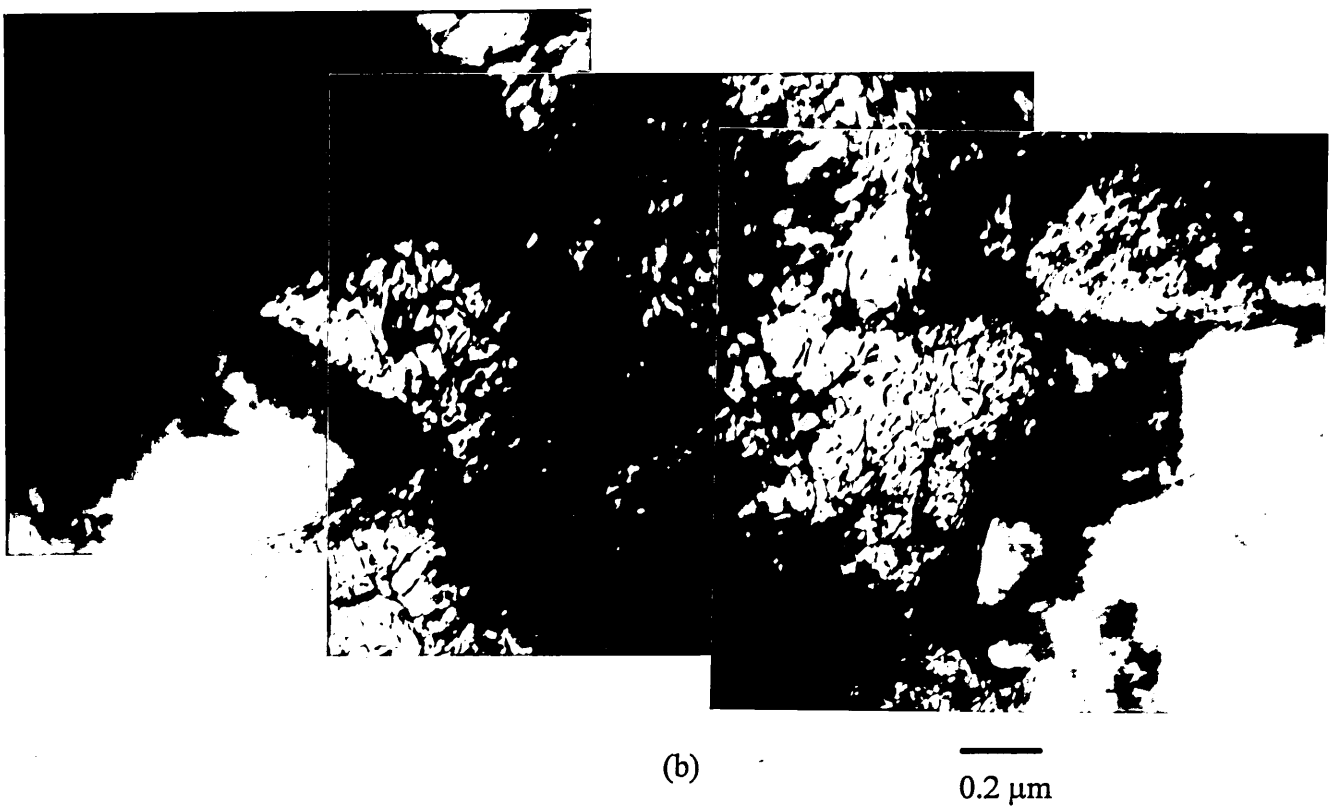

Fig. 4.25. Widmanstätten sawteeth with distinct boundary between phases; (a) optical micrograph, 2 % nital etched, and (b) TEM picture. Austenitised 20 min at 1150°C, isothermally held 24 hr at 555°C.

Massive Ferrite and Secondary Widmanstätten Lath

Since quenching into salt bath failed to bypass 557°C, as shown by thermal arrest in figure 4.15, specimens subjected to lower isothermal holding temperatures would contain partly transformed structures formed at 557°C. Nevertheless, different ferrite morphologies could still be identified and would therefore be treated as the representative structures that transformed at the corresponding holding temperatures lower than 557°C.

Figure 4.26 shows that Widmanstätten structure predominant at lower transformation temperatures. Lath type Widmanstätten structure was found to grow from grain boundary ferrite, either continuously or discontinuously. Widmanstätten structure could also form intragranularly (idiomorph) in the austenite grains. Figure 4.27 shows Widmanstätten ferrite nucleates at the ferrite grain boundaries and grows into laths structure with broad laths and not clearly distinguishable lath boundaries.

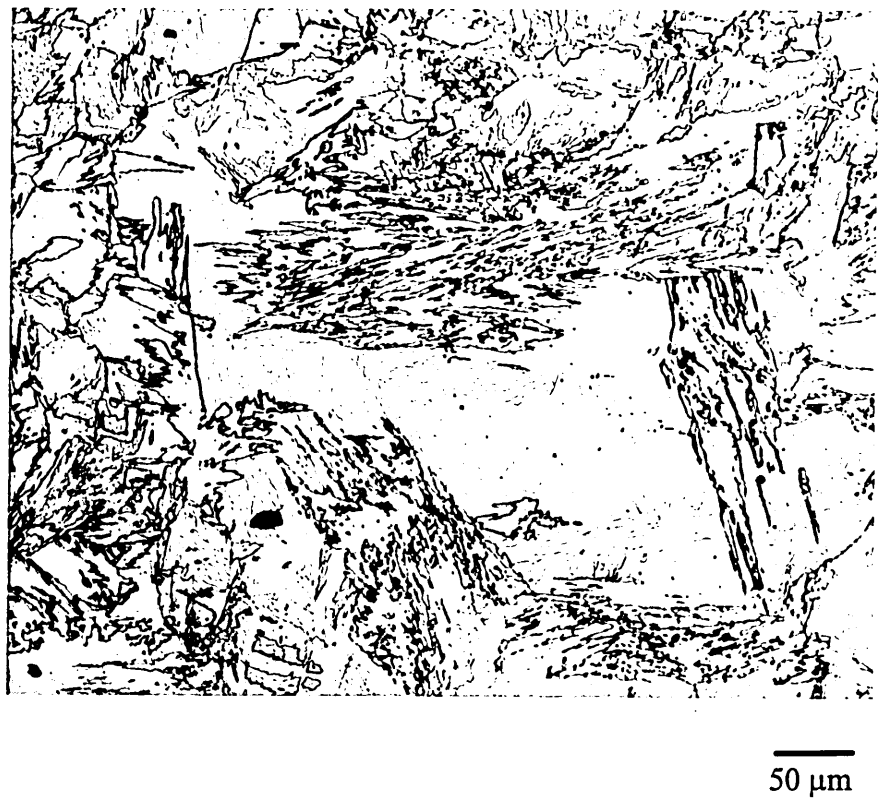

Fig. 4.26. General view of the Widmanstätten structure in a specimen austenitised 20 min at 1150°C followed by isothermally held at 545°C for 24 hr.

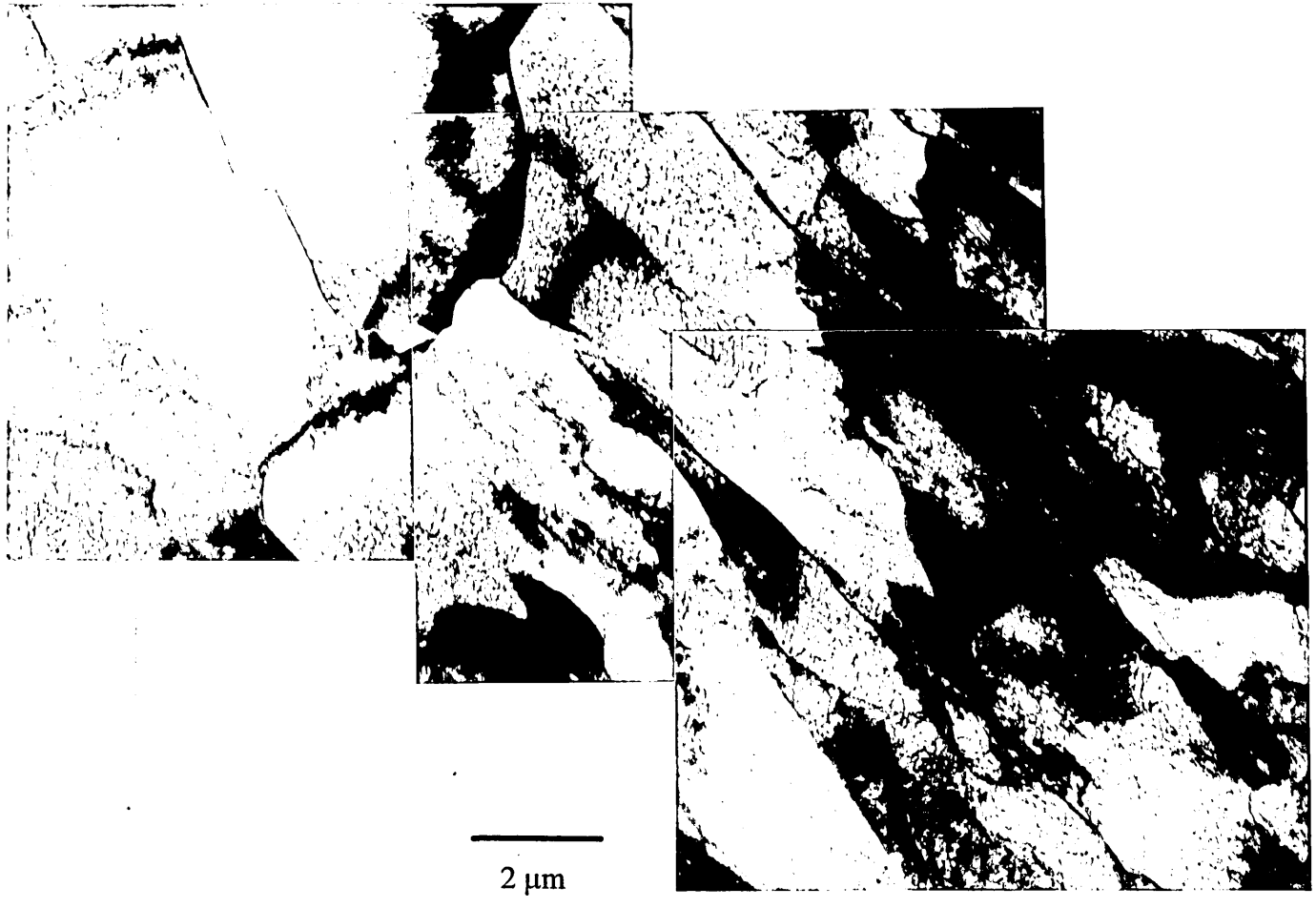

Fig. 4.27. TEM montage showing the secondary Widmanstätten laths nucleated and grew from ferrite grain boundaries, austenitised 20 min at 1150°C, isothermally held 20 min at 535°C for.

Comparing Widmanstätten structures with the isothermally transformed grain boundary allotriomorph formed at the higher temperature range, the identification of interface boundary (between the transformed structure and quenched matrix) was even more difficult at lower temperatures, unless the transformed region had subjected to prolong isothermal holding, as shown in figure 4.26. It was found that the Widmanstätten laths could in fact grow continuously to become martensite upon quenching without showing a distinct interphase boundary between the Widmanstätten ferrite and lath martensite, figure 4.28. Note also in figure 4.28, there is a distinct "step" on the Widmanstätten lath boundary.

Even though Widmanstätten laths predominate at lower isothermal transformation temperatures, a few ferrite grains were found on several occasions in transformed specimens at 535°C. The ferrite grain in figure 4.29 is rather irregular in shape and a discontinuous internal subboundary is revealed. This ferrite grain can therefore be regarded as massive ferrite. Figure 4.30 shows such ferrite grains under TEM. The dislocation lines in the grains are not evenly distributed and there are some internal subboundaries.

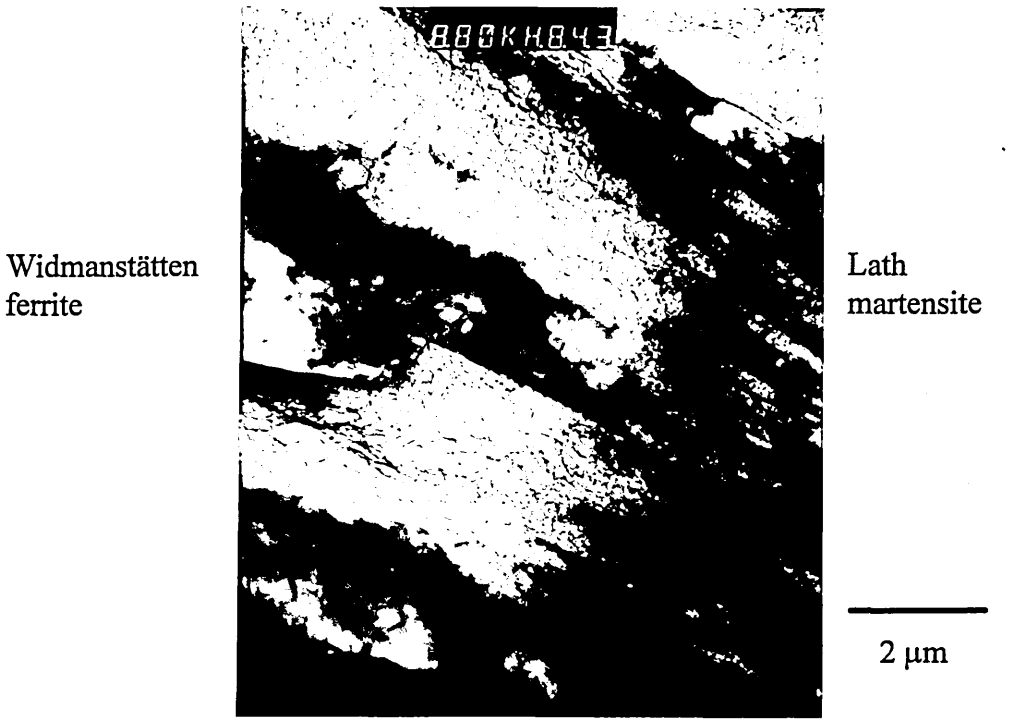

Fig. 4.28. A micrograph showing the absence of interphase boundary between Widmanstätten laths and lath martensite. Specimen austenitised 20 min at 1150°C, isothermal held 20 min at 535°C, followed by iced brine quenched.

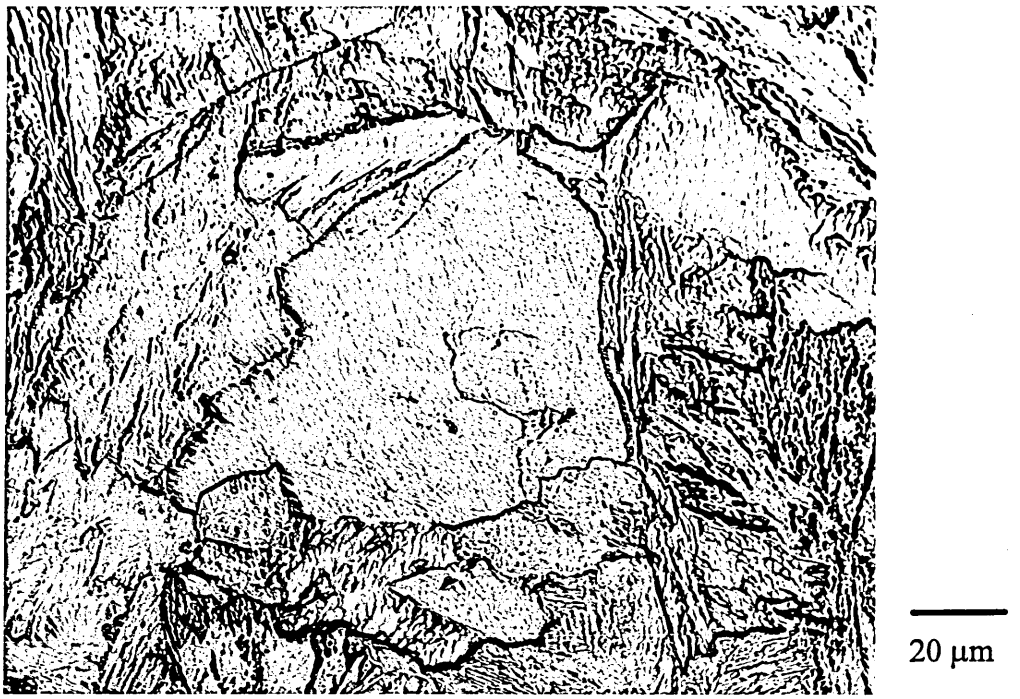

Fig. 4.29. Irregular single ferrite grain found in a specimen austenitised 20 min at 1150°C and isothermal held 20 min at 535°C. 2 % nital etched.

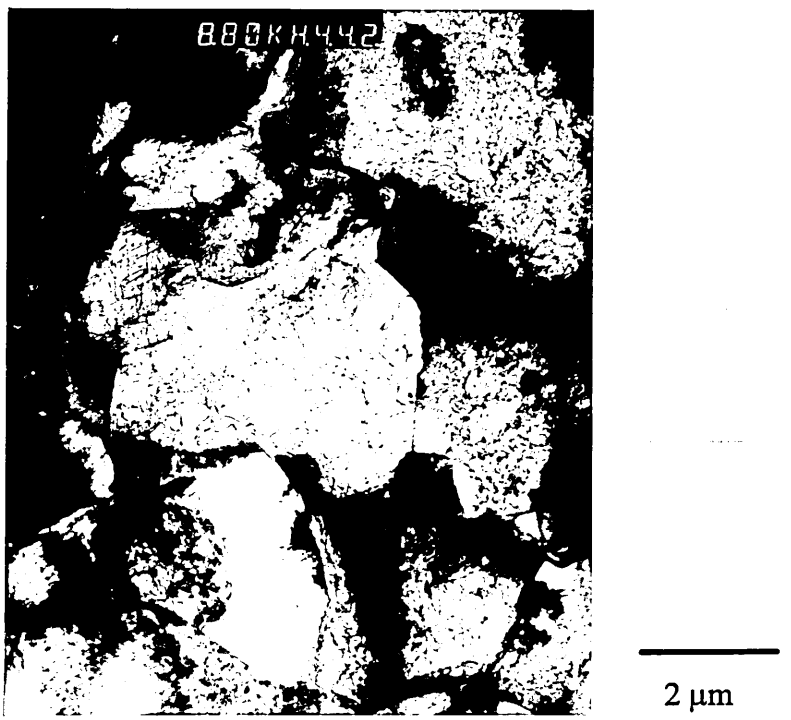

Fig. 4.30. Ferrite grains under TEM, austenitised 20 min at 1150°C, isothermally held 30 sec at 535°C.

Primary Widmanstätten Lath

At even lower degree of undercooling (515 and 495°C), it was found that the fine detail in the transformed phase was practically impossible to be revealed by nital etching. The isothermally transformed phase was essentially featureless, as shown by figure 4.31(a). However, with prolonged isothermal holding, the transformed structure could be recognised as the primary Widmanstätten laths that grew directly from the prior austenite grain boundaries, figure 4.31(b). The shape of Widmanstätten laths under TEM at this temperature range is shown in figure 4.32. Similar to the secondary Widmanstätten laths, these primary Widmanstätten laths transformed at lower temperature range are fairly broad and discontinuous laths boundaries are frequently observed .

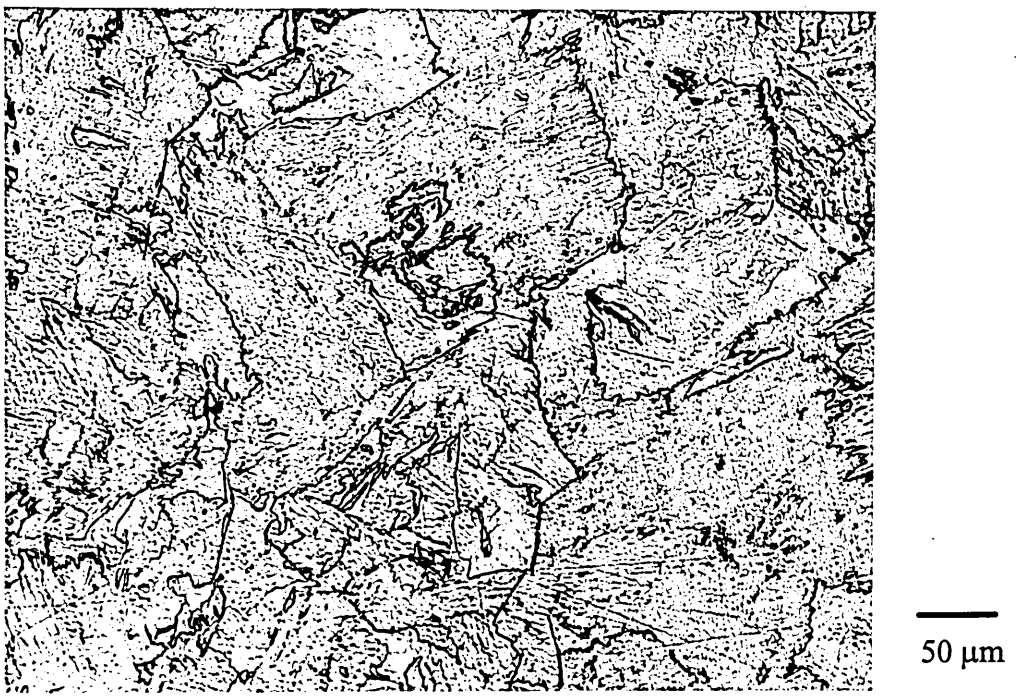

Fig. 4.31. (a) Optical micrograph of the transformed structure austenitised 20 min at 1150°C, isothermally held 1 min at 515°C. 2 % nital etched.

Fig. 4.31. (b) Optical micrograph of the transformed structure austenitised 20 min at 1150°C, isothermally held 24 hr at 515°C. 2 % nital etched.

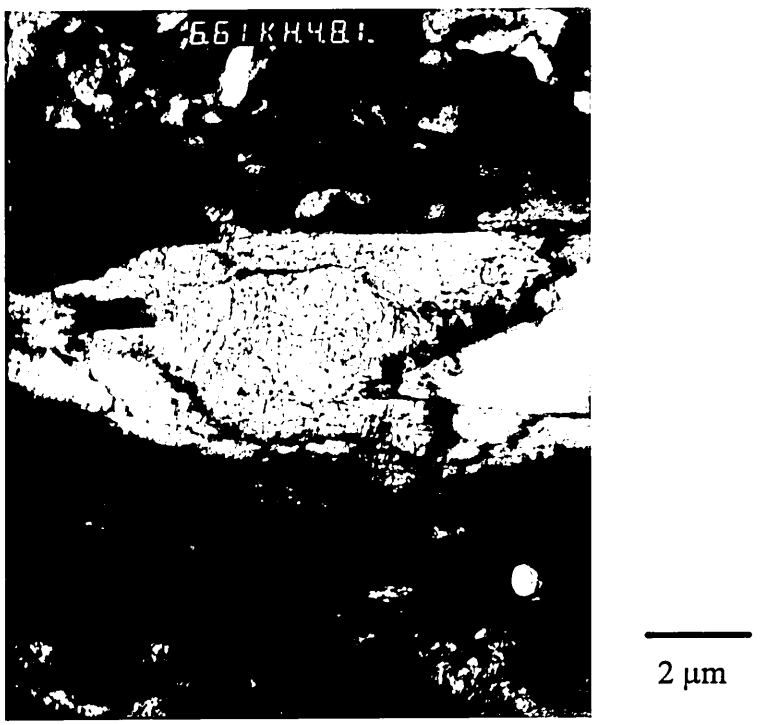

Fig. 4.32. TEM picture of Widmanstätten laths in a specimen austenitised 20 min at 1150°C, isothermally held 1 min at 515°C.

Bainitic Lath

Durferrit GS 430 salt starts to solidify at 495°C, in order to carry out isothermal transformation experiment at lower temperature range, the specimens would have to be quenched into another salt bath filled with Durferrit AS 140.

Thermal arrest result from continuous cooling experiment suggested bainitic transformation starts at ~486°C (table 4.1). In studying the transformation to bainite structure, isothermal holding at 450°C was attempted. Unfortunately, the cooling rate upon salt bath quenching was not rapid enough to pass the ferrite / Widmanstätten transformation range, as shown in figure 4.15. The transformed structures found in the specimens would require careful diagnosis to eliminate / discard the partially transformed structure that took place at higher temperatures.

Transformation did not go to completion, even after 24 hours. The nital etched bainitic structure appeared to be featureless, figure 4.33(a). This is quite different from the bainitic ferrite in OQ (figure 4.11(a) and WQ (figure 4.12(a)) specimens which show planar phase boundaries. Also, unlike the Widmanstätten structure that transformed in the higher temperature range, the fine feature of the laths remained unclear even with prolonged holding.

However, with picric etching, bainitic lath is revealed, showing the bainitic ferrite grows directly from the austenite grain boundaries, figure 4.33(b).

Under TEM inspection, the bainitic laths are much more orderly arranged compared with the Widmanstätten laths, and the lath boundary of bainitic ferrite is well defined, figure 4.34. After long period of isothermal holding, these laths started to break down into segments, presumably due to recovery, as shown in figure 4.35.

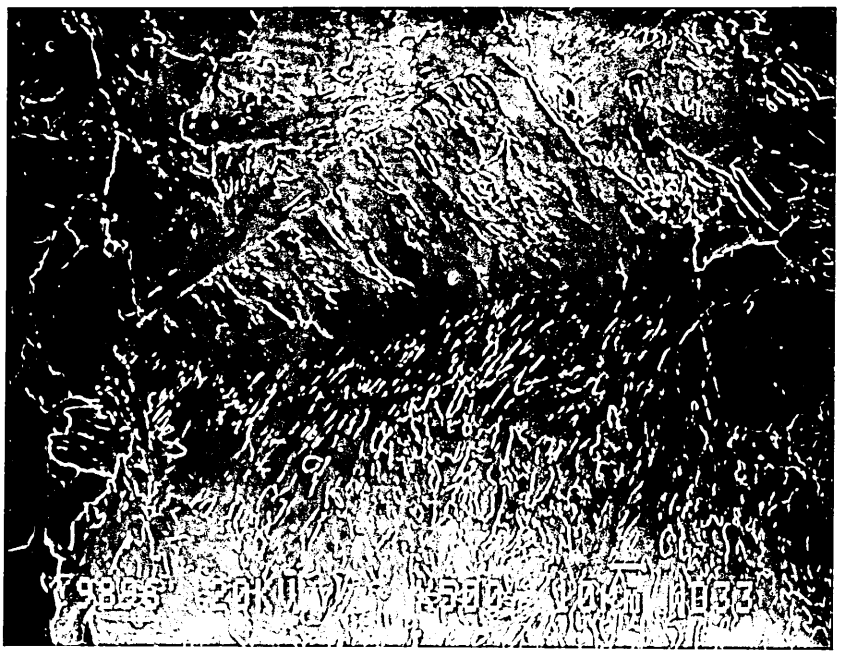

(a)

(b)

Fig. 4.33. Microstructure of bainitic ferrite in a VS2241A, Fe-9Ni specimen austenitised 20 min at 1150°C, isothermally held 24 hr at 450°C; (a) 2 % nital etched, (b) 4% picral etched.

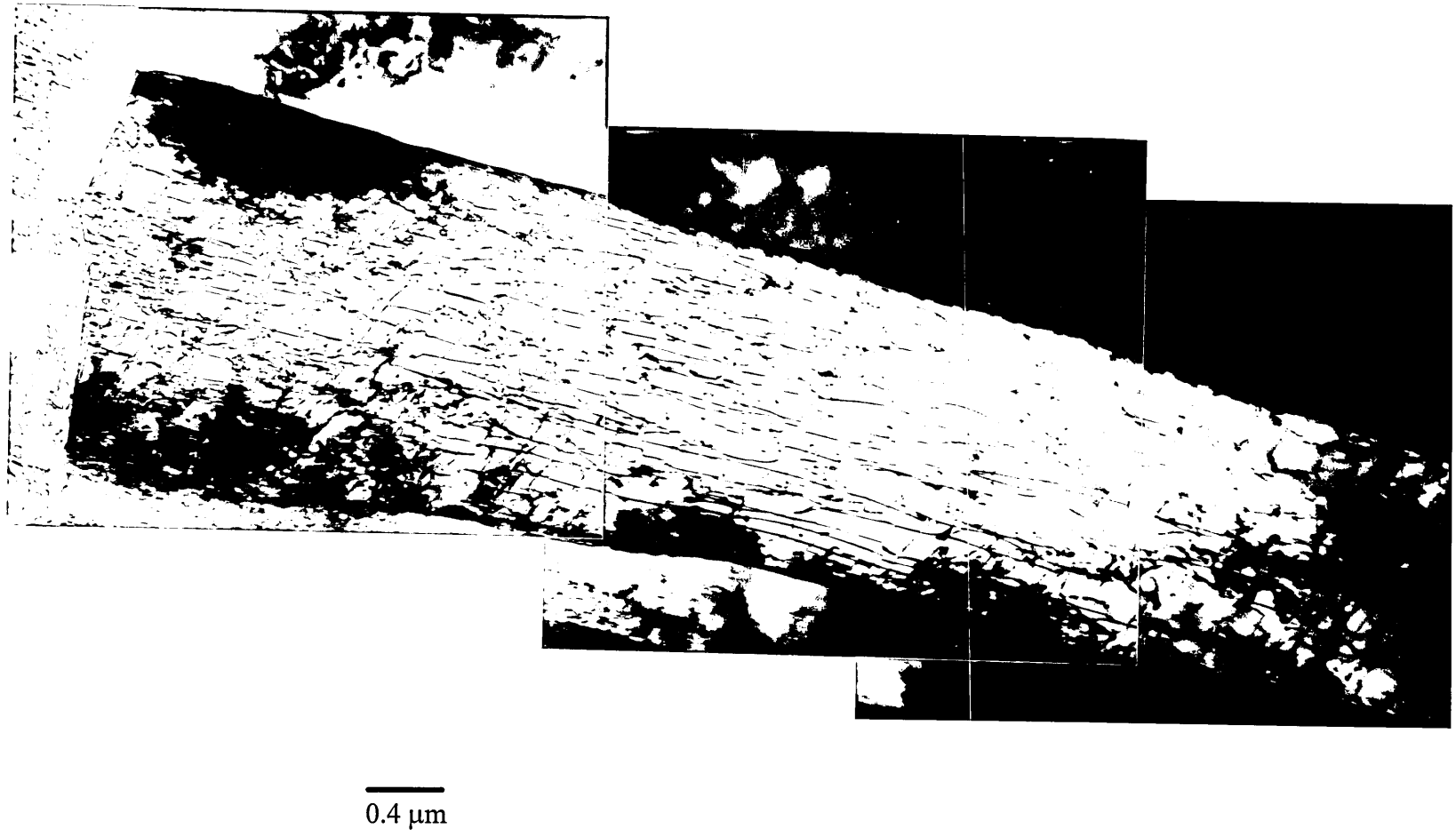

Fig. 4.34. TEM montage of a bainitic lath in Fe-9Ni alloy, VS2241A. Specimen austenitised 20 min at 1150°C, isothermally held 1 min at 450°C.

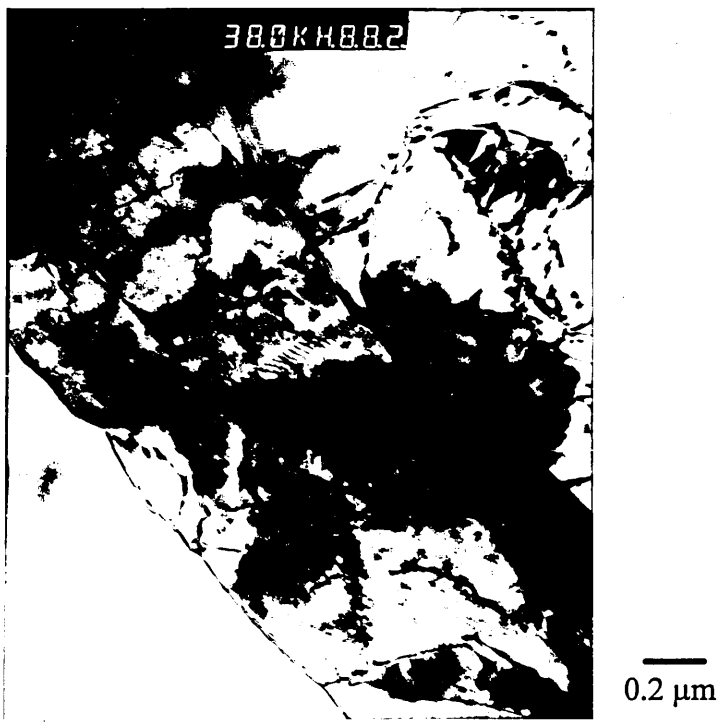

Fig. 4.35. TEM picture showing break down of bainitic lath by segmentation in Fe-9Ni alloy VS2241A, austenitised 20 min at 1150°C, isothermally held 24 hr at 450°C.

4.3. Mircoanaytical Results

4.3.1. Semi-Quantitative Analysis by TEM-EDX at Sheffield Hallam University

Thin foils from furnace cooled Fe-9Ni alloy, VS2241A, were prepared for the microanalysis to examine the composition invariant transformation to ferrite in this alloy. Figures 4.36 and 4.37 present the results of nickel distribution across ferrite grains which had been subjected to continuous and isothermal transformation respectively.

As mentioned in section 3.6.1, the smaller the spot size, the lesser the generated X-rays, and as a consequence, the larger is the experimental error. By choosing the spot size of 20 nm diameter and 50 seconds of counting time, an absorption number of around 400 was obtained under the nickel peaks. The error bar of ±0.5 wt.% Ni, as shown in figures 4.36 and 4.37, is based on the calculation below:

For n absorption number;

standard error, $\sigma = \sqrt{n}$

relative accuracy, $\frac{\sqrt{n}}{n} = \frac{1}{\sqrt{n}}$

if n is 400, then $\sigma = 20$

For 10% Ni:

Relative accuracy $= 10\% \times \frac{1}{20} = \mathbf{0.5\%}$

The points in figure 4.36 and 4.37 give average nickel content across the grain of 8.33 ± 0.12 wt.% Ni and 9.00 ± 0.19 wt.% Ni respectively. The composition profile in figures 4.36 and 4.37 shows no sign of nickel redistribution across the ferrite grains. This implies that as far as substitutional alloying element (nickel) is concerned, the $\gamma \rightarrow \alpha$ transformation is "diffusionless", i.e. the growth of α phase in this case is a composition invariant transformation.

Grain boundary analysis of the ferrite grains were also attempted on different locations and found no difference in terms of nickel content.

As a comparison, analysis was also carried out on the iced-brine quenched specimen which only consisted of lath martensite. The result is shown in figure 4.38. It is known that martensitic transformation is a diffusionless process in which decomposition of austenite to ferrite without change in composition. Spot analyses as shown in figure 4.38 with the average nickel content of 8.08 ± 0.12 wt.% Ni proved that the scatter of nickel content is simply due to experimental error.

Note no correction was made to calculate the actual composition in each of the spot analysis and it leads to slightly different weight percentage of Ni obtained from each foil.

4.3.2. Microanalysis by FEG-STEM at Liverpool University

Followed by unsatisfactory performance of TEM-EDX analysis, microanalysis on the same material was attempted using FEG-STEM, on ferrite phase of VS2241A, Fe-9Ni alloy that had been subjected to furnace cooling, and lath martensite obtained by iced brine quenching.

Lath Martensite

A lath at a very thin section adjacent to the perforated hole was chosen. 11 points were obtained with 10 nm interval. Very consistent values of nickel content for each point giving a mean value of 8.6 ± 0.1 wt.% Ni along the line. The thickness of the area selected was about 100.0 nm, and computed error was ±0.3 wt.% on each individual point, figure 4.39.

The individual spot analysis was done by the electron beam travelling across the selected line under computer control. It was found that the selected region had drifted after the analysis was completed. The location of each point in relation to the lath boundary was therefore not identified.

Spot analyses on the lath boundary were performed twice at different regions to see if there was any difference in composition at the lath boundary from the matrix. The results are shown in table 4.2 below.

In order to maximise the interaction of the electron probe with the boundary material, the spot analysis on the lath boundary was selected in such a way that the lath boundary aligned parallel with the electron beam through the thickness of the foil.

Table 4.2. Nickel composition in the matrix and the lath boundary of lath martensite in VS2241A, Fe-9Ni alloy. Specimen subjected to iced brine quenching.

Region	Location	Ni (wt.%)	Criteria
I	lath boundary	8.92 ± 0.2	100 seconds count time
	10 nm away	9.01 ± 0.2	100 nm foil thickness
			19.9 nm* beam broadening
II	lath boundary	8.60 ± 0.2	50 seconds count time
	50 nm away	8.98 ± 0.2	275 nm foil thickness
	1 μm away	8.76 ± 0.2	90.8 nm* beam broadening

*Beam broadening as nominal value.

In table 4.2, the computed error in composition was ±0.2% rather than ±0.3% as previously given in figure 4.39. The smaller error is due to longer counting time in region **I** and selection of a thicker section (275.0 nm) in region **II**. As we can observe from the results, there is no significant difference in nickel concentration at the lath boundary compared with the matrix.

Analysis Across Ferrite Grain

The same parameters were chosen in examining ferrite grains. A line was drawn across the grain boundary and 42 points were analysed with a counting error of ±0.2 wt.% for each point. Due to the scatter in the data, the average nickel content along the line was 8.8 ± 0.2 wt.%. The composition profile in figure 4.40 shows that the nickel concentration is constant throughout the grain, resembling the same result obtained from TEM-EDX analysis.

Again, due to drifting, the point corresponding to the grain boundary was not identified. In addition, the magnetic astigmatism was much more apparent due to the thicker foil for this sample and the ferromagnetism of the specimen. Consequently the effective electron beam was actually wider.

A different region was chosen in order to minimise the astigmatism effect, and the location of each spot was monitored to counteract drifting. Twenty one points on one line across the grain boundary were analysed. The results are given in figure 4..41.

In figure 4.41, it is very obvious that one point (on the grain boundary) shows a significantly higher nickel content. The computed results give an error of ±0.2%, beam broadening of 60.6 nm, with the foil thickness of 210.0 nm.

Grain Boundary Analysis

For the second attempt, the work was concentrated on the grain boundary analysis. Only good edge-on boundaries were selected. It is important not to work on inclined boundaries because the optimum results can only be obtained when the grain boundary is align parallel with the electron beam [DOIG and FLEWITT 1988].

For better statistical results, longer counting times were used (150 and 300 second). In order to counteract specimen drift, square boxes were drawn on the boundaries to allow the electron beam to scan across the grain boundaries. The position of the selected

boundary was closely monitored by the X & Y controls on the specimen stage to ensure that the grain boundaries stayed inside the predetermined scan box as the counting progressed. This approach also helped to avoid the build up of carbon contamination.

The same analysis was carried out for the matrixes adjacent to the selected grain boundaries. The calculation of foil thickness and beam broadening was performed on the matrix. The results are given in table 4.3.

Table 4.3. FEG-STEM microanalysis on massive ferrite in a furnace cooled specimen from Fe-9Ni alloy, VS2241A.

	Ni (wt.%)		Foil thickness	Beam broadening	Count time	Scan box
	Grain Boundary	Matrix	(nm)	(nm)	(second)	(nm)
1	8.81±0.11	8.61±0.12	190	52.1	300	3 x 3
2	11.05±0.18	8.73±0.17	115	24.5	300	3 x 3
3	8.48±0.24	8.88±0.23	65	10.4	150	3 x 50
4	8.65±0.15	8.77±0.14	190	52.1	150	3 x 50
5	8.98±0.15	8.80±0.13	210	60.6	150	4 x 15
6	9.49±0.12	8.70±0.13	240	74.0	150	7 x 50
7	9.57±0.15	8.73±0.15	200	56.3	150	3 x 30
8	12.98±0.43	8.81±0.40	40	5.0	150	1 x 7
9	9.60±0.17	8.94±0.23	120	26.2	150	2 x 12

Results in table 4.3 show that nickel content of ferrite grains is fairly constant in the matrixes, but varies at different grain boundaries. There are two cases (No. 3 and 4) where the nickel content is lower than in the matrices. Nevertheless, these values are within the error limit and therefore not significant. Other cases show higher nickel content in the grain boundary than the matrix.

In order to minimise astigmatism and beam broadening, a very thin area, No. 8 in table 4.3, of thickness 40 nm was chosen for analysis. Nickel content as high as 12.98 wt.% was detected from the grain boundary, and just 10 nm away from it, the nickel content reduces significantly to 8.81 wt.%. Figure 4.42 shows the corresponding spectra.

In addition to higher nickel content at the grain boundary, higher contents of copper and oxygen were also detected occasionally at the grain boundary. The results given in table 4.3 were calculated by omitting the copper peak which was very close to the nickel peak in the spectrum. The detection of the copper peak might probably be due to contamination from electropolishing solution. This solution was not fresh and had previously been used in polishing steel containing copper.

On one occasion, it was observed that the grain boundary appeared to be brighter in the annular dark field image, possibly implying heavy element segregation on the grain boundary. However, by comparing the spectra taken from the grain boundary with the adjacent matrix, no significant difference could be observed.

The spatial resolution of the field emission gun STEM is better than conventional STEM for microanalytical work, and is proven to be more efficient in detecting grain boundary segregation in various steels [FAULKNER et al 1990; SKOGSMO and ATRENS 1994]. Typically when the spatial resolution of the instrument is optimised, a distance limit as close as 2 nm can be achieved.

However, considering the poor image due to astigmatism in the present investigation, in addition to the beam broadening through the foil thickness, there is a possibility that the spectrum taken from grain boundary is actually not representative due to electron beam scattering, hence not able to show the true composition at the grain boundary. It is likely that the actual nickel content is higher than the measured results.

By compiling the results obtained from the analyses at different locations, the estimated beam broadening against foil thickness is plotted, figure 4.43.

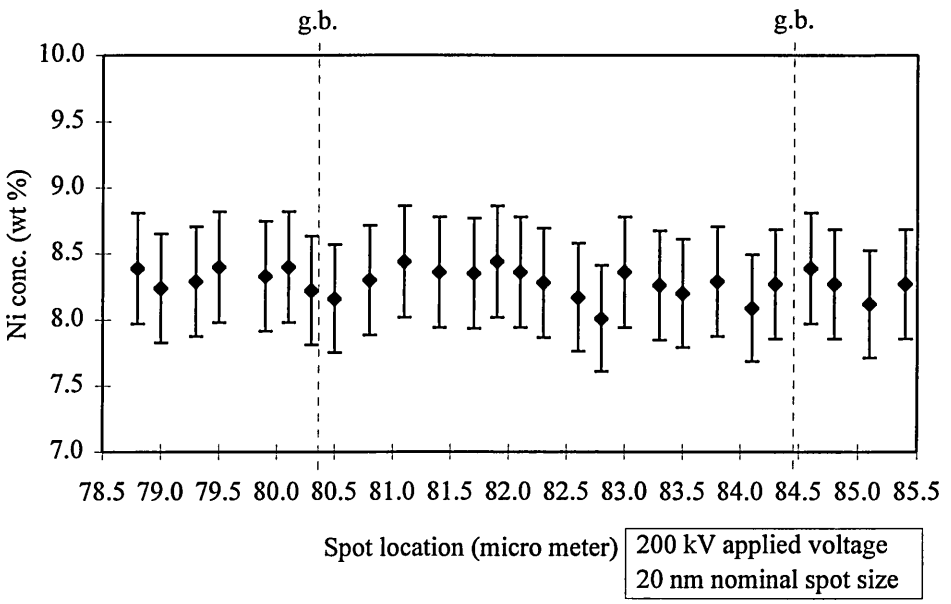

Fig. 4.36. TEM-EDX semi-quantitative analysis of nickel distribution across a ferrite grain in furnace cooled Fe-9Ni alloy, VS2241A. Thermal arrest at 555°C.
g.b. = grain boundary

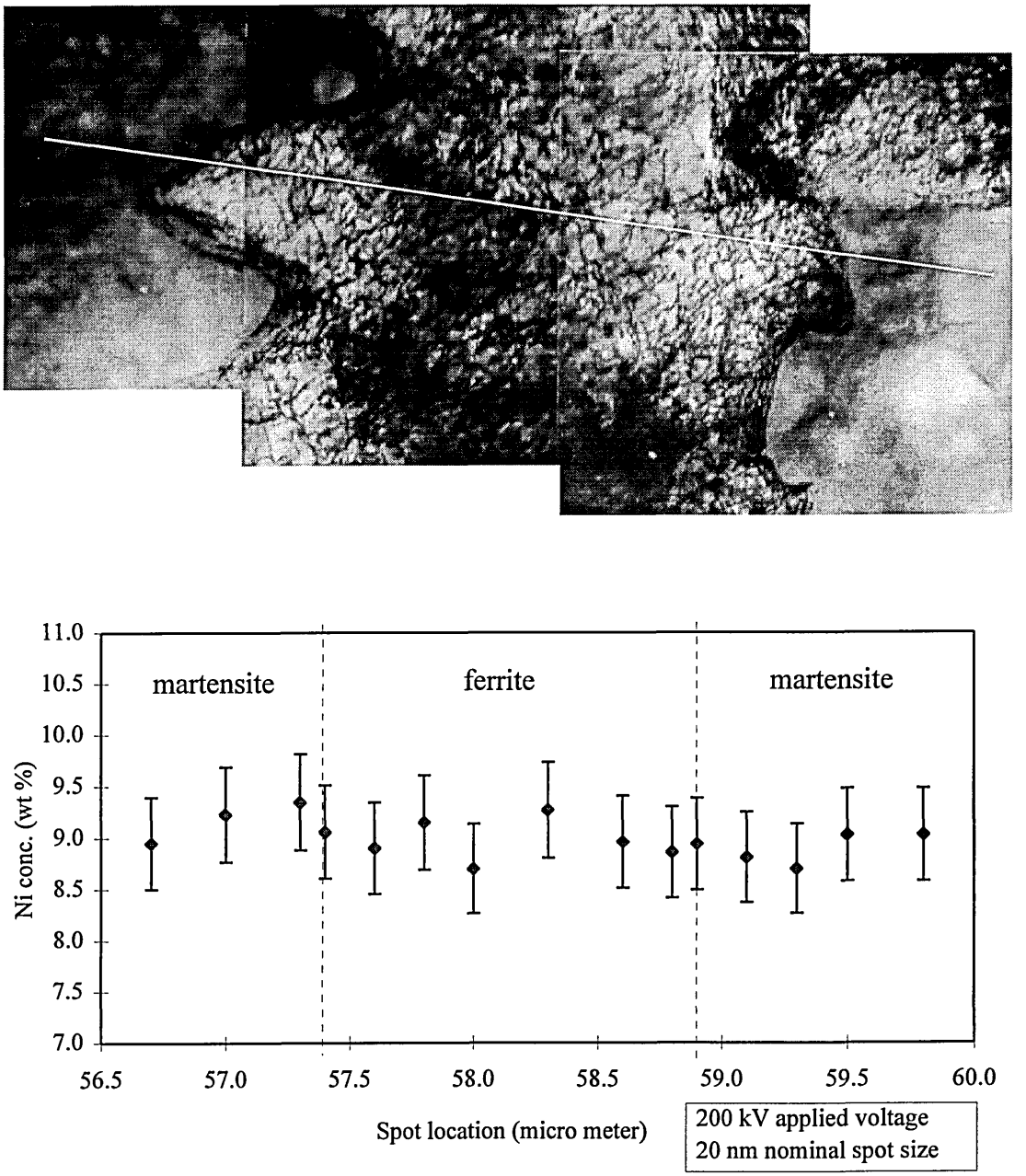

Fig. 4.37. TEM-EDX semi-quantitative analysis of nickel distribution across ferrite phase in Fe-9Ni alloy, VS2241A. Specimen austenitised 20 min at 1150°C, isothermally held 24 hr at 555°C.

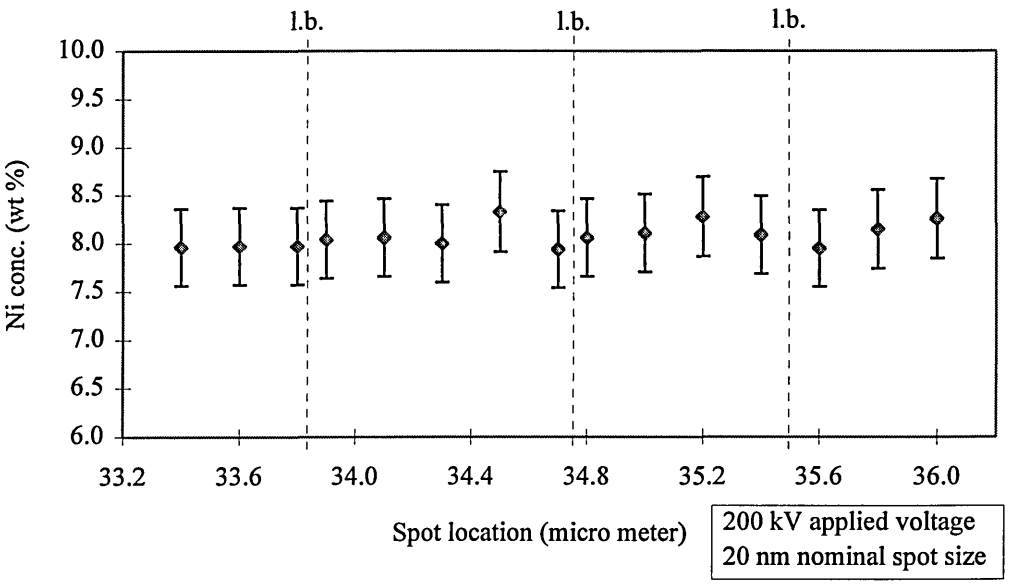

Fig.4.38. TEM-EDX semi-quantitative analysis of nickel distribution across lath martensite in iced brine quenched Fe-9Ni alloy, VS2241A.
l.b. = lath boundary

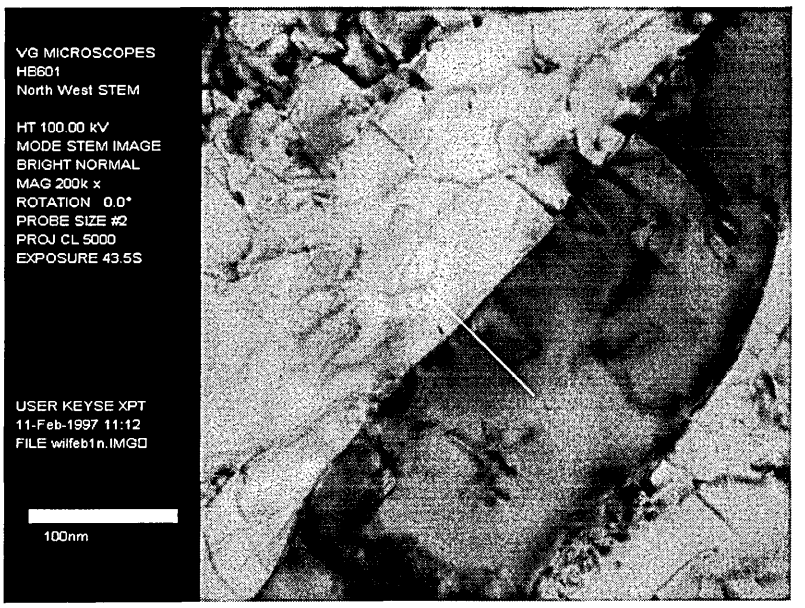

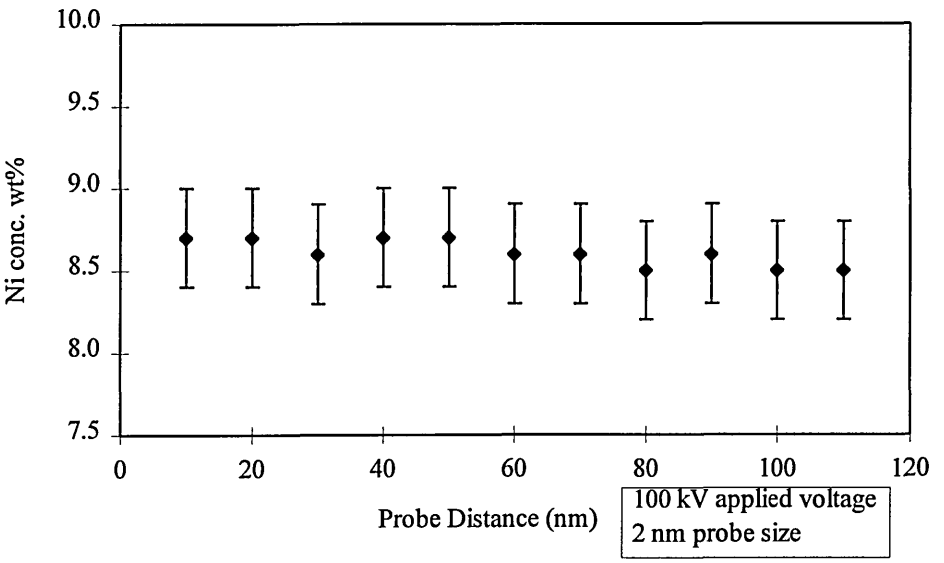

Fig. 4.39. Microanalysis by FEG-STEM showing the nickel distribution of lath martensite in an iced brine quenched Fe-9Ni alloy, VS2241A.

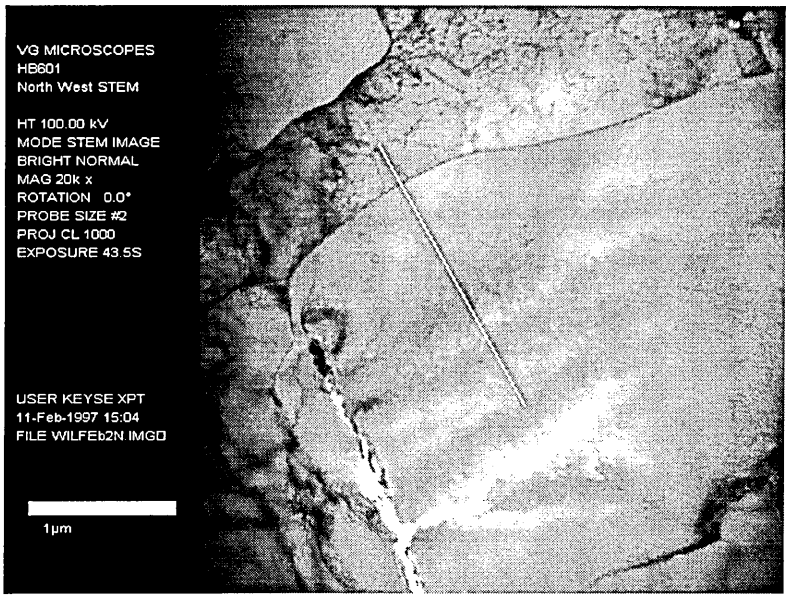

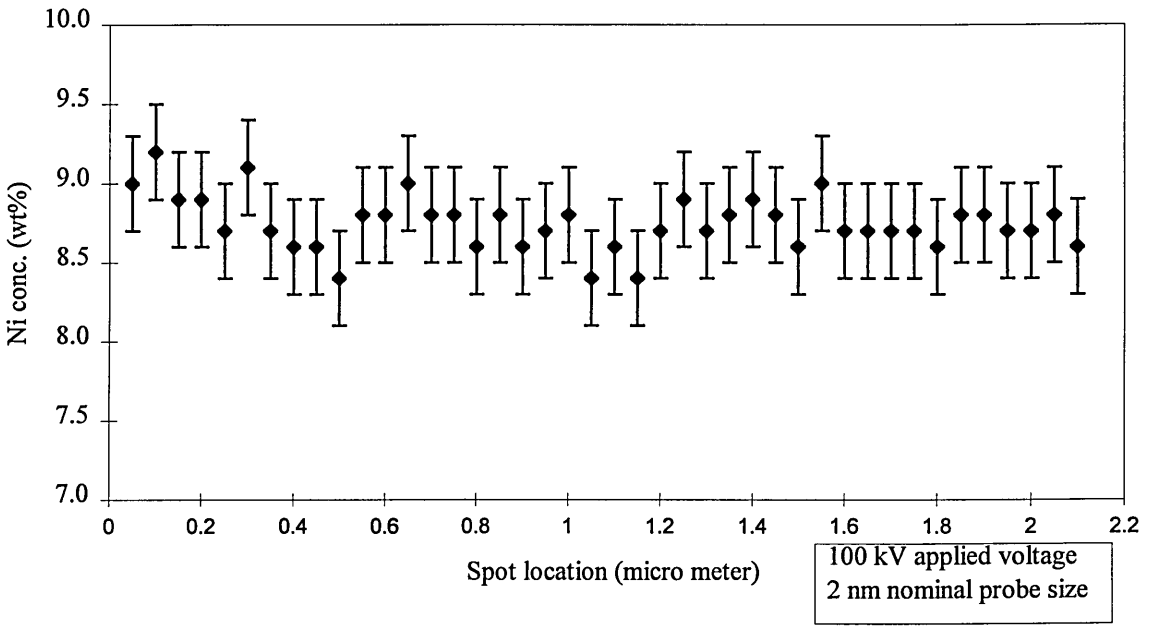

Fig. 4.40. Microanalysis by FEG-STEM showing the nickel distribution across ferrite grains in the furnace cooled Fe-9Ni alloy, VS2241A.

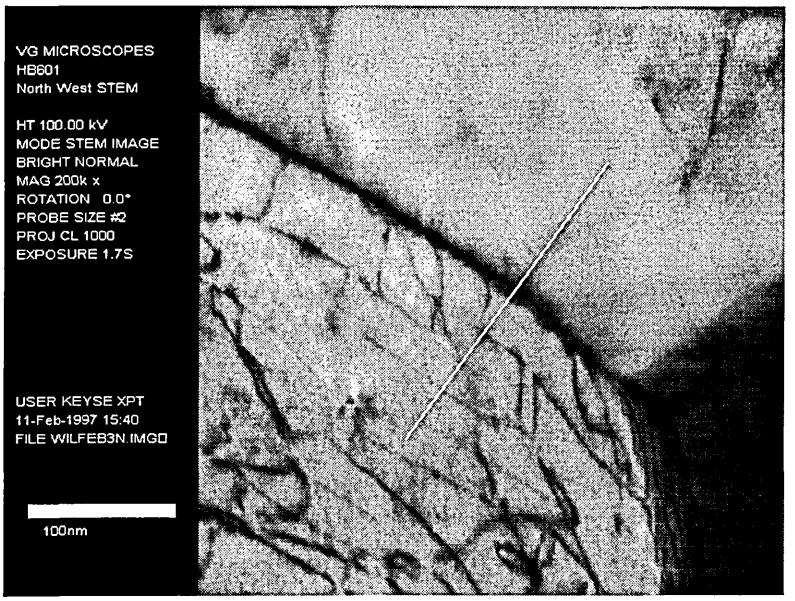

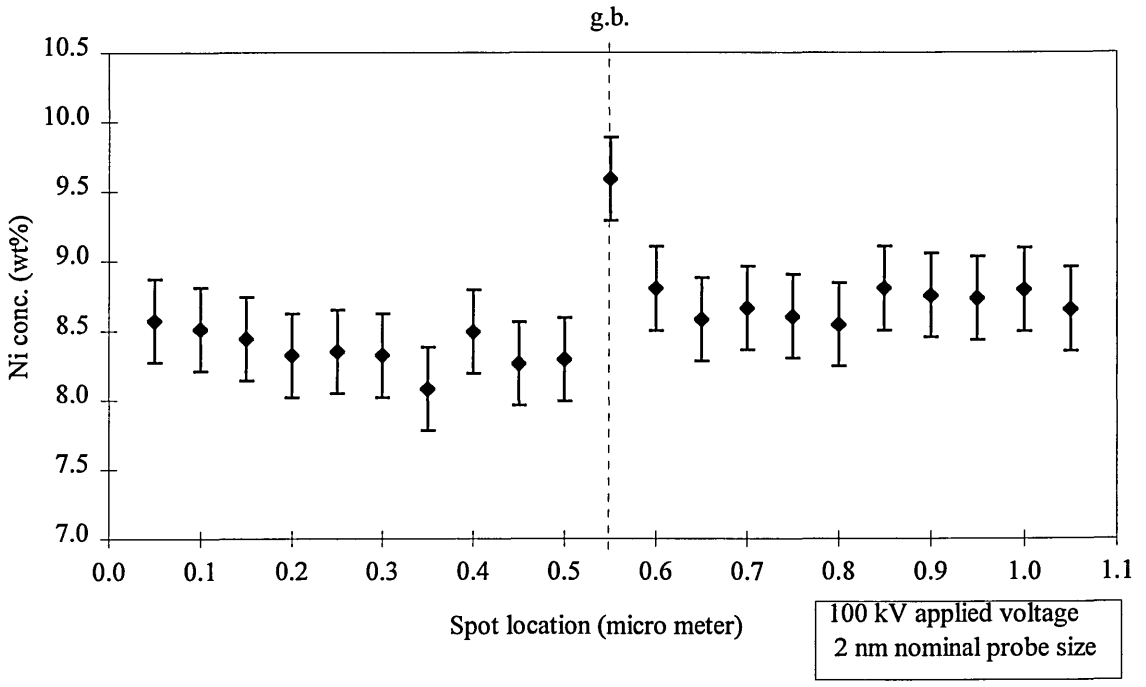

Fig. 4.41. Microanalysis by FEG-STEM showing the higher nickel content on the grain boundary from a furnace cooled Fe-9Ni alloy, VS2241A.
g.b. = grain boundary

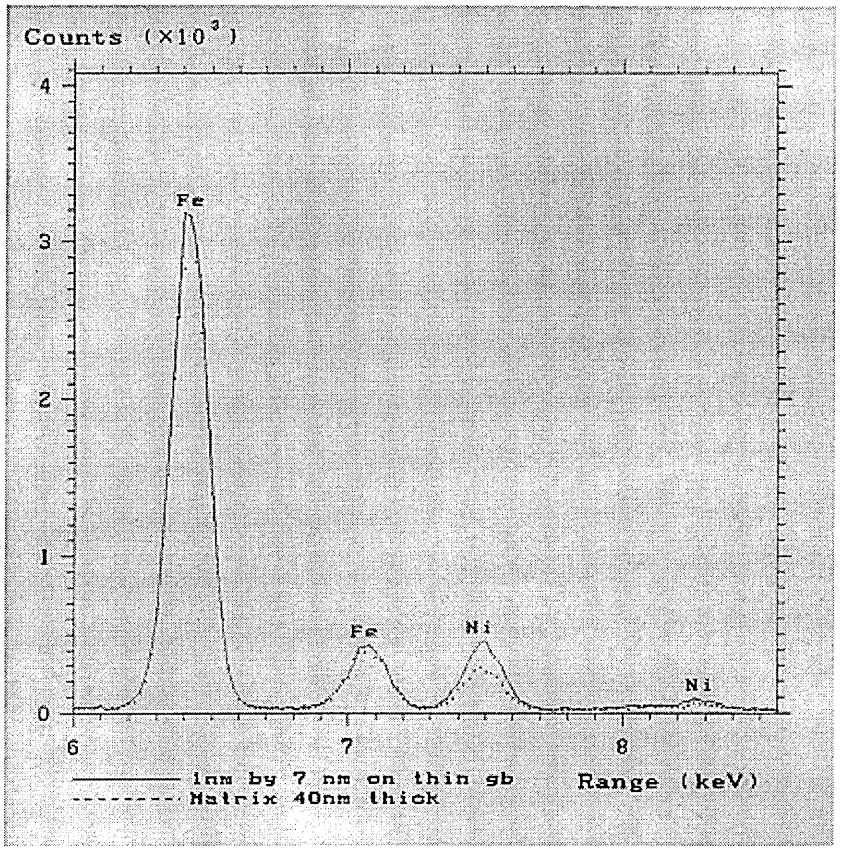

Fig. 4.42. EDX spectra showing the grain boundary and matrix composition in the furnace cooled Fe-9Ni alloy. Refer to No.8 in table 4.3.

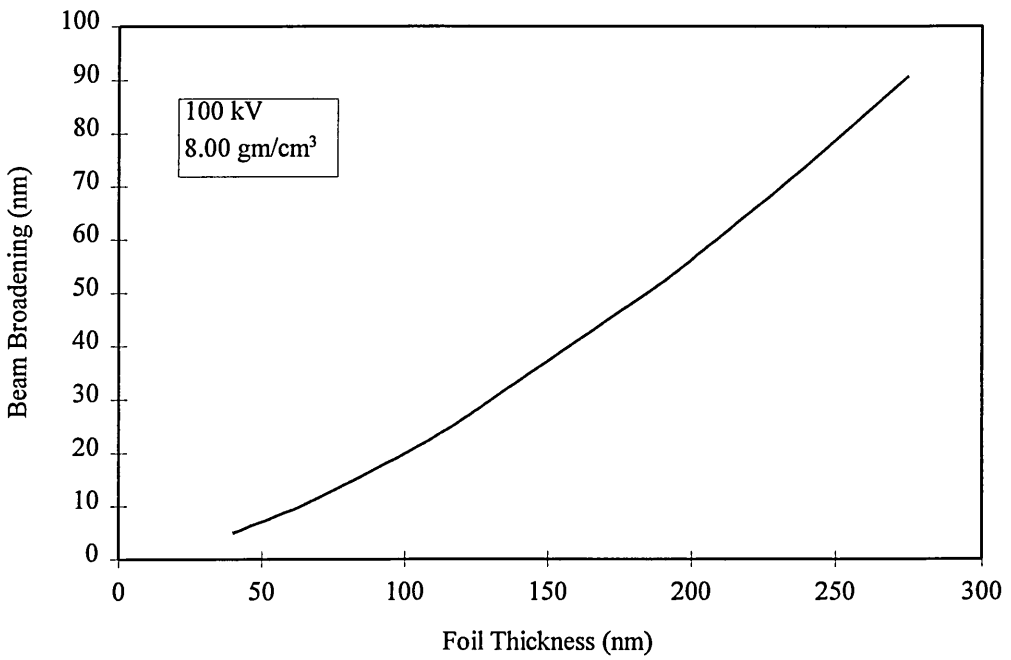

Fig. 4.43. Estimated beam broadening against foil thickness calculated from ZAF programme in VG HB601 FEG-STEM, with 2 nm probe size.

4.4. Dilatometric Analysis.

Dilatometry specimens were heated up to 1000°C and held for 20 minutes followed by cooling. Since the normal heating rate for a standard specimen is 0.83 $K.s^{-1}$ (50 $K.min^{-1}$) in the chamber, a specimen was allowed to cool at the same rate, i.e. 0.83 $K.s^{-1}$. Another specimen was allowed to cooled at the rate of 0.13 $K.s^{-1}$, corresponding to furnace cooling.

Upon heating, the change of dilatation curve was first started when austenite started to transformed, γ_s, and 25% transformation γ_{25} noted from the temperature / dilatation curve. Upon cooling, once again start temperatures α_s and temperatures corresponding to 25% transformation α_{25} were noted from the dilatation / temperature curves, see figure 4.44.

From the furnace cooled specimen, Widmanstätten laths formation with surface relief suggested that displacive transformation might have taken place during continuous cooling. Formulae which related to athermal martensite were therefore used in analysing the dilatation curve.

KOISTINEN and MARBURGER [1959] have shown for athermal martensite that the volume fraction transformed, y, at temperature T may be related to the martensite start temperature M_s by an expression of the form :-

$$y = 1 - \exp\{ \alpha (M_s - T) \} \qquad (4.1)$$

where α = constant, < 0, units K^{-1}

Rearranging and taking logarithms of equation 1 gives:-

$$\ln (1-y) = \alpha (M_s - T) \qquad (4.2)$$

By applying equation 4.2 to the present dilatometer results and it was found that -ln(1-y) did in fact vary linearly with temperature as shown in figure 4.45.

The fact that equation 4.2, originally applied to a displacive transformation (athermal martensite), applies to the present data below 558°C, figure 4.45, suggests that Widmanstätten ferrite (a reaction occuring martensitic-like, as shown by surface relief in figure 4.4(a) and 4.4(b)) is occurring in this temperature range, while massive ferrite forms in the temperature range 575 to 558°C.

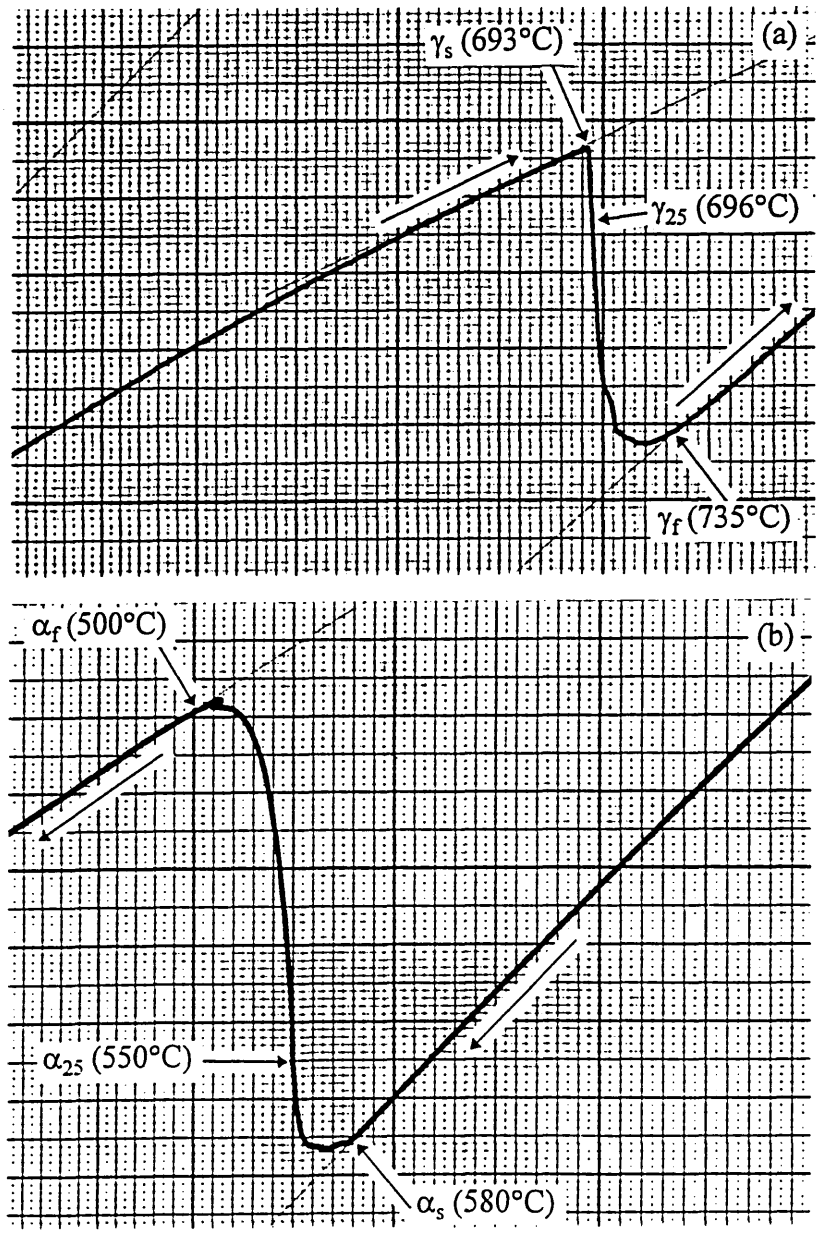

Fig. 4.44. Dilatation curves of VS2241A, Fe-9Ni alloy austenitised 20 min at 1000°C with, (a) heat rate 0.83 $K.s^{-1}$, and (b) cool rate 0.83 $K.s^{-1}$.

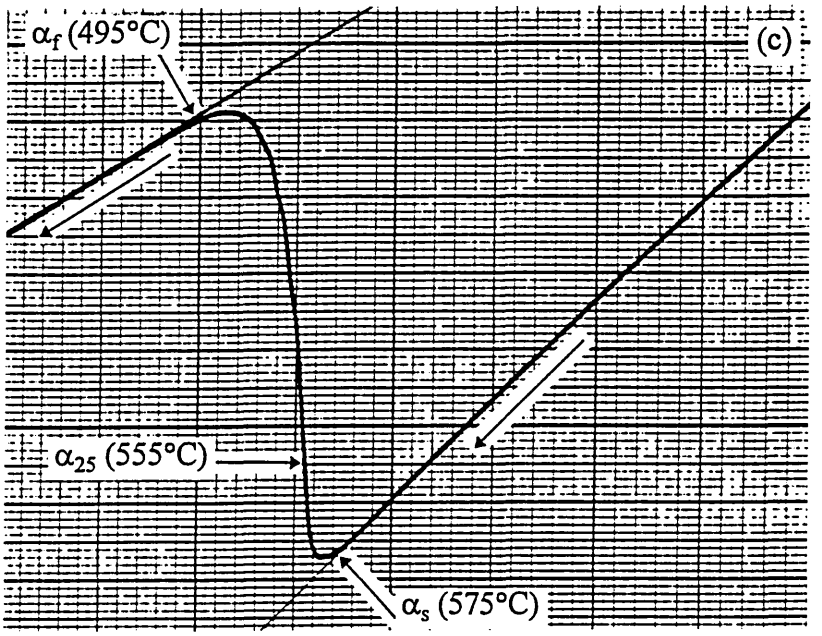

Continue:

Fig. 4.44. (c) Dilatation curves of Fe-9Ni alloy VS2241A, austenitised 20 min at 1000°C, cooled at 0.13 $K.s^{-1}$.

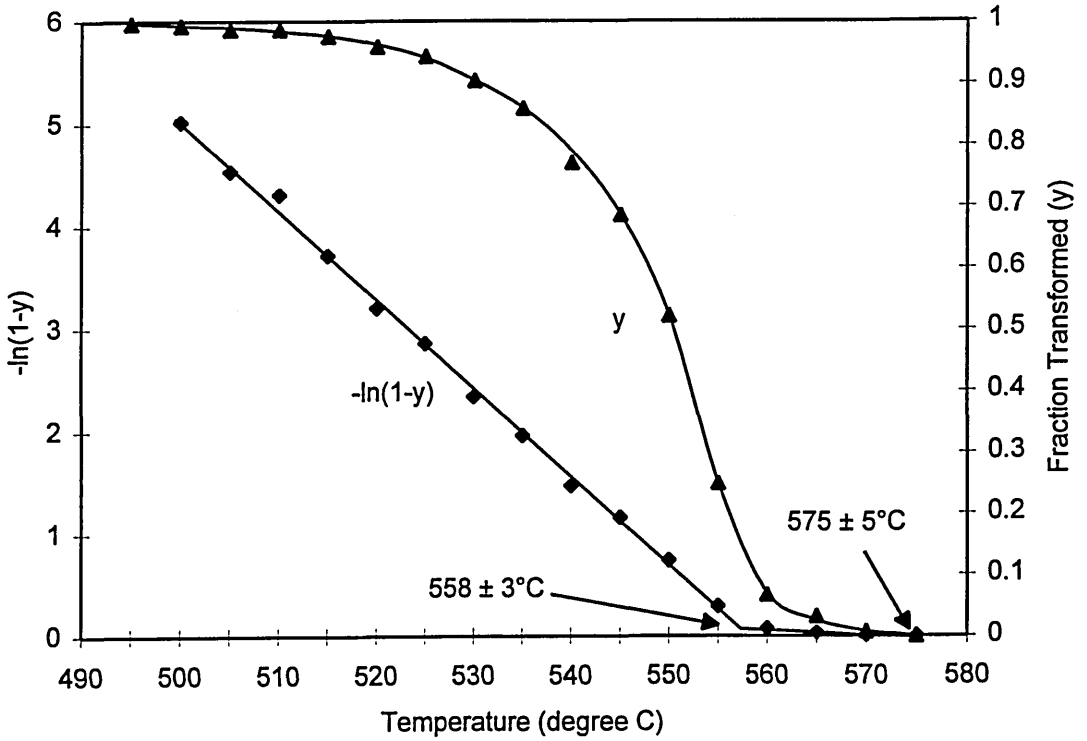

Fig. 4.45. Analysis of dilatation versus temperature curve for Fe-9Ni alloy VS2241A, austenitised 20 min at 1000°C, cooled at 0.13 $K.s^{-1}$.

4.5. Hardness

4.5.1. Hardness Results of Continuous Cooled Structures in VS2241A Fe-9Ni Alloy

Results of hardness measurement for the continuously cooled Fe-9Ni specimens are presented in figure 4.46 and table 4.4. Values obtained from both hardness and microhardness testing are fairly consistent, albeit with a larger error in microhardness results.

A particular specimen, coded 41AA in table 4.4, was subjected to air cool after long hours of austenitising treatment (microstructure refers to figure 4.10), the hardness of laths structure (Widmanstätten laths) inside this specimen is only slightly higher than the ferrite grain, but it is much lower then the laths structure (bainite or lath martensite) found in quenched specimens.

4.5.2. Hardness Results of the Isothermally Transformed Structures in VS2241A Fe-9Ni Alloys

Specimens for the second stage of experiment, isothermal transformation studies, were prepared from the homogenised block that had been heat-treated in the tube furnace instead of the sealed cast iron box. The difficulties of structural identification were mentioned in section 4.2. It was hoped that hardness measurement would provide some aid in terms of microstructural identification.

Figure 4.47 presents the microhardness results, showing the difference in hardness value of the isothermally transformed structures as compare with the quenched matrix. The matrix, which is composed of lath martensite, shows hardness values (HMV_{50} 224 maximum) much lower then the IBQ results (HMV_{50} 242 minimum) in figure 4.46, whereby the hardness of the ferrite grains (HMV_{50} 170 -178) agree well with the FC results (HMV_{50} 171.5 average). At a later stage, a specimen was quenched into iced

brine and the hardness measured was the same value as that obtained in the matrix in figure 4.47.

A plausible explanation for the hardness differences in iced brine quenched lath martensite from the first batch and second batch of materials is probably due to the minor difference in carbon (and / or nitrogen) content from these two different piece of homogenised blocks. A previous piece of Fe-9Ni block (used in continuous transformation experiments) contains slightly higher carbon then the later piece. The fact that M-A constituent (figure 4.9) is found in continuous cooling experiment supports this assumption.

At 535°C, isothermally transformed structures consisted of Widmanstätten laths and massive ferrite as described in section 4.2. Hardness of these structures is presented in figure 4.47. Massive ferrite in this case was identified by the hardness value, i.e. HMV_{50} 170. Hardness of Widmanstätten laths (HMV_{50} 205), was found to be very close to the quenched matrix.

At higher degree of undercooling, hardness measurement became meaningless in distinguishing the different microstructures. The hardness of the isothermally transformed Widmanstätten laths with higher undercoolings was found to be almost the same as the quenched matrix.

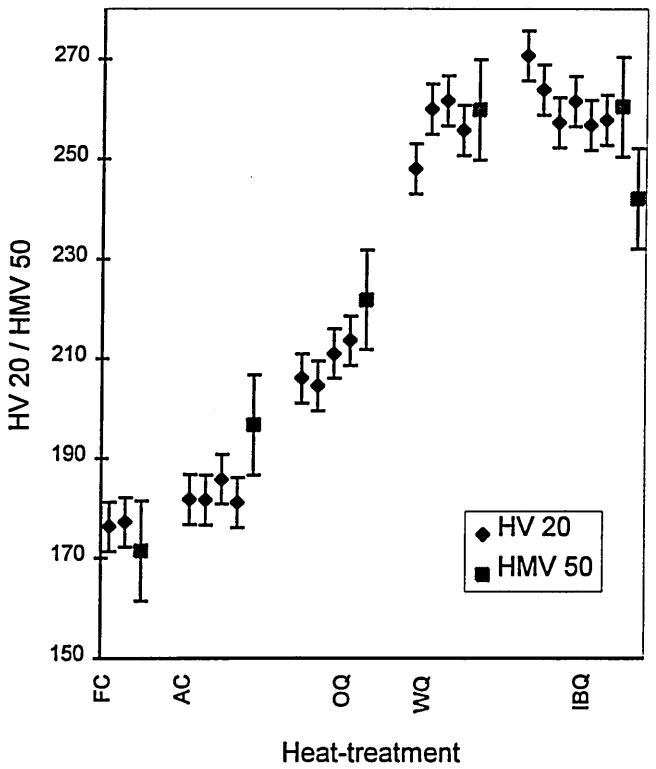

Fig. 4.46. Hardness diagram of Fe-9Ni alloy, VS2241A. Specimens subjected to continuous cooling transformation at different cooling rates.

Table 4.4. Hardness measurement of continuously cooled Fe-9Ni alloy, VS2241A samples.

Heat-treatment (main microstructure)	Sample	Hardness Value			
		20 kgf	Indent. No.	50 gf	Indent. No.
1000°C, 20 min, FC (massive ferrite)	907 (surface)	176.3 ± 3.3	12	171.5 ± 11.7	8
	907 (centre)	177.2 ± 3.0	12		
1000°C, 20 min, AC (massive ferrite)	942 (surface)	181.8 ± 4.6	11		
	942 (centre)	181.6 ± 6.9	12		
	912 (surface)	185.8 ± 5.2	11		
	912 (centre)	181.1 ± 6.0	10	196.7 ± 12.8	9
1000°C, 20 min, OQ (bainite)	944 (surface)	206.0 ± 5.2	10		
	944 (centre)	204.5 ± 3.8	10	221.8 ± 17.9	9
	947 (surface)	211.0 ± 7.9	10		
	947 (centre)	213.6 ± 8.5	10		
1000°C, 20 min, WQ (bainite)	96 (surface)	248.0 ± 5.8	8		
	96 (centre)	259.9 ± 2.9	8	259.8 ± 6.9	4
	911 (surface)	261.6 ± 4.7	12		
	911 (centre)	255.7 ± 2.6	12		
1000°C, 20 min, IBQ (lath martensite)	906 (surface)	270.6 ± 3.3	9		
	906 (centre)	263.8 ± 6.0	9		
	940 (surface)	257.2 ± 3.8	10		
	940 (centre)	261.5 ± 3.5	10	242.1 ± 12.7	7
1150°C, 20 min, IBQ (lath martensite)	908 (surface)	256.7 ± 3.0	8		
	(centre)	257.8 ± 3.9	10	260.4 ± 11.3	8
1200°C, 4 day, AC (Widmanstätten ferrite + massive ferrite)	41AA (surface)	161.6 ± 2.3	9	190.6 ± 10.3[a]	8
				158.3 ± 7.4[b]	7

NB: [a] Widmanstätten laths

[b] ferrite grains

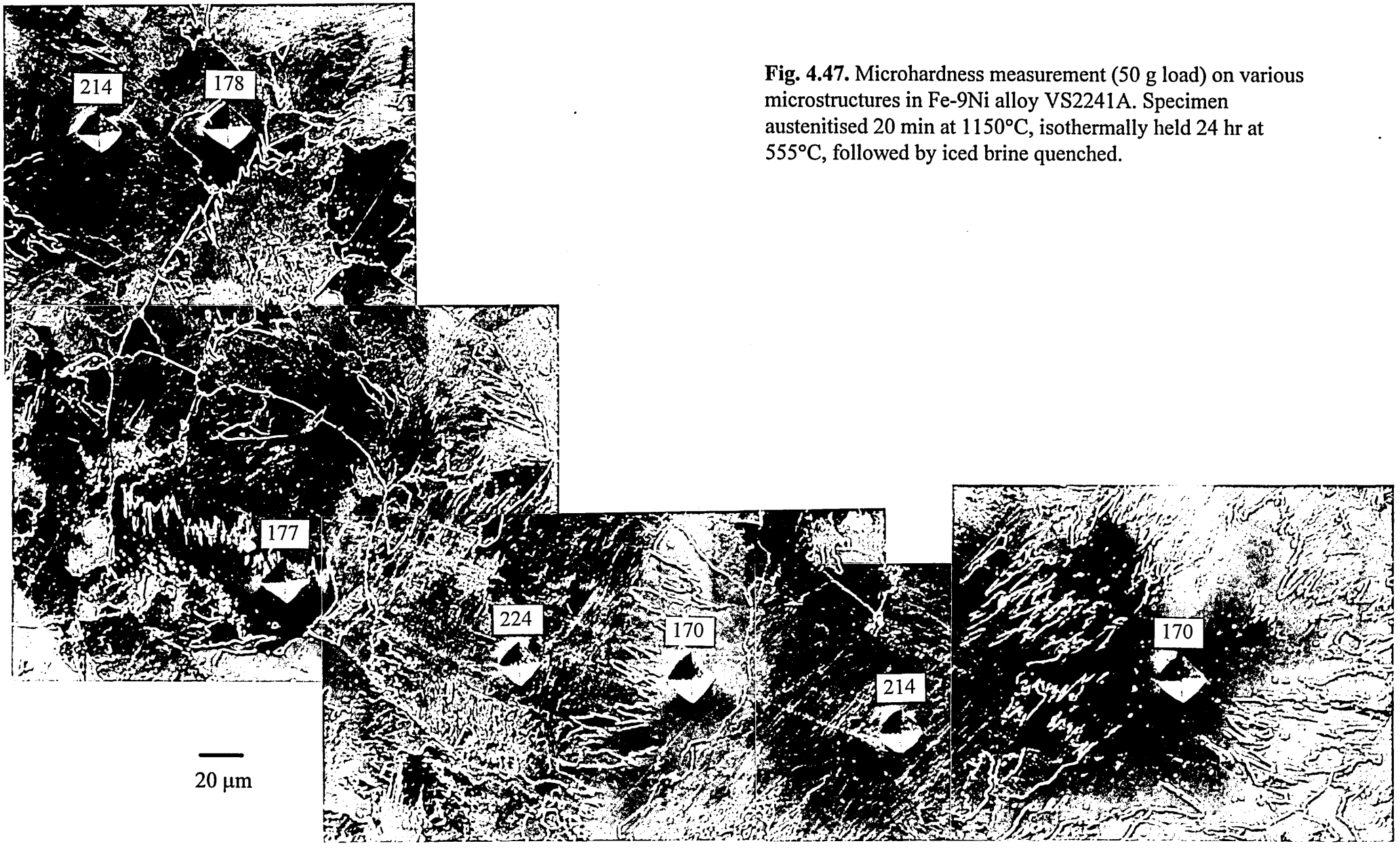

Fig. 4.47. Microhardness measurement (50 g load) on various microstructures in Fe-9Ni alloy VS2241A. Specimen austenitised 20 min at 1150°C, isothermally held 24 hr at 555°C, followed by iced brine quenched.

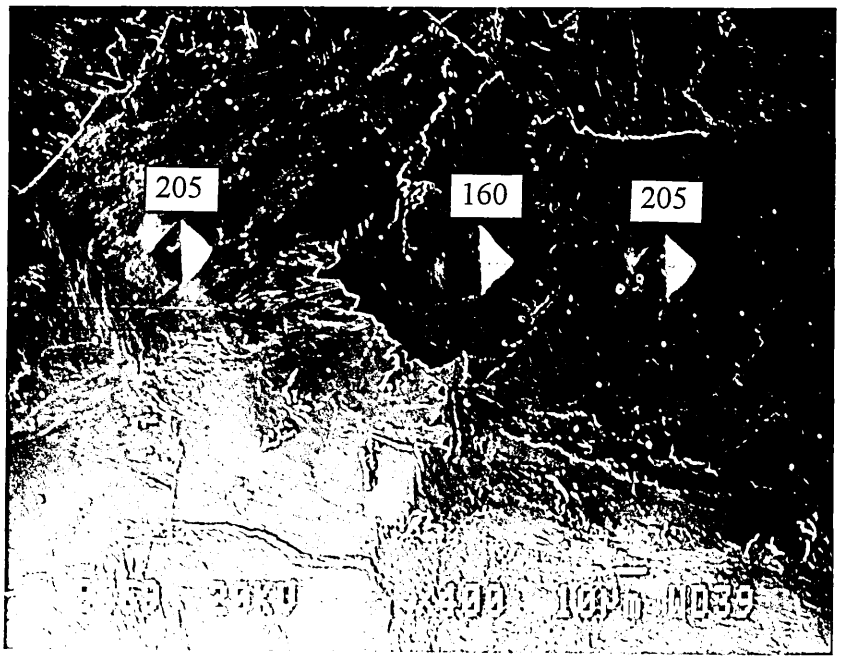

Fig. 4.48. Microhardness testing on the transformed structures in a specimen austenitised 20 min at 1150°C, isothermally held 2 min at 535°C.

5. Microstructural Observation on Other Materials

5.1. Air Cooled Fe-3.5Ni

In addition to the microstructural inspection of Fe-9Ni alloy, some studies were carried out on Fe-3.5Ni alloy, VS2239A. The chemical composition of this alloy is listed in table 3.2.

Continuous cooling experiments as described in section 3.2 was performed on this material. Air cooling indicated a thermal arrest at 707 ± 5°C at cooling rate of 4.4 $K.s^{-1}$. Thermal arrest result indicated transformation started below the α / γ + α line in figure 2.2, i.e. in the single phase region.

Equiaxed ferrite was obtained on air cooling, as shown by optical micrograph, figure 5.1(a) and TEM picture, figure 5.1(b). Equiaxed ferrite structure in this material showed smooth grain boundaries in contrast to the undulating and ragged boundaries of massive ferrite in Fe-9Ni alloy. This structure is much the same as the carbon depleted ferrite grains of proeutectoid ferrite. Compared with the ferrite grains from furnace cooled Fe-9Ni alloy, these equiaxed grains contain a lower dislocation density. Also note the absence of substructure inside the equiaxed grains.

No results were obtained from the water quenched experiments and therefore there was no further investigation on this material.

(a) 20 μm

(b) 2 μm

Fig. 5.1. Equiaxed ferrite in air-cooled Fe-3.5Ni alloy, VS2239A; (a) optical micrograph, 2 % nital etched, and (b) TEM picture.

5.2. Iced Brine Quenched Fe-4Cu

This material, Fe-4Cu alloy, had been studied by WILSON [1968]. Only an optical micrograph of the massive ferrite was presented in this reference and no further detailed work was carried out on this alloy. The same alloy was used again to reproduce the same microstructure by applying the same heat-treatment parameters mentioned in this reference.

A piece of Fe-4Cu plate with 5 mm thickness was subjected to 1050°C austenitising temperature in tube furnace for 3 days followed by iced brine quenching. The transformed structure is shown in figure 5.2. The etching reaction on this alloy was so rapid that only very dilute nital (1/2%) needed to reveal the microstructure. Ragged boundaries of massive ferrite predominate. Lath martensite or bainitic ferrite could only be found in a very small proportion at the edge of the specimen.

It was suspected that the transformed structures could be hidden by the darkening effect of the nital etch. Using cotton dipped with 2 % nital and mopped across the fined polished surface, the etched microstructures were then exposed, as shown by SEM micrograph, figure 5.3. It was found that Widmanstätten ferrite also present, which was lighter and therefore not revealed by light etching.

Figure 5.4(a) present the TEM montage of massive ferrite structure in this specimen. Due to long period of austenitising treatment, the grains are fairly large. A particular region showing irregular type of grain boundary is shown at higher magnification, figure 5.4(b). Electron diffraction, figure 5.4(c), indicates that these two adjacent grains are misoriented with 6°.

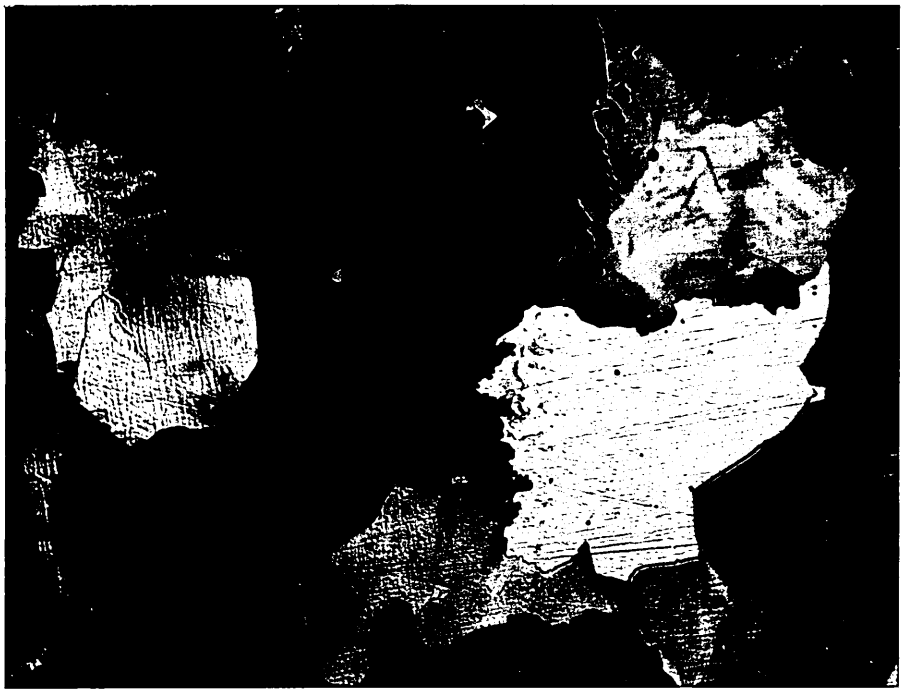

Fig. 5.2. Massive ferrite in an iced brine quenched Fe-4Cu alloy, austenitised 3 days at 1050°C, 1/2 % nital etched.

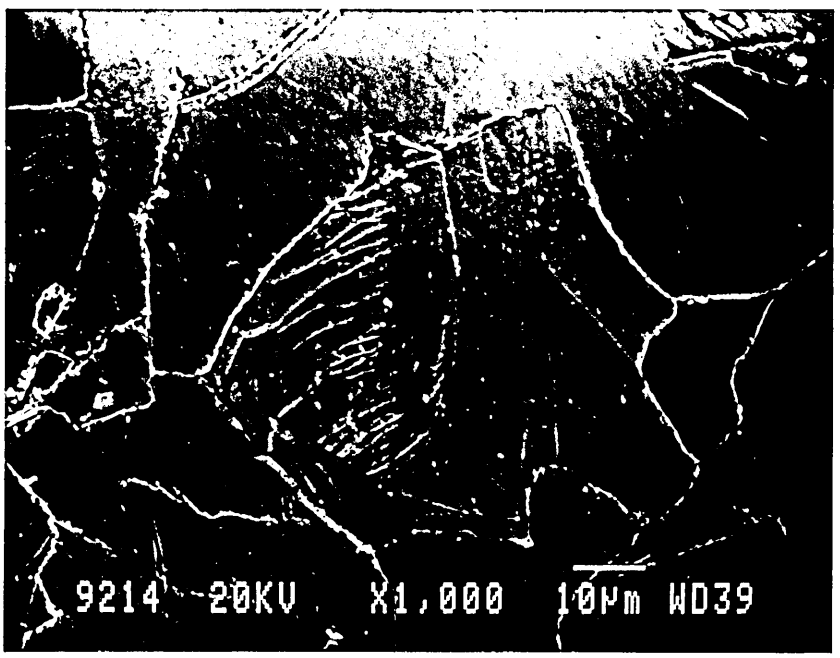

Fig. 5.3. Widmanstätten structure found in iced brine quenched Fe-4Cu alloy, austenitised 3 days at 1050°C, 2 % nital etched.

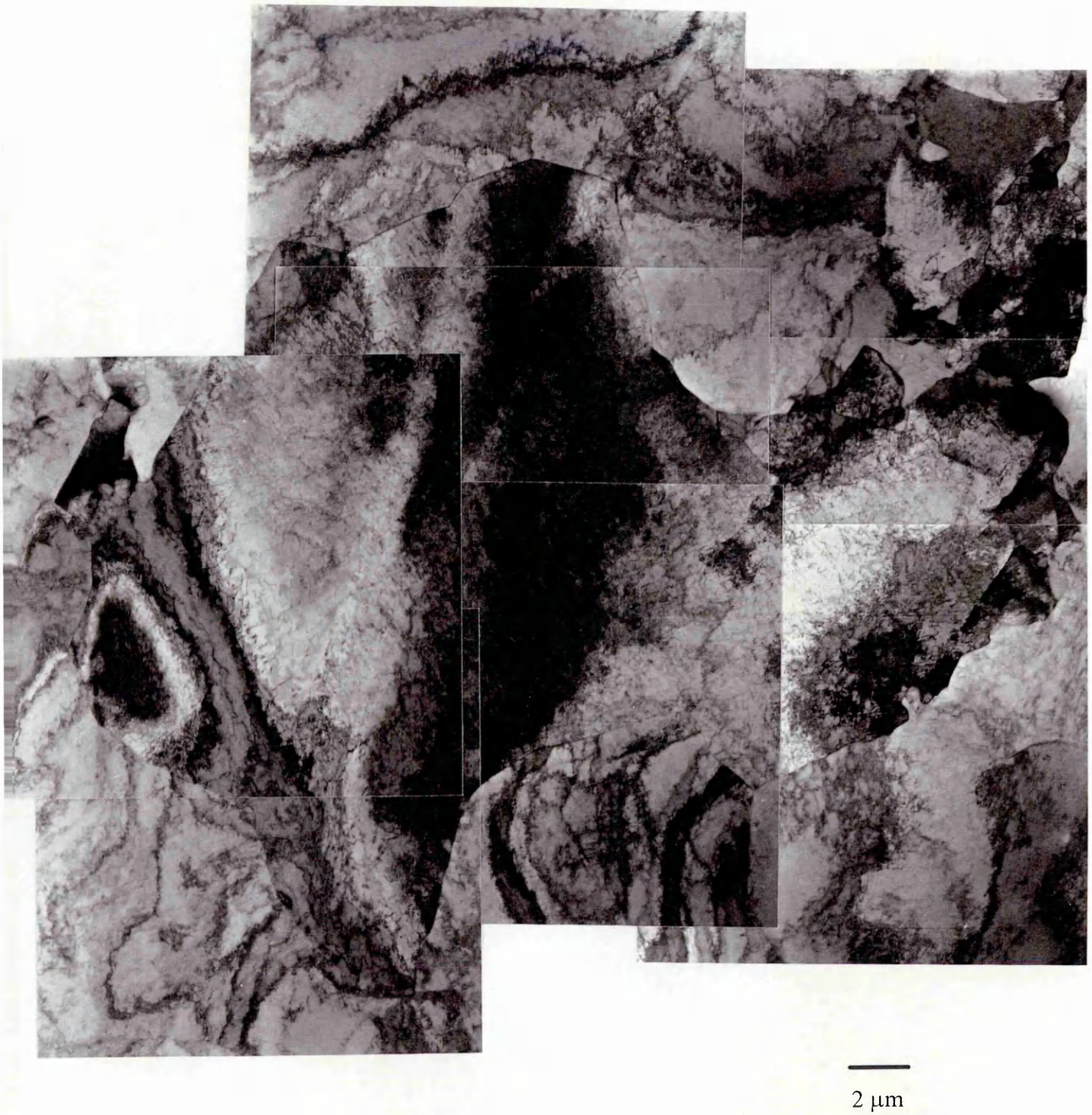

Fig. 5.4.(a) TEM montage of massive ferrite structure in Fe-4Cu alloy, austenitised at 1050°C for 3 days followed by iced brine quenched.

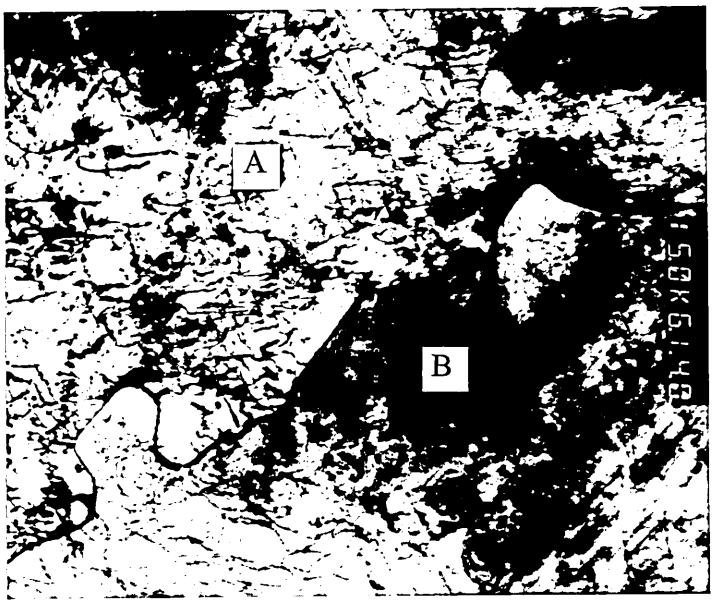

(b) 1 μm

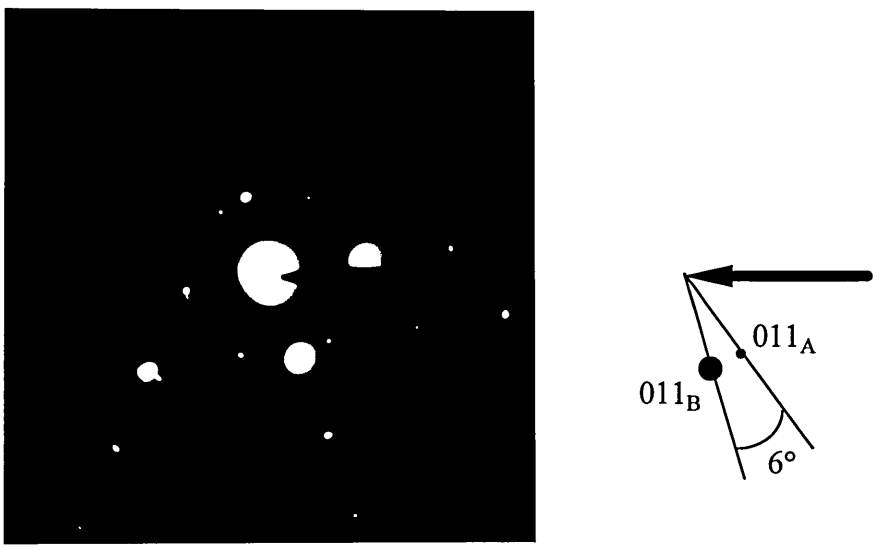

(c)

Continue:

Fig. 5.4. (b) Irregular grain boundary of the massive ferrite, (c) electron diffraction pattern of two adjacent grains.

6. Discussion

6.1. Transformation Start Temperature of Various Structures in Fe-9Ni Alloy Upon Continuous Cooling

It was mentioned in the section 3.1 that because the thermal arrest experiments were not carried out using the dedicated quenching chamber used by previous workers, the thermal arrest results obtained from continuos cooling experiments shown in table 4.1, require careful diagnosis to evaluate their degree of fruitfulness.

Transformation temperatures of various structures in Fe-Ni alloys for 9 % nickel were interpolated from the rationalised diagrams constructed by different parties, listed in table 6.1. Particular attention was paid to Goodenow and Hehemann's work [GOODENOW and HEHEMANN 1965] as their results were obtained directly from experimental work using 9 % nickel, figure 6.1.

Plateau IV, which is referred to as twinned martensite transformation, was not obtained in the present work. Extremely high cooling rate would be needed to allow twinned martensite transformation to take place. Specimen designed for use in the present work, figure 3.1 would not be able to achieve the high cooling rate necessary to suppress the transformation of lath martensite. The lowest transformation arrested in present work, 384°C, obtained by iced brine quenching, agree with the temperature of plateau III, refers to lath martensite transformation. IBQ specimens show blocky structure under optical microscope, figure 4.13(a), representing a packet of lath martensite. Each packet or block consists of a group of laths aligned in parallel, separated by low angle boundary, whereby individual block can be distinguish because of different orientation with the adjacent blocks. The etching reagent Sodium metabisulphide ($Na_2S_2O_5$) can be used to enhance the appearance of the blocky structure. The feature of lath martensite in Fe-Ni alloys had been described in detail by MARDER and MARDER [1969] and identical features are observed in the IBQ specimen confirming the presence of lath martensite. Transmission electron microscopy inspection did not find any twinned martensite.

Table 6.1. Transformation temperatures of Fe-9Ni reported by various workers.

Plateau	WILSON [1984]	BORGENSTAM and HILLERT [1996]	ZHAO [1992]	MIRZAYEV et al [1973]
I	532°C	520°C	524°C	537°C - 508°C
II	440°C	437°C	420°C	-
III	382°C	380°C	393°C	356°C
IV	318°C	326°C	310°C	322°C

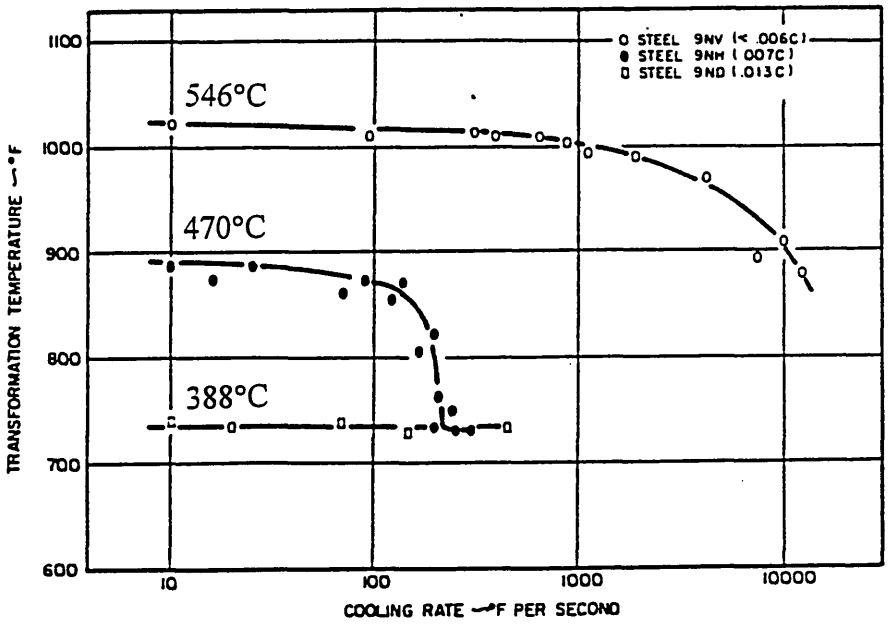

Fig. 6.1. Plateaux temperatures obtained by GOODENOW and HEHEMANN [1965] in various Fe-9% Ni alloys of different carbon content.

Thermal arrest results for OQ and WQ again agree with the temperature of plateau II. Plateau II is generally regarded as a bainitic transformation. Bainitic transformation for plateau II is evident by the lath formation. With the absence of carbide precipitation, the bainitic structure is very similar to lath martensite.

Under optical microscope, planar boundaries are revealed by nital etching. Picral etch on the other hand, produces different appearance by revealing prior austenite grain boundaries, and the laths parallel with the surface of the specimen are exposed, but not exhibiting blocky appearance like martensitic structure. Interestingly, $Na_2S_2O_5$ etching reagent, can be used to enhance the laths appearance of lath martensite, but can not produce the same effect on the bainitic ferrite. The differences in etching reaction for bainitic laths as compare with lath martensite indicate that these two structures transform by different mechanism, and therefore react differently with the same etching reagents.

Transformation plateaux of II, III refer to bainitic ferrite and lath martensite formation respectively are generally in agreement with researchers from different schools. However, discrepancies arise in discussing plateau I transformation. It is generally perceived that a massive transformation is responsible for the formation of plateau I. Thermal arrest of 555°C and 535°C for the FC and AC experiments fall into this category. WILSON [1984, 1994] believed that equiaxed ferrite and massive ferrite could be distinguished in the massively transformed structures and therefore two plateaux should exist. GOODENOW and HEHEMANN [1965] reported acicular structure for the transformation arrested at 548°C. BORGENSTAM and HILLERT [1996] favour plateau I as being due to Widmanstätten ferrite. MOISEYEV et al [1981] reported irregular shape of ferrite grains with high dislocation density and "comb" type of structures.

The actual plateau I temperature for this alloy, VS2241A has not been determined in the present studies. However, because bulk specimens were used in the present work, thorough examination on the transformed structures was feasible. All the transformed structures mentioned by different workers above were indeed observed in present work. Mixed structure of massive ferrite and Widmanstätten structure (comb and lath) were identified, taking place in this transformation temperature range.

It was also found that austenitising condition played an important role in determining the presence of transformed structures. High austenitising temperatures or long holding period produced large austenite grain size, as a consequence, promoting Widmanstätten lath formation, and vice versa for the ferrite grains, even if the same cooling rate was

applied. Apparently, the factor of austenitising condition and hence the austenite grain size, has been neglected while comparing the results from different workers. This led to dispute in observing different structures for the same material.

6.2. A_3 and T_0 Temperature of Fe-9Ni Alloy, VS2241A

The A_3 line represents the solvus line separating γ / $\alpha + \gamma$. Referring to ROMIG AND GOLDSTEIN [1980], figure 2.2 and SWARTZENDRUBER et al [1991], figure 2.3, a value of 711 ± 12°C represents the A_3 temperature for the alloy in this studies.

T_0 can be defined as temperature at which metastable austenite and metastable ferrite of the same composition are in metastable equilibrium [ZENER 1946; KAUFMAN and COHEN 1956]. Martensitic and massive transformations involving a composition invariant process must occur at temperatures below T_0. T_0 can be determined experimentally from the following expression [KAUFMAN and COHEN 1956; WILSON 1965]:

$$T_0 = 1/2\ (\alpha_f + \gamma_f) \qquad (6.1)$$

where α_f = temperature for the $\gamma \rightarrow \alpha$ transformation to produce fraction f transformation product without change in composition.

γ_f = temperature for the reverse transformation, $\alpha \rightarrow \gamma$ under the same conditions as for α_f.

From the dilatation curves in figure 4.43(a) & (b), in which the specimens were subjected heating and cooling at the same rate, the 25% of transformation upon heating (γ_{25}) and cooling (α_{25}) were found to be 696°C and 550°C respectively. Applying equation 6.1, a value of 623 ± 5°C was therefore obtained representing T_0 temperature with f = 0.25. Comparing the interpolated values from Fe-Ni diagrams drawn by various parties, we obtained 621°C from JONES and PUMPHREY [1949] with f = 0.10; 616 ± 5°C ($1/2(\alpha_s + \gamma_s)$) from WILSON [1965] for Fe-9.57 at.% Ni; 627°C from

SWARTZENDRUBER [1991]. Apparently, the experimental T_0 value of 623 ± 5°C in the present work is in good agreement with other workers.

The theoretical T_0 determined from thermodynamic data can vary significantly from the experimental values given above, being very dependent on the value of $\Delta G_{Fe}^{\gamma\rightarrow\alpha}$ used in the free energy calculation. The chemical driving force for the $\gamma \rightarrow \alpha$ transformation for Fe-Ni binary system is given by:

$$\Delta G^{\gamma\rightarrow\alpha} = (1-X)\Delta G_{Fe}^{\gamma\rightarrow\alpha} + X\Delta G_{Ni}^{\gamma\rightarrow\alpha} + \Delta G_m^{\gamma\rightarrow\alpha} \quad (6.2)$$

where $\Delta G_{Fe}^{\gamma\rightarrow\alpha}$ = chemical driving force for $\gamma \rightarrow \alpha$ transformation in pure iron

$\Delta G_{Ni}^{\gamma\rightarrow\alpha}$ = hypothetical chemical driving force for fcc → bcc transformation of nickel.

$\Delta G_m^{\gamma\rightarrow\alpha}$ = free energy of mixing for Fe-Ni transformation.

X = atomic fraction of nickel.

For a transformation without change in composition, KAUFMAN and COHEN [1956] derived the following parameters:

$$\Delta G_{Ni}^{\gamma\rightarrow\alpha} = 3700 - 7.09 \times 10^{-4} T^2 - 3.91 \times 10^{-7} T^3 \text{ cal.mol}^{-1} \quad (6.3)$$

$$\Delta G_m^{\gamma\rightarrow\alpha} = -X(1-X)[3600 + 0.58T(1 - \ln T)] \text{ cal.mol}^{-1} \quad (6.4)$$

where T is the transformation temperature in kelvin.

There are three sources from which the data for $\Delta G_{Fe}^{\gamma\rightarrow\alpha}$ can be obtained, i.e.:
(i) reference KAUFMAN, CLOUGHERTY and WEISS [1963],
(ii) $\Delta G_{Fe}^{\gamma\rightarrow\alpha} = -1474 + 3.4 \times 10^{-3} T^2 - 2 \times 10^{-6} T^3$ [GILBERT and OWEN 1962], or
(iii) $\Delta G_{Fe}^{\gamma\rightarrow\alpha} = -1202 + 2.63 \times 10^{-3} T^2 - 1.54 \times 10^{-6} T^3$ [KAUFMAN and COHEN 1956].

Ignoring the minor elements in VS2241A alloy, we take the chemical composition of VS2241A alloy as Fe- 8.74 at.% Ni, and substitute the X value with the atomic fraction of nickel element, i.e. 0.0874 in equations 6.2, 6.3 and 6.4.

Various $\Delta G^{\gamma \rightarrow \alpha}$ against transformation temperature for Fe-8.74 at.% Ni were calculated and drawn in figure 6.2. T_0 temperatures correspond to $\Delta G^{\gamma \rightarrow \alpha} = 0$ were obtained from this plot. Value of 577°C, 596°C and 603°C were found for (i), (ii), and (iii) respectively.

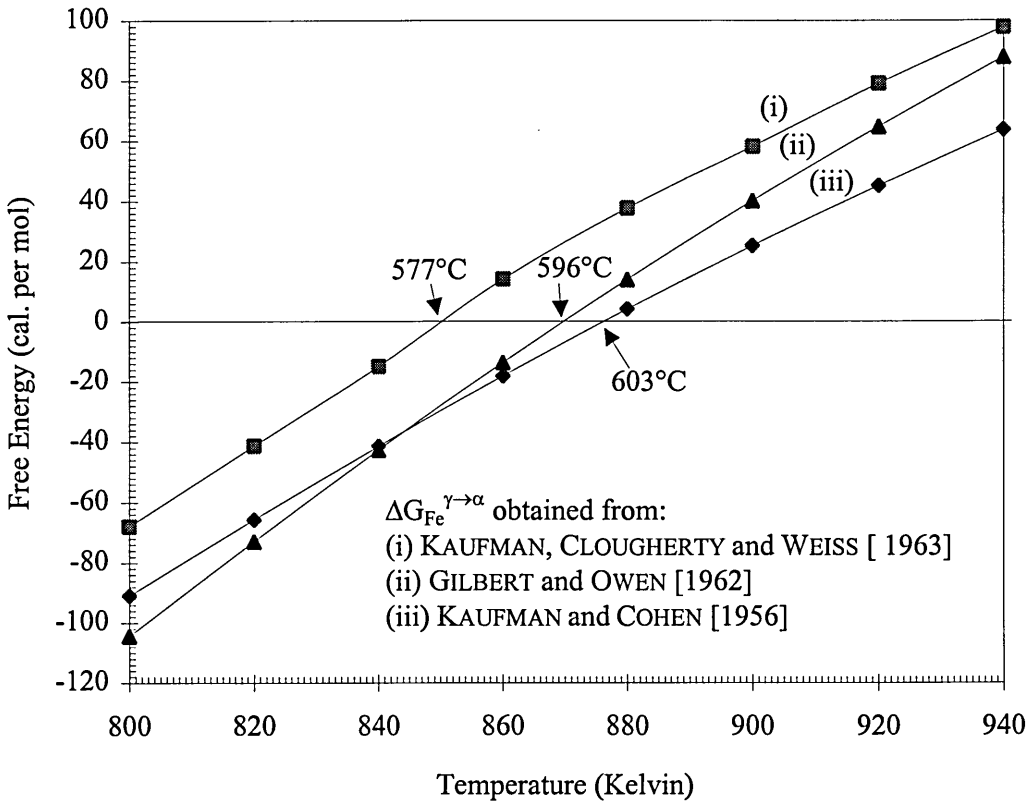

Fig. 6.2. Chemical driving force versus temperature for composition invariant transformation in Fe-8.74 at.% Ni binary alloy.

Thus the theoretical estimates of T_0 differ appreciably from the experimental values. However, the most recent data of 614 ± 5°C from BORGENSTAM and HILLERT [1997] is probably the best theoretical estimate of T_0 for Fe-8.74 at.% Ni. This data was derived from the thermodynamic data bank of The Steel Research Group Martensite Database, Northwestern University.

In spite of these different values of T_0, the data confirm that the massive ferrite transformation occurs in the two phase field and below A_3 and T_0.

Dilatometric analysis suggested that massive ferrite transformation occurred in the temperature range 575 - 558°C on continuous cooling, whilst microstructural observation from isothermal transformation studies suggested the temperature range of 565 - 535°C. The lower transformation range in the later case can be explain by the fact that higher austenitising temperature (1150°C) was applied for the isothermal transformation studies and as a consequence, suppressed the transformation start to lower temperatures.

6.3. EDX Microanalysis on Massive Ferrite Grains

The fact that there was no change in composition profile across the grains from both continuously cooled structure, figure 4.36 and isothermally transformed structures, figure 4.37 proved that transformation did indeed take place with the absence of redistribution of substitutional element.

The higher nickel content on the ferrite grain boundaries can be detected only by FEG-STEM with 2 nm probe size but not with TEM Philips CM20 of 20 nm probe size means that the segregation of nickel on the grain boundaries is only within a very narrow band width.

SKOGSMO and ATRENS [1993] suggested the proportion of X-rays signal obtained from the grain boundary region can be improved by reducing foil thickness and incident electron probe size and increasing electron accelerating voltage. For the dedicated FEG-STEM system developed to date, 2 nm probe size is considered as the optimum condition and anything smaller this that would not improve the performance from statistical point of view [TITCHMARCH 1997]. From the present work, the optimum result was obtained by selecting the thinnest region, usually the region adjacent to the perforated hole. This would minimise the astigmatism (since the material is magnetic) and the beam broadening is minimised. X-rays signal collected would be more representative as localised area covered, albeit with a higher experimental error.

In the case of equilibrium segregation on the grain boundaries, the solute element would be concentrated to a few atomic layers, i.e. about 1 nm. It means the area covered by the electron beam would always be wider than the width of the grain boundary. The true concentration at the grain boundary is therefore always higher for segregated elements or lower for the desegregated elements.

The massive transformation can be regarded as a process involving short range diffusion whereby the moving of the growing phase is by atomic jumps across the massive / matrix interface. It is assumed that moving interfaces are incoherent type of boundaries [MASSALSKI 1958, 1970]. A composition spike might exist along with the moving interface as far as diffusional process is concerned; the higher the growth rate, the thinner is the spike [HILLERT 1975]. In addition to that, solute drag effort would be quite significant due to the large composition change during the trans-interphase diffusion for Fe-9Ni binary alloy [JÖNSSON 1990].

The study of the solute atoms at the γ / α interface became possible only when the microprobe was developed. Using STEM-EDX with 10 nm diameter electron probe, RICKS et al [1981] discovered the nickel and chromium enrichment at the equiaxed ferrite / lath martensite interface in partially transformed Fe-7Cr-2Ni. Limited by the relatively large electron beam as compared with the grain boundary, the difference between the grain boundary and the matrix were just outside the experimental error, table 6.2. These workers tentatively suggested that solute drag effect are likely to take place in the ferrite transformation of carbon free iron alloys.

With the latest development of field emission gunned FEG-STEM used in the present work provide much higher resolution (2 nm probe size contain 90% of the beam current). It allows better results to be achieved as compared with Ricks et al's work which conventional thermionic emission gunned STEM was used. Nickel enrichment on the grain boundary as high as 12.98 ± 0.43 wt.% was detected (matrix 8.81 ± 0.40 wt.%). It is now proven that decomposition of austenite by a composition invariant massive transformation, is *not* by all means a "diffusionless" process.

Table 6.2. Microanalysis at the ferrite-martensite interface in a Fe-7Cr-2Ni alloy isothermally transformed 30 min at 640°C. After RICKS et al [1981].

		Cr (wt.%)	Ni (wt.%)
Region I	Matrix	7.8 ± 0.2	2.1 ± 0.2
	Interface	8.2 ± 0.2	2.2 ± 0.3
Region II	Matrix	7.2 ± 0.2	2.1 ± 0.2
	Interface	7.8 ± 0.2	2.7 ± 0.2

However, 2 nm diameter of the electron beam would still be larger than the width of the grain boundary, and the inevitable beam broadening would result in a lower experimental value than the actual. According to the local equilibrium model, composition spike would exist in front of the growing interphase, solute drag effect resulted and slowed down the speed of grain boundary propagation. Ideally, since cooling rate as low as 0.13 $K.s^{-1}$ initiated the transformation start at 575°C for the ferrite formation upon furnace cooling, nickel content as high as 22.3 wt.% at the peak of the spike could form, 22.3 wt.% Ni being the A_3 composition at 575°C.

Nickel enrichment was not detected in all chosen boundaries suggesting that the growth of massive phase is unidirectional. The chosen boundaries might be of the product of high growth rate but weak solute drag type of massive phase, rather than the product of low growth but strong solute drag effect, as predicted by JÖNSSON and ÅGREN [1990]. It has been reported that no nickel enrichment was detected on the grain boundaries by FEG-STEM in an air-cooled Fe-3Ni alloy [VORLICEK and FLEWITT 1994]. Thermal arrest of air-cooled Fe-3.5Ni of the present observation (section 5.1) suggested that the massive ferrite transformation in this case thought to be equiaxed ferrite, take place in the single phase region on air cooling. Therefore, nickel enrichment would not be detected on the grain boundaries of this massive structure due its high growth rate and weak solute drag effect with a very thin spike on the growing interphase [JÖNSSON and ÅGREN 1990].

6.4. Hardness Testing

In the case of ultra low carbon steels, bainitic ferrite appears in various morphologies under optical microscopy, and is only distinguishable from lath martensite by microhardness testing as lath martensite would be significantly harder [SHIBATA and ASAKURA 1995].

However, when microhardness testing was applied in the present studies, bainitic laths of WQ specimens were essentially the same hardness as the IBQ lath martensite. Widmanstätten laths from AC specimens, on the other hand, showed considerably lower hardness values.

Compared with the martensite in continuously cooled specimens, results from the isothermally transformed specimens show much lower hardness value on the martensitic structure. In addition to that, the hardness of Widmanstätten laths isothermally transformed at 495 - 535°C temperature range is almost the same as the martensite matrix.

Different part of the ingot was cut out and subjected to different method of homogenisation treatment for different experiment. It can therefore be assumed that different IBQ hardness from the first batch specimens for continuous cooling experiment and the second batch for the isothermal transformation experiment is because of different carbon (or / and nitrogen) levels, being higher in the first batch. The chemical composition of Fe-9Ni alloy, VS2241A as shown in table 3.2 was analysed using sample taken from the first homogenised block.

The same hardness from WQ and IBQ implies that both bainitic ferrite and lath martensite are saturated with the interstitial element (C and N), this result is in contradiction to Shibata and Asakura's work. Hardness of bainitic ferrite from OQ specimen is significantly lower than the WQ bainitic lath due to lower cooling rate for OQ, allowing the bainitic laths to recover, and therefore contain lower dislocation density. Referring to ISIJ nomenclature, bainitic ferrite from WQ and OQ would be categorised differently as α°_{B} and α_{B} respectively [ARAKI et al 1992].

Nickel alloying does not have much effect on the strength and hardness in steels (figure 2.15). Changes in hardness with different cooling rates are therefore mainly controlled by the carbon (0.002 wt.%) and nitrogen (0.008 wt.%), and transformation strengthening mechanism. In the second batch of materials, the carbon and / or nitrogen content is assumed to be lower than the first batch. The slight difference in the hardness value of the isothermally transformed Widmanstätten lath from the quenched lath martensite is merely due to the higher dislocation density in lath martensite. When the interstitial alloys content has fallen to a very low level, the microstructural identification by hardness measurement would become insignificant and unjustifiable.

6.5. M-A Constituent

M-A (martensite-austenite) constituent was observed in both the FC and AC specimens even with such a low carbon content (0.002 wt.%). This minor secondary phase is so minute and small amount that it is practically invisible under optical microscope. With higher carbon content, bigger M-A constituent is formed, generally on ferrite grain boundaries. Figure 6.3 shows the M-A constituent in a furnace cooled VS2241B alloy containing 0.029 wt.% C. Apparently, nickel depresses pearlite and promotes the M-A constituent formation. Similar effect is shown by other alloying elements such as Mn and Mo [WANG and YANG 1992; CAWLEY, HARRIS and WILSON 1994]. EDX analysis shows no difference in nickel content in M-A constituent with the adjacent matrix suggests that it forms under paraequilibrium condition, as originally described by HULTGREN [1947].

The presence of M-A constituent in such low carbon condition implies that carbon, even at extremely low level, can exert a significant influence on the transformation behaviour and it is therefore difficult to ignore its role in massive ferrite and Widmanstätten formation, as commented by MASSALSKI [1970].

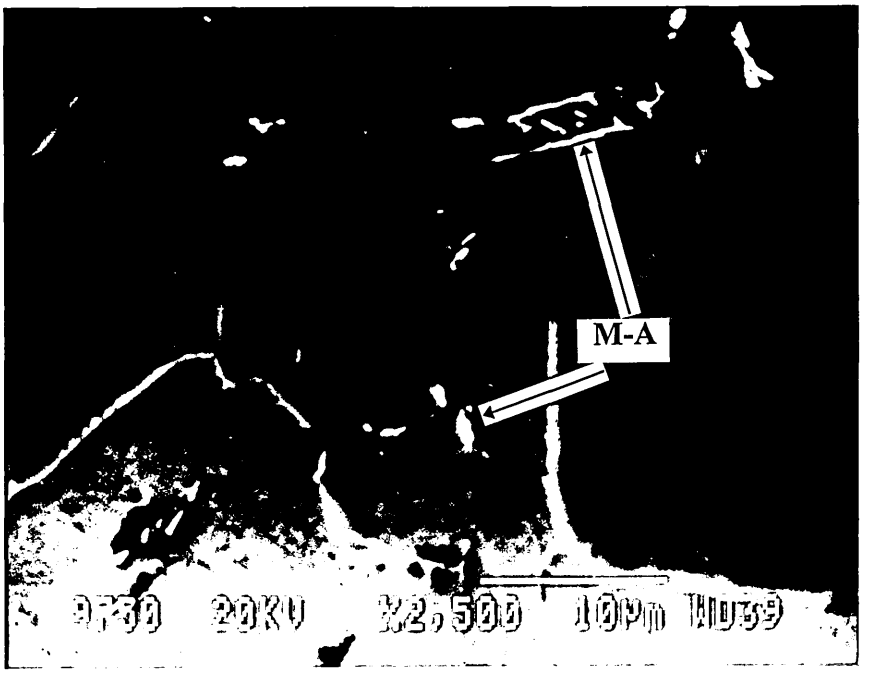

Fig. 6.3. M-A constituent on the ferrite grain boundaries in furnace cooled VS2241B alloy containing 0.029 wt.% C.

NB: Even relative "pure" metals, very small quantities of impurities undoubtedly contribute to grain boundary "dragging" during phase transformations and resulted complex microstructures instead of equiaxed morphology even if the cooling rate is low - MASSALSKI [1970], p454.

6.6. Massive Transformation

Compositions in diffusion controlled reactions under local equilibrium are similar to the calculation of phase equilibria, whereby the ordinary mass balances is replaced by flux balances. If there was no diffusion in the phase interface the growing α phase would inherit the composition of the matrix and local equilibrium would not be maintained, for example in martensitic transformation. The amount of solute that must diffuse in the moving phase interface depends upon the growth rate. The concentration gradient is maintained along with the travel of the interface. If the composition change is large, the reaction will slow down and this effect is referred to as *solute drag.*

A massive transformation in which the product inherits the composition of the parent, similar to martensitic transformation involving shear mechanism, is not truly a diffusionless transformation process. It is believed that massive transformation involving trans-interphase diffusion by atomic jumps across the interphase. HILLERT [1984] perceived the natural limit for the massive transformation is the single-phase boundary and the reaction takes place under local equilibrium condition. MASSALSKI [1975] reported a massive transformation in Fe-8.7 at.% Ni in the two phase field. This implies that the local equilibrium model does not apply to the massive transformation in the two phase field.

In view of this observation, local equilibrium model was then improved and applied to Fe-Ni and Fe-C system by Ågren and Jönsson [ÅGREN 1989; JÖNSSON and ÅGREN 1990; JÖNSSON 1990] to account for the massive transformation in the two phase field.

Dilatometry indicated that the massive ferrite transformation started at 575°C in the present studies. Local equilibrium model for the diffusional transformation of Fe-9Ni can be represented by figure 6.4(a) in which the correspond α phase would contain 5.5 wt % Ni, and the composition spike as high as 22.3 wt.% Ni, evaluated from the phase diagram in figure 2.3 and 2.4. For transformation at 555°C, the α phase would contain 5.8 wt.% Ni and the tip of the composition spike, 25.0 wt % Ni. Obviously, the composition profile of the transformed structure either via continuously cooling, figure 4.36 or isothermally, figure 4.37 do not comply with this model. Instead of figure 6.4(a), figure 6.4(b) represents the solute distribution at the γ/α during massive growth in Fe-9.14 wt.% Ni at 575°C.

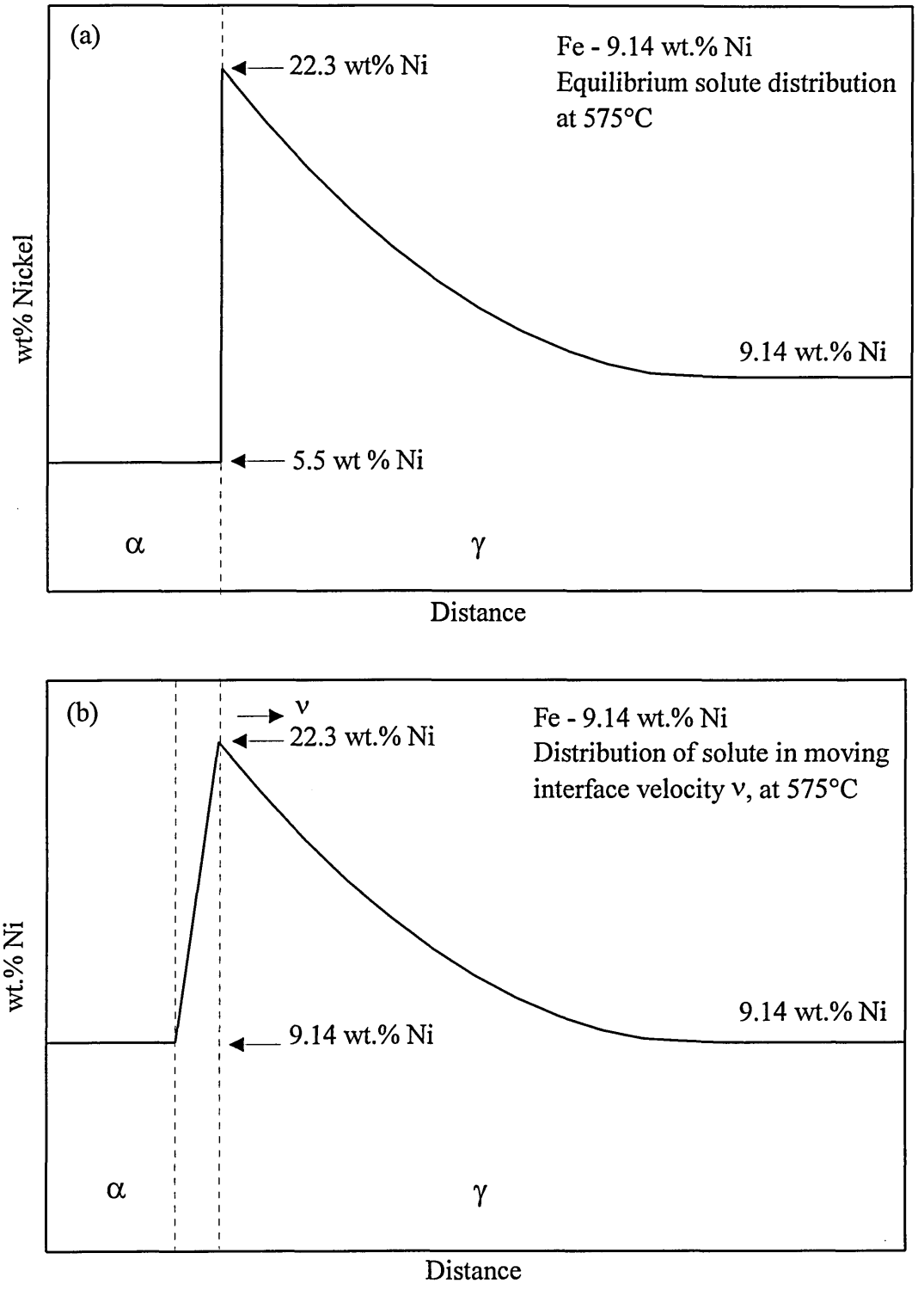

Fig. 6.4. (a) Solute distribution for the growth of ferrite by diffusional under local equilibrium; (b) by massive growth in Fe-9.14 wt.% Ni at 575°C.

According to ÅGREN [1989], as the supersaturation is increased above a critical level, a diffusion controlled reaction will gradually developed into a diffusionless massive, occurring by *dynamic nucleation process*. At this composition, transformation will occur from the supersaturated matrix at temperature below T_0.

Dynamic nucleation proposed by HILLERT [1975] however, is highly hypothetical, being derived from mathematical model to account for the nucleation under a supersaturation condition. Figure 4.17 presents a ferrite grain at the triple point of the austenite grain boundary implying that classical nucleation at grain corner with one coherent interface. However this specific orientation relationship between parent phase and the precipitate product is unable to explain the present of austenite grain boundaries 'inside" the single ferrite grain. The present observation seems to support Massalski's concept whom regarded massive grain nucleation without crystallographic orientation relationship requirement between the parent and the product phases [BHATTARCHARYYA, PEREPEZKO and MASSALSKI 1974].

On the other hand, AARONSON [private communication 1998] commented that if there are three instead of a single grain in the feature portrayed in figure 4.17, it is possible that each of the austenite grains forming this particular grain corner had a {111} plane nearly parallel to its area near the corner, a relatively planar and simple partially coherent interface (as described in RIGSBEE and AARONSON [1979]) would inhibit growth normal to each such boundary. This fortuitous crystallography would also encourage nucleation at each of these boundaries in the described relationship. Note that both the rationally and the irrational orientation relationships interfaces of grain boundary allotriomorphs are partially coherent [FURUHARA and AARONSON 1991], contrary to usual opinion. The interfaces of such case would be more nearly planar and have fewer growth ledges than is usual for the interfaces enclosing grain boundary allotriomorphs.

Alternatively, the appearance of austenite grain boundaries are simply delineated by the impurities segregation or the carbide precipitation. The possibility of carbide can be ignored as the inspection on the thin foils shows the absence of any particle precipitation on the grain boundaries (figure 4.19 & 4.20). Impurities segregation is possible by the fact that impurities were detected while performing grain boundary analysis using FEG-STEM on the furnace cooled specimens, see section 4.3.2.

As there are only few austenite grain corner nucleated ferrite grains present in the isothermally transformed specimens, the observation of figures 4.17 and 4.19 can not be justified with statistical meaning. For the grain boundary ferrite, the trace of austenite grain boundary is shown in figures 4.18, 4.20, but not in figures 4.21, 4.22, and 4.25.

The author is of the opinion that the preservation of the austenite grain boundaries inside the transformed region is merely delineated by the immobile heavy element segregation in austenite. The presence of planar boundaries in figures 4.5, 4.17 and 4.19 suggested that the massive phase nucleated coherently with at least one planar facet. Coherent interface establishes an orientation relationship with the parent phase. The other nonplanar interfaces would be of incoherent type. This incoherent interface would allow the growth of massive phase by rapid atomic transfer across interphase interfaces, with the coherent interface keeping pace with the incoherent boundaries by lateral movement of ledges. For the austenite grain corner nucleated massive phase, the volume change could be absorbed by the austenite grain boundaries to give a low dislocation density grain. As for the massive phase nucleated at austenite grain boundaries at lower temperature range, the volume change during growth would not easily be absorbed by the austenite grain boundaries and as a consequence resulting in a heavy dislocation density within the ferrite grain, figures 4.18 and 4.20 [WILSON 1984, 1994, and private communication 1998].

Equiaxed ferrite transformation is a high temperature reaction. Growth of equiaxed ferrite would be very rapid and not impeded by the solute pinning with weak solute drag effect. As a consequence, the final product appears to be equiaxed-like with low dislocation density and absence of dislocation substructure inside the grains. Air cooled Fe-3.5Ni alloy of figure 5.1 shows the typical feature of equiaxed ferrite, and it is forming in the single phase region. However, with 9% nickel addition into iron, the transformation is taking place in the two phase region and being suppressed to a much lower temperature range that the transformation to equiaxed ferrite is suppressed. Generally, the ferrite grains in Fe-9Ni alloy posses undulating type of boundaries, as described by MCEVILY et al [1967] for the massive ferrite in Fe-3Ni-3Mo alloy, as shown in figure 4.6, or irregular type of boundaries with the observation of substructures

inside the grains, such as figure 4.7. Such ferrite grains are generally regarded as massive ferrite or quasi-equiaxed ferrite (α_q).

Widmanstätten structure with high dislocation density was observed in the same temperature range as the ferrite in Fe-10Cr alloy, led BEE and HONEYCOMBE [1978] to draw the conclusion that the ragged features in massive ferrite are a result of Widmanstätten ferrite impingement.

Isothermal transformation studies in Fe-9Ni alloy in the present studies discovered massive ferrite and Widmanstätten ferrite in about the same temperature range. In the high temperature range, massive ferrite and Widmanstätten ferrite form at the austenite grain boundaries as grain boundary allotriomorph and Widmanstätten sawteeth respectively. At lower temperature range, the transformation of massive ferrite and Widmanstätten ferrite can take place at austenite grain boundaries or intragranularly (idiomorphs). Both the massive ferrite and Widmanstätten ferrite posses the characteristics of subgrain and sublath boundaries respectively. At a further lower temperature range, only the formation of primary Widmanstätten ferrite laths is possible. Regarding massive ferrite and Widmanstätten ferrite as the same transformed product is therefore not acceptable. The co-existence of Widmanstätten structure as well as irregular massive ferrite in iced brine quenched Fe-4Cu alloy also confirms this argument. Nevertheless, it is possible, if the transformation is taking place in the high temperature range, that recovered Widmanstätten will resemble massive-like structures in the end product.

In the present isothermal transformation studies on Fe-9Ni alloy, Widmanstätten structure is preferred as the transformed product at such a relatively low temperature range, especially with large austenite grains (due to high austenitising temperature). HAYZELDEN and CANTOR [1985] managed to produce massive ferrite in Fe-25Ni in melt spun Fe-Ni alloy because of fine austenite grains (3 μm) and hence providing excessive large number of potential heterogeneous nucleation site for the massive ferrite nucleation. Under normal circumstances, lath martensite will form even if a slow cooling rate is applied in this Fe-25Ni alloy [KAUFMAN and COHEN 1956; WILSON 1965].

Massive transformation based on Fe-9Ni alloy of the present studies show a high degree of similarity with the decomposition of austenite in steels governed by long range carbon diffusion. The Dubé classification can be applied to describe the morphologies found in this Fe-9Ni alloy, VS2241A. Grain boundary allotriomophs in steels were once regarded as bounded by disordered and incoherent type of boundaries which can propagate unrestricted [AARONSON 1962]. The later work, LANGE, ENOMOTO and AARONSON [1988] perceived ferrite grains being bounded by partial coherent boundary, and grew by ledge mechanism, as evident by the presence of faceted type of boundary. On the other hand, faceted massive phase of ζ_m separating the β matrix of a Ag-26 at.% Al alloy was found to be a partial coherent type of boundary [MOU and AARONSON 1994]. One might suggest that growth of massive ferrite might not be solely attributed to the propagation of incoherent type of boundary.

If the growth of Widmanstätten structure was by all means the movement of planar boundary via ledge mechanism, and can take place continuously from the ferrite grain formation, as shown by the protuberance in figure 4.23, it would be plausible to suggest that ferrite grain of such was partly bounded by partially coherent boundary to facilitate the change in growing phase from a fairly equiaxed-like grain to become ragged and extended to laths formation eventually. i.e. massive transformation allowed the change of morphology from equiaxed-like to laths-like. Such arguments have also been pointed out by MENON et al [1987].

The propagation of massive phase in Fe-9Ni with cooling rate about 10 $K.min^{-1}$ advances by faceted as well as undulating type of boundaries was observed by in situ studies [MOISEYEV et al 1981]. In situ studies on $\beta \rightarrow \zeta_m$ massive transformation in a Cu-24.3 at.% Ga also shows movement of planar facet and ledge-type structure at one instant can be quickly replaced by a smooth curved interface at another [KITTL and MASSALSKI 1967]. These two cases suggest that the growth of massive phase is viable either by the propagation of incoherent boundary or by the ledge movement of the partially coherent boundary, or both operating at the same time. Connecting the above observations to the present studies of Fe-9Ni alloy, we can also regard the Widmanstätten ferrite as a product of a massive transformation.

Regardless of which either mode of phase boundary movement occurs, growth of massive phase is in such a way that the volume interdiffusivity in the matrix phase is very small, the solute concentration in the matrix will remain the same as the bulk alloy. Therefore, solute from parent phase is 'trapped" by the advancing interphase boundary [PEREPEZKO 1984; MENON et al 1988; AARONSON et al 1994].

6.7. Laths Formation Associated with Widmanstätten, Bainite and Martensite

Widmanstätten Ferrite

Generally it is believed that the non-crystallographic related surface rumpling effect is for massive ferrite / grain boundary ferrite due to the volume change on transformation, with growth occurring by the migration of a high angle or disordered interphase boundary.

On the other hand, if the phase transformation is an ordered type whereby the motion of transformed phase is in co-ordinate manner, it often produces geometric surface relief. The best example would be the surface tilt resulted by the plate formation of martensitic transformation. The observation of surface relief has long been regarded as due to invariant plane strain (IPS) associated with martensitic transformation, which is best described by PTMC.

In the 50's, the observation of surface relief in the high temperature range in steel had led KO [1953] to propose that the Widmanstätten ferrite plates formation is due to the displacement of substitutional atoms simultaneously with the diffusion of interstitial atoms.

At a later date, CLARK and WAYMAN [1970] and WATSON and MCDOUGAL [1973] found that the growth of carbon depleted Widmanstätten ferrite plates in Fe-C alloy show some aspects of an apparent displacive reaction, notable surface relief. In determining the orientation relationship of Widmanstätten ferrite plates in Fe-C alloys, WATSON and MCDOUGALL [1973] reported the results of average habit plane $(0.5057, 0.4523, 0.7346)_{\alpha}$ and direction (-0.8670, 0.4143, 0.2770). KING and BELL [1975]

reported the Widmanstätten grows in the direction of $<110>_{\gamma}$ most nearly parallel to a $<111>_{\alpha}$.

In analysing Watson and McDougall's result, AARONSON et al [1975] however, found that plate formation by shear in the proeutectoid transformation temperature range is thermodynamically not viable.

Aaronson's group [AARONSON 1969; KINSMAN, EICHEN and AARONSON 1975; HALL and AARONSON 1994] discovered that the surface relief due to plates or laths formation of proeutectoid ferrite in Fe-C alloys is tent-shape. These workers suggest that such surface relief for Widmanstätten ferrite cause by the glide of growth ledges with dislocation character along the α/γ interface. These plates are found to form in a single crystal, which is different from that the observation of surface reliefs consisting of two or more tilted planar surfaces associated with the requirements and predictions of the PTMC [AARONSON et al 1990; AARONSON and HALL 1994].

In the present studies, it was found that Widmanstätten ferrite and massive ferrite co-exist in the furnace cooled Fe-9Ni alloy. Figure 4.3 and 4.4 show that Widmanstätten ferrite form via sympathetic nucleation on the ferrite grain at the prior austenite grain boundaries. Isothermal transformation studies confirm that Widmanstätten structure is in the same (or slightly lower) temperature range as the massive ferrite transformation. Surface relief of these laths is tent-shape. In the lack of direct experimental evidence, it is thought that formation of these laths via short range diffusion transformation with the atomic jump across the interphase interfaces in much the same way as the massive ferrite formation. In contrary to massive ferrite, the growth of Widmanstätten structure does not involve the propagation of incoherent boundaries without specific orientation relationship requirement, rather, by means of ledge mechanism in a much co-ordinated manner. The growth posses anisotropic character in which forward growth is preferred to the lateral growth, resembling laths structure after transformation is completed. The observation of "steps" on the Widmanstätten lath in figures 4.8(a) and 4.28 support such an explanation.

On the other hand, the wavy form of the lath boundaries shown in Widmanstätten ferrite, figures 4.8(a) and 4.27 suggest that these laths, formed during slow cooling or isothermally transformed at relatively high temperature range, facilitate dynamic recovery and strain relaxation to take place during the process of transformation, resulting the annihilation of adjacent laths and / or showing discontinuous lath boundaries characteristic.

Co-existence of Widmanstätten structure and ferrite grains was also found in Fe-0.003%C by KINSMAN, RICHMAN and VERHOEVEN [1976]. In their observation, a large austenite grain size encouraged the formation of Widmanstätten structure formation first, followed by the formation of ferrite grains.

In fact, Widmanstätten ferrite in carbon free alloys was also found by BEE and HONEYCOMBE [1978] and RICKS, HOWELL and HONEYCOMBE [1979] in Fe-Cr and Fe-Cr-Ni alloys respectively. They too observed "steps" in Widmanstätten structure and suggested the ledge mechanism of Widmanstätten ferrite growth. They also reported cube-cube related $\{111\}_{\alpha'}//\{111\}_{\alpha}$ $<110>_{\alpha'}//<110>_{\alpha}$ of ferrite (α)-martensite(α') implying K-S relationship of Widmanstätten ferrite in respect with austenite.

It should be noted that the Widmanstätten structure is almost unidentifiable after short period of isothermal transformation as mentioned in section 4.2.2. With longer isothermal holding period, the growth of laths stopped at certain stage, because of losing driving force for the lattice atom jump across the interphase interfaces by the apparent solute drag effect, and as a consequence, the movement of the growing ledge losses its mobility. Prolong isothermal holding resulted segregation of impurities and hence delineate the phase boundaries between the transformed phase and the quenched matrix. In addition to that, prolong holding also allows recovery to take place.

Widmanstätten laths formed during the growing stage, would be of the partially coherent type. Since the isothermally transformed Widmanstätten laths and quenched martensite structure are both in bcc structure due to low carbon content (high carbon martensite forms bct structure), the lattice misfit at the phase boundary might tend to form low angle boundaries with a blurred α_W/α' interfaces, for instance in figure 4.24. Poor

quenching is thought to be another reason for blurred α_W/α' interface since relatively large size (5 x 5 mm) of the isothermally transformed specimens were used.

A recent conference* [1994] demonstrated that there are quite a few incidents in which plate precipitation showed surface relief. The motion of growth ledges which have dislocation character in the fully or partially coherent precipitates can give rise to a lattice site correspondence even if the occupation of these sites may change, becoming more solute rich as solute rich phase grows into the low solute matrix. Very much the same principles can be applied in the present studies. As far as solute distribution is concern, Widmanstätten ferrite in Fe-9Ni alloy of present studies, can also be regarded as massive transformation, as evident by the composition invariant microanalysis result in figure 4.37. The only difference with massive ferrite transformation is that Widmanstätten ferrite transformation acquired a specific orientation relationship with the parent phase and is therefore the propagation of Widmanstätten structure can be stopped by the austenite grain boundary, as evident by figure 4.4(b).

Bainite

Bainitic transformation of Fe-9Ni alloy takes place at much lower temperature as compared with the Widmanstätten ferrite. Thermal arrest results suggest that bainitic ferrite in Fe-9Ni alloy starts to transform at temperature ~ 480°C. Perfect laths are observed if the continuous cooling is sufficiently high. "Steps" character found in Widmanstätten laths is absent in bainitic laths. Even though surface relief evident is not presented in this thesis, it is believed that the formation of bainitic laths take place by shear mechanism.

In spite of the high degree of morphological similarity between bainitic laths and laths martensite, there is a different chemical reaction to $Na_2S_2O_5$ etching on lath martensite (in IBQ specimen) and bainite (in WQ specimen). This suggests that while martensitic transformation is by all means displacive and diffusionless with no diffusion of substitutional and interstitial atoms, this is not the case for bainitic transformation. Bainitic transformation is diffusionless in respect to substitutional atoms, diffusion of the interstitial elements such as carbon and nitrogen, however, is possible as these atoms

posses high diffusivity. Colouring agent of $Na_2S_2O_5$ etching reagent is so sensitive that a minor difference in chemical composition of the microstructures can be distinguished, and suggesting the different transformation mechanism between martensite and bainite. In fact, using atom probe field ion microscopy (AP-FIM), BASH et al [1980] already demonstrated that carbon spike existed but not for other substitutional elements in the bainite / austenite interface in a low alloyed Cr-Mo alloy steel, figure 6.5.

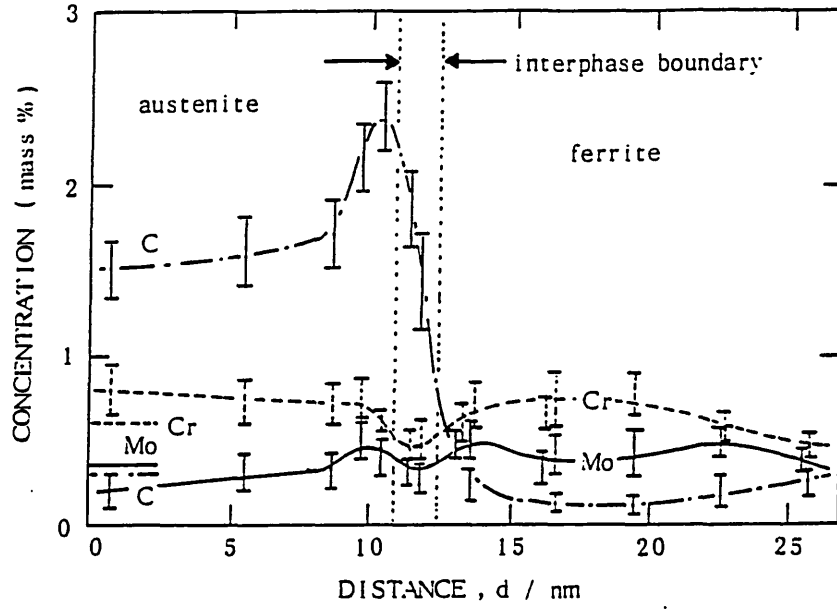

Fig. 6.5. Composition profiles across bainite (ferrite) - martensite (austenite) interface in a commercial Cr Mo steel, AISI H10, showing lower carbon concentration in the ferrite (bainite). After BASH et al [1980].

TSUZAKI et al [1994] found that bainite transformation in silicon bearing steels, carbide precipitated *after* bainitic laths formation, and these laths are highly supersaturated with carbon, i.e. carbon diffusion is restricted from achieving local equilibrium condition. RAO and WINCHELL [1967] also demonstrated that bainite growth in Fe- 9%Ni-C would be too low to be determined solely by carbon diffusion.

By isothermal holding at 450°C, transformation reached to optimum level at the very early stage, and the transformed laths did not thicken with prolong isothermal holding. This suggest that the interface had already lost its mobility as a glissile interface at 450°C after a short period of isothermal holding. Because of relatively high reaction

temperatures, after the stopping of the glissile movement, diffusion might take place in order to release the strain energy caused by shear, which can be compared with the process of tempering martensite.

Cambridge workers found bainitic ferrite in carbon free Fe-Cr, Fe-Cu-Ni and Fe-Cr-Ni alloys [BEE and HONEYCOMBE 1978; RICKS, HOWELL and HONEYCOMBE 1979; RICKS, BEE and HOWELL 1981]. In their works, trans-lath subgrain boundaries observed in bainitic lath after prolong isothermal holding referred as 'recovery-controlled shear mechanism", suggested by BOLTON, PETTY and ALLEN [1971].

As far as ferrous bainites are concerned, Christian sees bainite as plates or laths formation with the absence of "superledges", and the mobility of iron and all substitutional solutes are negligible [CHRISTIAN 1990].

Despite the lack of convincing experimental evidence in the present studies, the author advocates the displacive model in bainite transformation. Bainitic laths formation in Fe-9Ni alloy can be viewed as shear transformation product, perhaps not in the same way as martensitic transformation. Note WILSON et al [1982] have tentatively suggested that there is a difference in habit plane for the bainite and martensite in Fe-15%Ni.

It is quite interesting to find that in the study of bainitic ferrite formation in Fe-29.8 wt.% Ni with less then 0.01 wt.% C by YANG et al [1994], bainite was found to grow by ledge mechanism with the thickening rate of 2×10^{-10} cm.s^{-1} at isothermal temperature 300°C, and claimed to be consistent with the diffusion rate of nickel atoms. However, 300°C is well above T_0 (~180°C according to BORGENSTAM and HILLERT [1997] and ~210°C according to Kaufman and Cohen [1956]), therefore the transformed structure may not be of the bainitic type.

Similarly, a perfect c-curve of Fe-12%Ni presented in figure 2.6 by MOISEYEV et al [1981] with the nose of the curve around 420°C. The reported structures as comb-like and plate- like crystals. These structures may be regarded as Widmanstätten structure.

In the present work, the author failed to establish experimentally a TTT diagram for Fe-9Ni. RICKS, BEE and HOWELL [1981] and MCEVILY et al [1967] however, managed to present a distinct transformation curve for bainite in carbon free Fe-Cr-Ni and Fe-Ni-Mo alloys respectively. In view of the low diffusivity of nickel atoms in iron, bainitic transformation would have to take place via shear transformation. In the mean time, the establishment of an independent C-curve for carbon free bainitic ferrite might be best described as *time-dependent shear transformation process* [BOLTON and PETTY 1971; RICKS, BEE and HOWELL 1981].

Widmanstätten-Bainite-Martensite Relationships

Widmanstätten laths formation at high temperature is thought to occur via short range diffusion of nickel atoms by ledge mechanism movement. Martensite transformation is purely by shear without any degree of atomic diffusion. However, figure 4.28 clearly shows that Widmanstätten ferrite grow continuously into martensite upon quenching, suggesting that the ledge growth mode of transformation can in fact convert into shear mode. Successful application of the formulation for athermal martensite to the dilatometric results for Widmanstätten formation (see section 4.4) also implies martensitic characteristic to Widmanstätten ferrite.

Hillert's theoretical derivation demonstrated that diffusional transformed Widmanstätten ferrite in Fe-C can grow continuously into martensite when the carbon content is reduced to a critical level [HILLERT 1975]. He viewed Widmanstätten ferrite, upper bainite, lower bainite and lath martensite as a continuous series of related product. Bainite plates in partially transformed Fe-C alloys were shown, by up-quenching, to continue their growth as Widmanstätten plates while maintaining the same morphology they had as bainite. Similarly, continued growth of Widmanstätten plates as martensite plates parallel to the original ferrite plates was shown by down-quenching partially transformed structure [PURDY and HILLERT 1984]. He also suggested that the effort on proposing different mechanisms in separating pearlite / bainite transformation in Fe-C as unnecessary as there are both transformed by diffusional process. Bainite does not grow with a purely martensitic type of interface but may become more and more coherent at lower temperatures [HILLERT 1994].

Generally speaking, there are scholars who in favour of plate formation using ledge mechanism model, refer to as *diffusionists*, there is another group of scholars in favour of PTMC to explain the plate / laths formation, i.e. *shearists* (see AARONSON et al [1990] and conference* [1994]). In reviewing the topic of bainite transformation, DOHERTY [1996], whom is neither a diffusionist nor shearist in the study of bainite transformation, commented that the problem for the research on bainite is not the shortage of quantitative data, but lack of agreed theory.

Having said that, the development of invariant line strain concept in place of the invariant plane strain model based on PTMC seems to have found the common ground where these two parties can stand together. Using invariant line model, DAHMEN [1987] demonstrated how Ag-rich precipitated plates of hcp γ from fcc Al-Ag could produce surface relief effect. On the other hand, ARAKI et al [ARAKI, SHIBATA and NAKAJIMA 1992; ARAKI and SHIBATA 1995] also proposed bainitic ferrite transformation based on invariant line model in combination with interstitial spike to account for bainite formation in low carbon steels. CHRISTIAN [1994] viewed the invariant line concept as applicable onto needles or laths formation. HOWE [1994] viewed that as long as there is an atomic site correspondence across the interface, either diffusional and martensitic phase transformations would produce surface relief.

No doubt, extensive studies on plate / laths formation in solid-solid transformation will still go on until a commonly agreed explanation is found.

**Conference: "Roles of Shear and Diffusion in the Formation of Plate-Shaped Transformation products", Kona, Hawaii, 18-22 December 1992. Published in Met. Mat. TransA, V25A, September 1994.*

6.8. Incomplete Transformation Phenomenon

Incomplete transformation has always been associated with bainitic transformation in steels, which bainite transform rapidly but cease shortly afterwards and never reaches completion (i.e. transformation stasis), but the remaining untransformed austenite will however, transform into pearlite after extended isothermal holding [BHADESHIA and EDMONDS 1979].

In steels, bainitic transformation takes place at sufficiently large undercoolings and the maintenance of local equilibrium with bulk partitioning is impossible. Partitioning of substitutional alloying elements which can occur in pearlite transformation by diffusional process is therefore not likely to occur in the displacive mode of bainitic transformation. Paraequilibrium model was therefore applied to the bainitic transformation where diffusion of interstitial elements (carbon especially) still occurred [HULTGREN 1947].

In view of high diffusivity of carbon even at the intermediate transformation temperature range, T_0' (the metastable equilibrium temperature for α and γ at the same composition in the presence of strain energy, W and is defined as $\Delta G^{\gamma\rightarrow\alpha} + W = 0$) is the limit of bainitic transformation beyond which bainitic transformation would not proceed and the remaining untransformed austenite become saturated with the rejected carbon atoms from the transformed bainite [BHADESHIA and EDMONDS 1980; CHRISTIAN and EDMONDS 1984; BHADESHIA 1992], i.e. incomplete-reaction phenomenon is dependent on the effective T_0' temperature. In fact, ZENER [1946] had proposed a long time ago that B_s temperature would also be the T_0 temperature.

On the other hand, Reynolds et al [1990] found that the incomplete character of bainite transformation in Fe-C-Mo depends on the carbon and molybdenum content, and is not observed in low carbon or low molybdenum alloys, i.e. incomplete transformation is not a general feature for bainite transformation.

OHMORI et al [1994] have demonstrated that W_s and B_s are above T_0 in high carbon steels, but fall below T_0 when the carbon content is decreased to a certain level. In the present studies, carbon content in Fe-9Ni alloy is so low that it's role in the process of

transformations is minimised. Transformation starts only with large undercoolings, well below T_0 temperature. Incomplete reaction phenomenon may therefore be applied not just to the bainite transformation, but also for massive ferrite and Widmanstätten transformation. The cessation of massive ferrite growth under isothermal condition is probably due to solute drag effect. The T_0 line (and possibly T_0') is therefore the limit of transformation above which partitionless transformation would not take place. In addition to that, such phenomenon occurs only for the transformations in the two phase ($\alpha + \gamma$) field.

In the alloyed steels, the residual austenite which enriched in carbon would transformed via reconstructive manner into pearlite after prolonged isothermal holding [BHADESHIA and EDMONDS 1979]. In the case of Fe-9Ni alloy, it is expected that the untransformed austenite would be undergoing decomposition process by nickel diffusion into equilibrium $\alpha + \gamma$, if an excessive long period of isothermal holding is allowed.

6.9. Schematic Isothermal Transformation Diagram for Fe-9Ni Alloy

The present investigation suggests that the transformation of the massive ferrite, Widmanstätten ferrite, bainitic ferrite and lath martensite are of the sequential transformed structure in Fe-9Ni alloy as the transformation temperature decreases. At the highest temperature range, massive ferrite transformation takes place by short range diffusion across interphase interfaces. There is a mixed mode of phase boundary migration, i.e. propagation of incoherent, disorder as well as partial coherent phase boundaries might occur. Massive phase growing across austenite grain boundary is due to the disorder type of boundary movement. Coherent type of phase boundary (planar boundary at least in macro scale) may not posses sufficient mobility and therefore tends to propagate laterally by ledge mechanism.

At lower temperatures, the migration of incoherent type of phase boundary may give way to the partially coherent type of boundary movement by ledge mechanisms. Ledge movement is of anisotropic type of growth and as a consequence producing elongated transformed phase- laths or plates, i.e. the Widmanstätten structure.

The movement of interfaces by ledge mechanism would be much more restricted at lower temperature range, and eventually replace by the shear transformation so that the high strain energy can be accommodated under the low temperature circumstances. Bainite transformation takes place at the intermediate temperature range above martensitic transformation but below Widmanstätten ferrite formation. Interstitial atom diffusion may be possible, but the diffusion of substitutional atoms would be negligible.

At the lowest temperature where the diffusion process is completely prohibited, it is only shear mode of martensitic transformation can take place and both interstitial and substitutional elements are trapped in the transformed structure.

Schematic TTT diagram is constructed based on the microstructural observation, figure 6.6. Transformation start lines only are drawn because of the incomplete transformation character for all the structures. 2 distinct C-curves are proposed for massive ferrite and Widmanstätten ferrite transformation, drawn overlapping with each other. It is expected that these two different ferrite morphologies are competing among themselves as the thermally activated transform products. Present studies found that massive ferrite transformation prevails as the first transformed product. KINSMAN, RICHMAN and VERHOEVEN [1976] observed Widmanstätten ferrite transformed first in Fe-0.003C. It is thought that the competition between these two structures would be largely governed by the austenite grain size whereby formation of lath structure (Widmanstätten ferrite) is promoted by large austenite grain size.

By continuous cooling, bainite reaction starts (B_s) at temperature around 480°C regardless of cooling rate (figures 4.1(c), 4.1(d) and 4.14). Results from the thermal arrest experiments suggest a plateau-like for bainite C-curve. The plateau characteristic for bainite C-curve is also appear in 9 % nickel steel, figure 2.16.

Since the present experimental results obtained lath martensite at the highest cooling rate, martensite C-curve for lath martensite is therefore presented in figure 6.6. Twinned martensite was not found in the present studies and therefore not included. Note that equilibrium transformation by diffusional process is also ignored as the transformation reaction would be situated very far to the right on the TTT diagram.

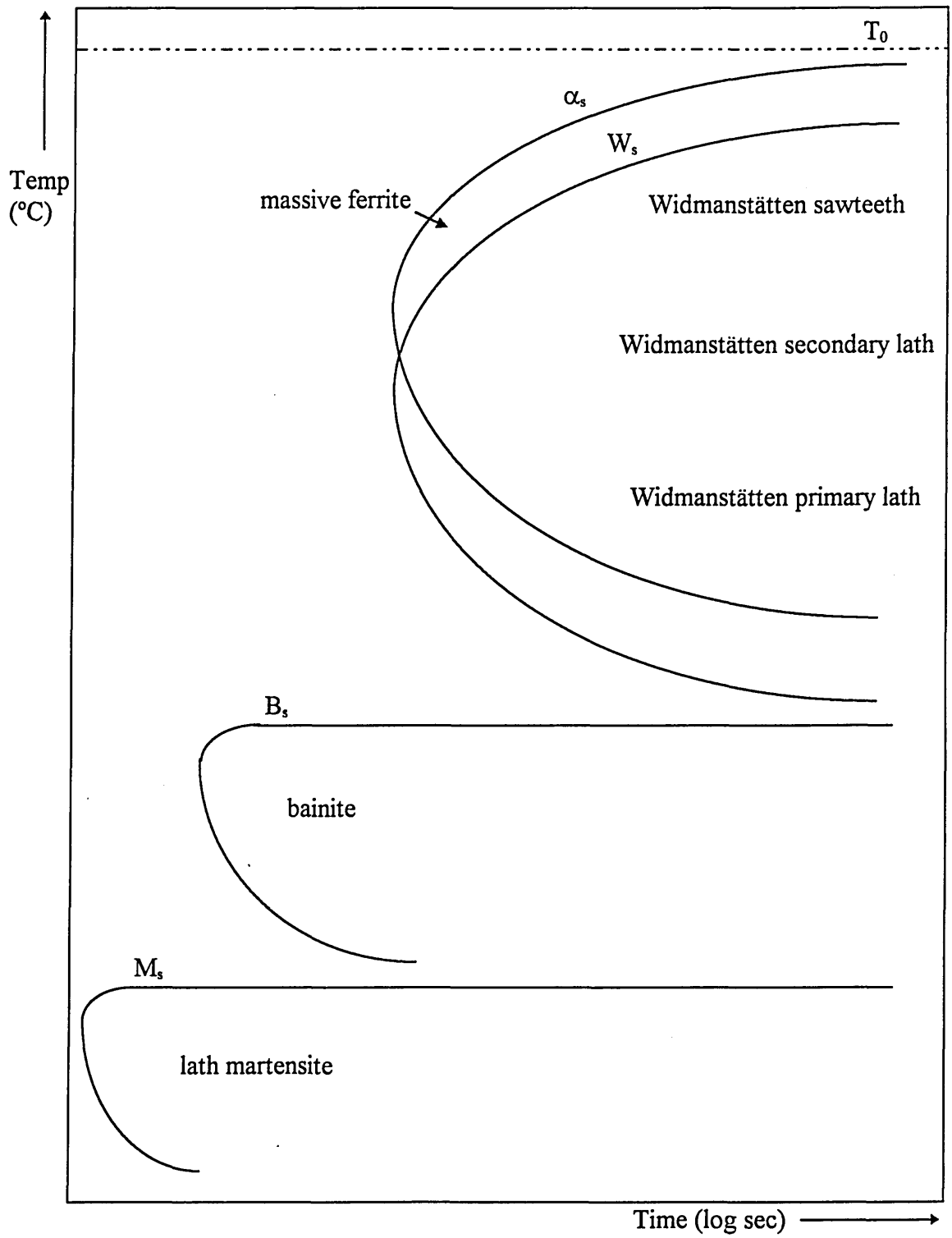

Fig. 6.6. Schematic TTT diagram for the Fe-9Ni alloy. Only transformation starts are indicated.

7. Impact Toughness of Fe-9Ni Alloy

7.1. Heat-treatment and Grain Size Measurement

After transformation experiments, it was decided to compare the toughness properties of massive ferrite and bainitic ferrite structure by air cooling and water quenching. From the hot rolled plate, it was found that an austenitising treatment of 20 minutes at 1000°C followed by air cooling, gave variable grain size, with excessive large grains at the centre of the specimen. These large grains often consisted of Widmanstätten structure rather than massive ferrite. After a few trials, it was decided to adopt austenitising at 900°C for one hour in producing smaller and fairly consistent grain size throughout the cross-section of the plate, as a consequence, the presence of Widmanstätten structure was minimised on air cooling.

Grain size measurement by mean linear analysis was carried out on about 500 ferrite grains, the average ferrite grain size was estimated to be around 10 μm. One should note that the identification of the grain boundary sometime found to be rather ambiguous as mentioned in section 4.1.2, therefore the term "estimate" was used to indicate the uncertainty of the figure. The measurement was performed on selective areas wherever the grain boundaries were identifiable.

For the water quenched bainitic structure, picral etching was used to reveal the prior austenite grain boundaries. Measured from about 500 grains, the calculated average (austenite) grain size around 20 μm.

A closer look at the polished and etched microstructures, trace of lines composed of holes and grooves were identified, found in both the water quenched and air cooled specimens, revealed by nital etching, probably due to impurities segregation at the austenite grain boundaries, i.e. the lines delineating the prior austenite grain boundaries, figure 7.1. This was only observed in plate which had been hot rolled and then re-austenitised.

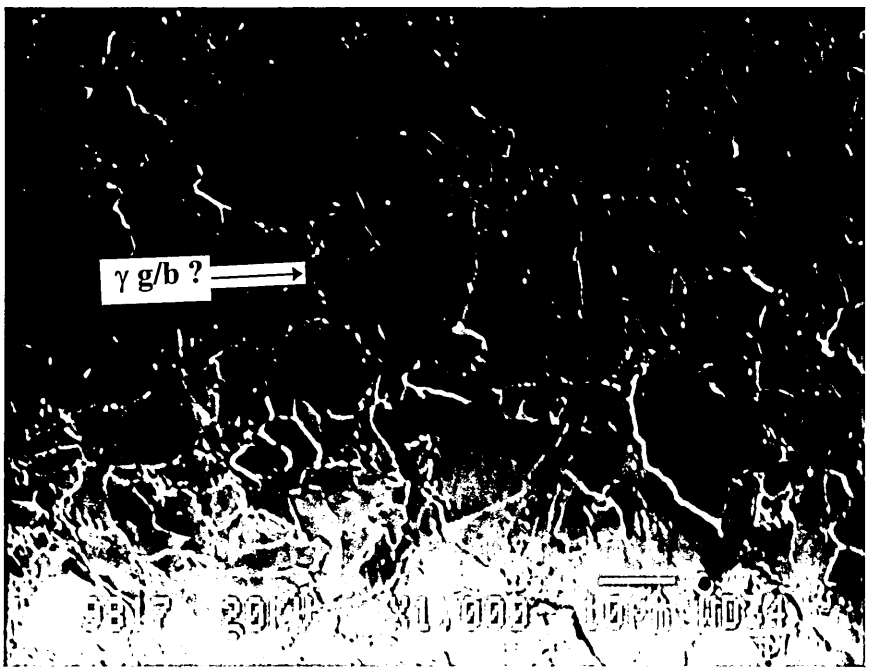

Fig. 7.1. Microstructure of Fe-9Ni alloy, VS2241A from the hot rolled plate subjected to 900°C austenitising treatment for one hour followed by air cooled, showing massive ferrite and trace of austenite grain boundaries (γ g/b), 2 % nital etched.

7.2. Charpy Impact Results of Fe-9Ni Alloy

Figure 7.2 presents the impact-energy curves obtained from subsize Charpy V-notch VS2241A specimens. Experiment results using K3393 (Fe-8.94%Ni-0.012%C-0.018%S), carried out by BASTON [1991], is also included.

For alloy VS2241A, it is quite clear that AC massive ferrite exhibit lower ductile-brittle transition temperature (DBTT) as compared with the WQ bainitic structure, which is about -140°C and -100°C respectively, the later also shows lower impact energy at the upper shelf. K3393 alloy shows much higher DBTT temperature which is around +60°C.

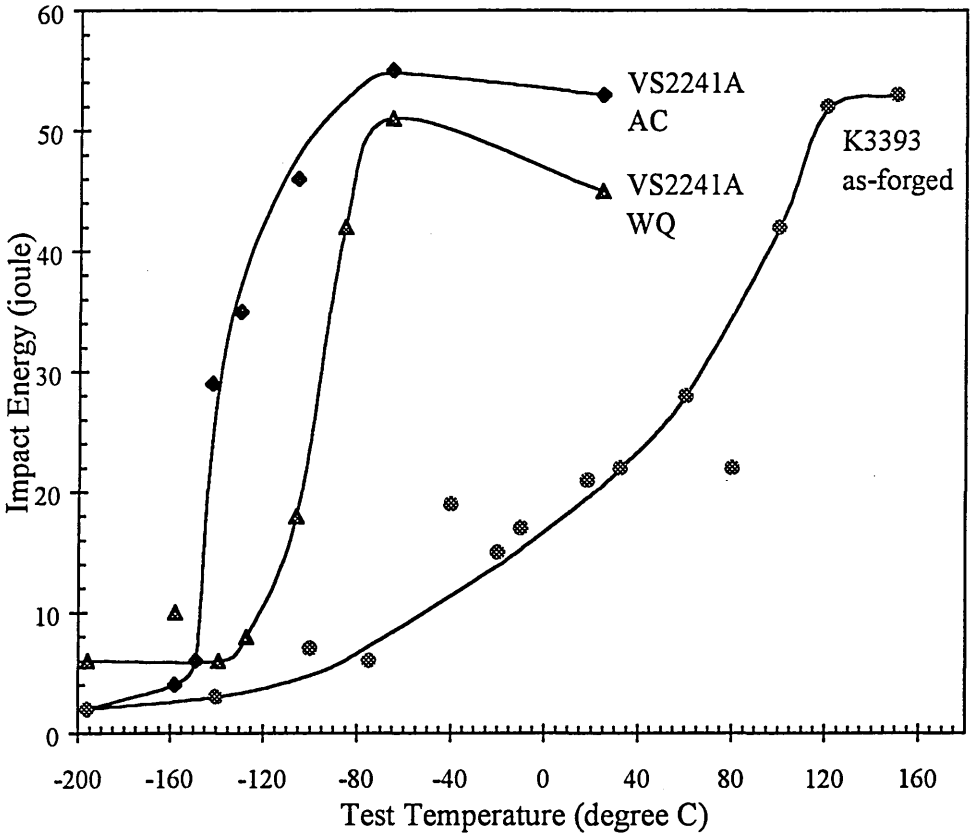

VS2241A, 900°C 1hr, WQ: γ grain size ~20 μm, HV_{20} = 213, DBTT ~-100°C

VS2241A, 900°C 1hr, AC: α grain size ~10 μm, HV_{20} = 168, DBTT ~-140°C

K3393 as-forged: α grain size ~20 μm, HV_{20} = 173, DBTT ~+60°C

Fig. 7.2. Impact transition curves for Fe-9Ni alloys, VS2241A and K3393.

Figure 7.3(a) shows the fracture surface of a WQ specimen of VS2241A failed at -196°C, clearly indicate a mixed mode of transgranular fracture and intergranular crack. Note even at -196°C temperature, the fracture is not completely in a brittle manner, a small amount of ductile rupture can still be observed, figure 7.3(b).

AC specimen of VS2241A as shown in figure 7.2, is more brittle at -196°C with impact energy as low as 2 joule only. Figure 7.4(a) shows a general view of the fracture surface dominated by cleavage. Intergranular cracks are also found. Interestingly, even with 2 joule of energy absorption, ductile rupture is still observed, figure 7.4(b). Compared with

WQ specimen, tongue-like cleavage would be more apparent in AC specimen, figure 7.4(c).

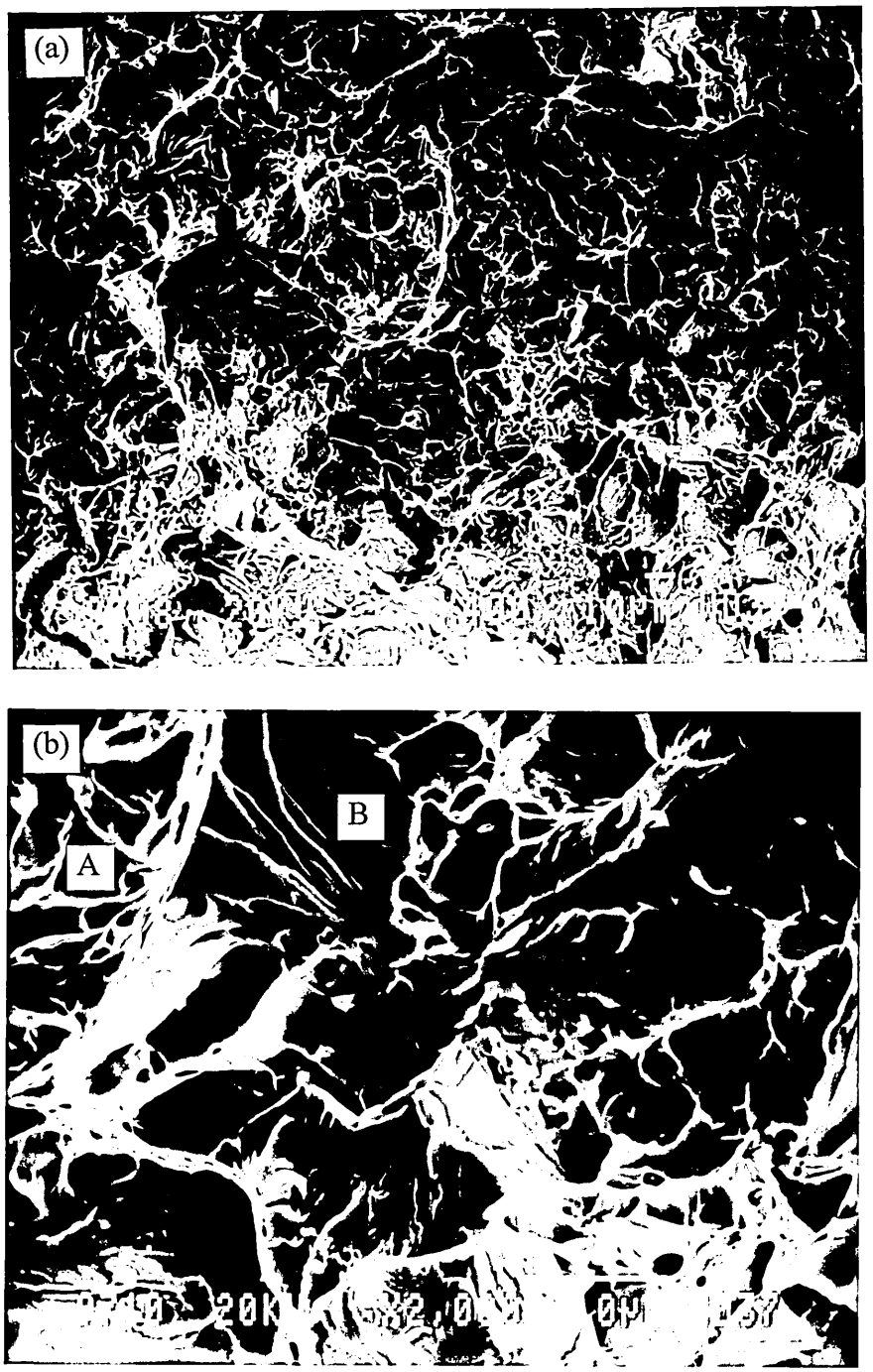

Fig. 7.3 (a) Fracture surface of a WQ specimen, Fe-9Ni alloy VS2241A broken at -196°C, showing a mixed mode of intergranular and transgranular failure. (b) Magnified fracture surface showing the ductile rupture (A) and river-line cleavage (B).

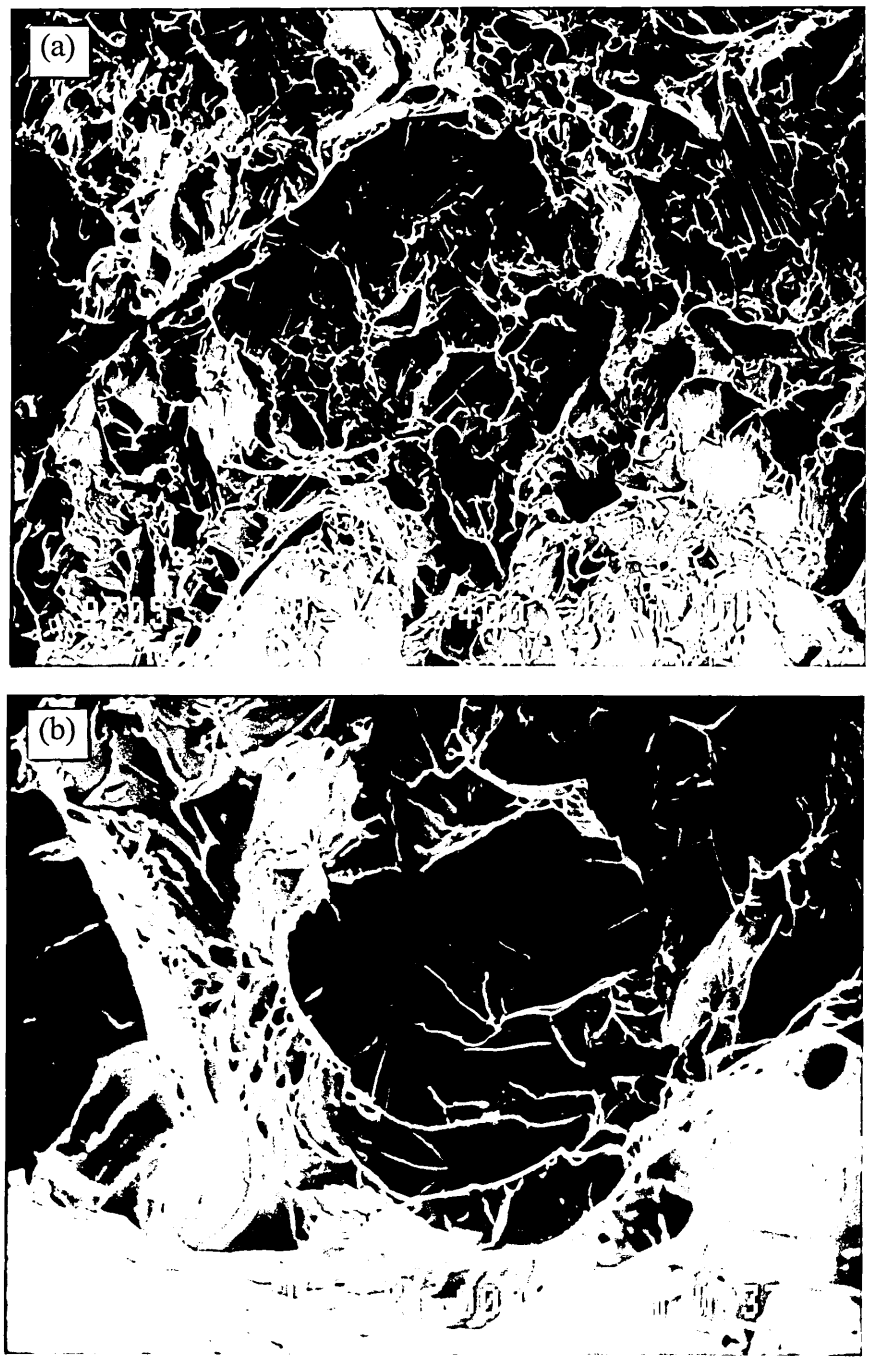

Fig. 7.4. (a) General feature of the fracture surface of a AC Charpy specimen, Fe-9Ni alloy VS2241A broken at -196°C, showing cleavage and cracks along grain boundaries. (b) Fracture surface showing ductile dimple in some areas from the same specimen.

Fig. 7.4. (c) Fracture surface of the AC specimen, Fe-9Ni alloy VS2241A broken at -196°C, showing cleavage tongues.

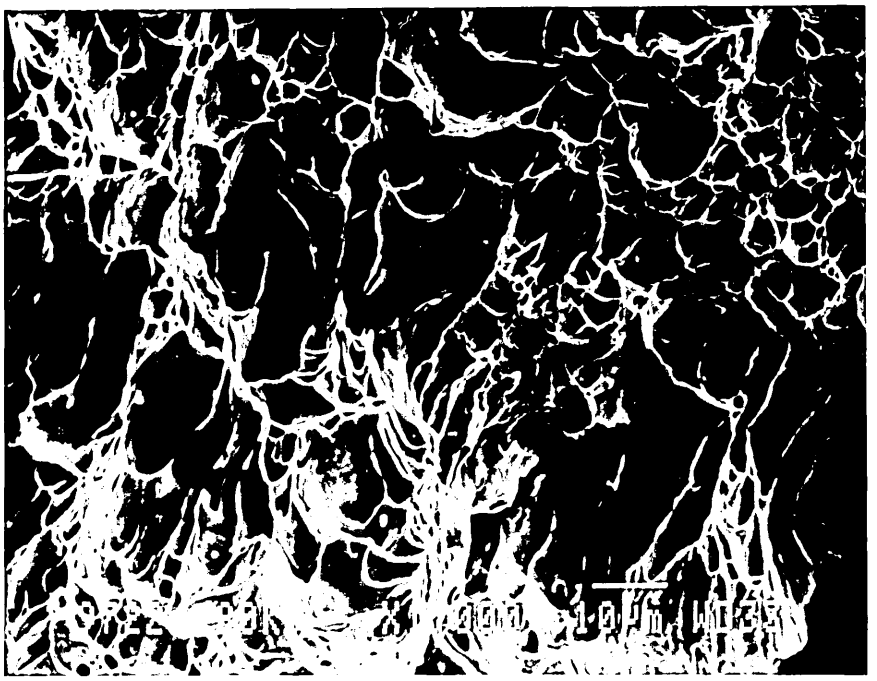

Fig. 7.5. Ductile failure of an AC Charpy specimen, Fe-9Ni alloy VS2241A broken at room temperature.

Room temperature impact test resulting ductile failure, figure 7.5. The formation of dimples clearly exhibit tearing effect parallel with the direction of the impact. With such a "pure alloy", crack nucleation on the inclusion site is not apparent, rather, few cracks as shown in figure 7.5 suggested cracks propagation along the grain boundaries. Such cracks are observed from both the AC and WQ specimen. It is thought that these crack paths are associated with the prior austenite grain boundaries.

7.3. Discussion

Fe-9Ni alloy, K3393 shows a much higher DBTT than the VS2241A AC specimens ,albeit there being not much difference in grain size and hardness. Higher DBTT for K3393 material is attributed by its low level of cleanliness. The importance of steels cleanliness in affecting DBTT is very obvious.

Compare with AC massive ferrite, WQ bainitic ferrite established higher DBTT due to its higher strength and hardness with higher dislocation density. The formation of packets of laths upon bainite transformation allows transgranular failure along the well defined crystallographic planes [NAYLAR and KRAHE 1975; EDMONDS and COCHRANE 1990].

Fracture at -196°C on both the WQ and AC specimens of VS2241A alloy show some degree of intergranular fracture. This is possibility due to impurities segregation on the prior austenite grain boundaries, suggested by the nital etched micrograph in figure 7.1. Note that impurities segregation was detected, particularly oxygen segregation, while performing microanalysis by FEG-STEM on a furnace cooled specimen (section 3.6.2). It was not sure if the chosen grain boundary was in fact the transformed ferrite grain boundary or the trace of prior austenite grain boundary (the preservation of austenite grain boundary upon decomposition is mentioned in section 4.2.2). The argument of oxygen segregation on grain boundary being detrimental to toughness in iron alloys had been subjected to critical studies by many researchers for decades [FAST 1950; REES and HOPKINS 1952; RELLICK and MCMAHON 1970; PICHARD, RIEU and GOUX 1976; KUMAR and RAMAN 1981]. KIMURA [1994] managed to produce iron of 99.999% purity and

found that the addition of oxygen into iron did in fact promote intergranular fracture and raised the DBTT, even though the effect was not drastic.

It should also be noted that M-A phase was detected upon slow cooling (FC and AC) in continuous cooling experiments. M-A phase is commonly found in weld metals on grain boundaries and can act as nucleation point of brittle crack. Decreasing the amount of M-A phase would improve the low temperature toughness in low alloy steels [FURUKIMI et al 1987; ASKSELSEN, SOLBERG and GRONG 1988]. However, with such a small amount of M-A phase present in these specimens, whether it would cause significant effect on toughness is difficult to justify.

With low nickel content, the ferrite grain size dependency in lowering DBTT about 6 to 7 $K.mm^{-1/2}$ was reported by LESLIE [1971]. For high nickel alloys, it was found that grain refinement lowered the DBTT 6 $K.mm^{-1/2}$ in Fe-12Ni-0.3Ti [SASAKI and YOKOTA 1975] and 8 $K.mm^{-1/2}$ in Fe-8Ni-2Mn-0.15Ti alloy [JIN, HWANG and MORRIS 1975]. In the case of high nickel ferrous alloys, austenite grain size was considered. Fe-12Ni-0.25Ti alloy with fine grain size of 0.5~2 μm produced by thermal cycling without the presence of reverted austenite fracture in ductile manner near helium gas temperatures (-267°C) [JIN, MORRIS and ZACKAY 1975]. Fe-8Ni-2Mn-0.15Ti alloy with the grain size of 1.5 μm showed DBTT around -118°C, lowering the DBTT further required the presence of reverted austenite [JIN, HWANG and MORRIS 1975].

Assuming the grain size dependency on DBTT is 6 $K.mm^{-1/2}$ for both the austenite grain and ferrite grain for Fe-9Ni alloy VS2241A, reducing the austenite grain size for bainitic structure from 20 μm to 2 μm could lower the DBTT from -100°C down to -176°C. As for massive ferrite structure, if the ferrite grain size was reduced to 2 μm, DBTT could be lowered further 74°C from -140°C down to -214°C, i.e. below the temperature of the liquid nitrogen (-196°C).

Having said that, impurities segregation on the austenite grain boundary, to a certain degree, deteriorated the impact toughness and raised the DBTT temperature for both the WQ bainitic structure and AC massive ferrite. Grain boundary weakening by impurities segregation is significant even for ductile failure. In view of significant amount of

impurities segregation found on the prior austenite grain boundaries from these Charpy specimens, no doubt, promoting a small amount of reverted austenite precipitation by tempering treatment would be essential to improve toughness and lower the DBTT. KIMURA [1994] had demonstrated that an iron of 99.999% purity showed transgranular fracture below -223°C whereas an iron of 99.99% purity showed intergranular fracture even at -196°C. For the case of 9 % nickel ferrous alloys, the practical mean of "purifying" the ferrite phase would be introducing reverted austenite act to *scavenge* the impurities.

8. Conclusions

The continuous cooling studies using Fe-9Ni alloy, VS2241A observed massive transformation on furnace cooling. Grain boundary of the massive ferrite appeared to be irregular or undulating. These grains were found to:-

(a) nucleate on the austenite grain boundary or grain corner and often grow across the austenite grain boundaries;

(b) produce surface rumpling on the prepolished surface;

(c) contain high dislocation density and low angle subboundaries were often observed inside the grains.

Microanalysis across massive ferrite showed the composition invariance of the $\gamma \rightarrow \alpha$ reaction in this alloy. Nickel enhancement as high as 12.98 ± 0.43 wt.% was observed on the massive ferrite grain boundaries but not on the lath boundary in lath martensite. These observations confirmed the nature of trans-interphase diffusional process involved in massive transformation with a composition spike in the growing interface.

Both massive ferrite and Widmanstätten laths formed under slow cool condition. Dilatometry analysis suggested massive ferrite started to form at 575°C at cooling rate 0.13 $K.s^{-1}$, and subsequently Widmanstätten ferrite formed at 558°C. The experimental T_0 was calculated to be 623 ± 5°C (as compared with a theoretical value of 614 ± 5°C from BORGENSTAM and HILLERT [1997]), implying the transformations occurred below the T_0 temperature in the two phase field.

Bainite transformation was found to take place upon oil quenching and water quenching at temperature around 482°C and lath martensite transformation took place around 384°C upon iced brine quenching. The difference between these two structure was also observed by their response to etching in $Na_2S_2O_5$ reagent.

Under isothermal transformation, after a high austenitising treatment, decomposition of austenite started at 565°C. Transformed structures conformed with Dubé classification. Ferrite (massive) phase was found to nucleate at austenite grain boundary and grain corner, i.e. referred as grain boundary allotriomorphs according to Dubé classification.

Widmanstätten ferrite could be distinguished as Widmanstätten sawteeth, primary lath or secondary lath.

The observations of tent-shape surface relief; the existence of "steps" on lath boundaries; and isothermally transformed about the same temperature range as massive ferrite led to the suggestion of short range diffusion occurring during the formation of Widmanstätten ferrite and the propagation of interface by ledge mechanism. Separate but overlapping C-curves for massive ferrite and Widmanstätten ferrite in the TTT diagram for Fe-9Ni alloy were proposed.

Bainite and lath martensite were regarded as transformed products forming by shear. It was thought that diffusion of interstitial elements might occur in the bainite transformation but not in the formation of lath martensite.

M-A phase was observed under slow cool condition in VS2241A alloy even with carbon content as low as 0.002%C. TEM-EDX analysis found that the nickel content in M-A phase was consistent with the matrix.

Based on the observation of incomplete transformation for all the isothermally transform structures in Fe-9Ni alloy, it was thought that "incomplete transformation phenomenon" might not only be confined to the bainite transformation only but applied to all the transformations in the two phase field below T_0 (or T_0') temperature, due to solute drag.

Upon air cooling, the transformation start of Fe-3.5Ni alloy, VS2239A was found to take place in single phase region with the thermal arrest temperature of 707 ± 5°C. The transformed microstructure was equiaxed ferrite with smooth grain boundaries and the absence of substructures.

Austenitised an Fe-4Cu alloy for 3 days followed by iced brine quenching produced mixed structures of massive ferrite and Widmanstätten ferrite. The ragged boundary separating two ferrite grains was found to be misoriented by 6°.

Charpy impact testing of Fe-9Ni alloy, VS2241A observed DBTT of -140°C and -100°C for air cooled massive ferrite and water quenched bainitic ferrite respectively. The transition curve of massive ferrite structure showed higher absorb energy in the upper shelf.

9. Suggestions for Further Work

It was thought that the transformation of Widmanstätten ferrite in Fe-9Ni alloy involved ledge movement, thermally activated by short range diffusion of substitutional element. Microanalysis needs to be carried out on Widmanstätten ferrite to confirm this.

The percentage of transformation in Fe-9Ni alloy upon isothermal holding presented in figure 4.16, determined by point counting is only an approximation, due to problems in identifying different structures. Percentage transformation by dilatometry experiments might be more appropriate in plotting the transformation curves.

Both the present work and MOISEYEV et al [1981] failed to determine experimentally the TTT diagram for Fe-9Ni alloy. It is recommended to use smaller or thinner specimens to carry out the experiment.

After long periods of austenitising, bainite transformation was observed on air cooling. This led to suggestion that the C-curve for massive ferrite could be pushed to the right of the TTT diagram by producing larger austenite grains, i.e. holding the Fe-9Ni specimens for a longer period or at a higher austenitising temperature may permit the TTT diagram for massive ferrite to be determined by metallography. Alternatively, one could use an Fe-Ni alloy with slightly higher nickel content, for instance 10-12 wt.% Ni. Higher nickel would slow down the transformations.

The present work provides little experimental evidence to distinguish the differences between bainitic ferrite and lath martensite in Fe-9Ni alloy. Further work would be needed to extend the present arguments. Crystallographic analysis by hard TEM work, for instance habit plane determination, would be paramount in studying the differences between bainitic lath and lath martensite.

References

AARONSON, H. I., 1962: in "Decomposition of Austenite by diffusional Processes", ed. V. F. Zackay and H. I. Aaronson, Interscience, New York (1962), p387.

AARONSON, H. I., C. LAIRD and K. R. KINSMAN, 1968: Scripta Metall., 2 (1968), p259.

AARONSON, H. I., M. G. HALL, D. M. BARNETT, and K. R. KINSMAN, 1975: Scripta Metall., 9 (1975), p705.

AARONSON, H. I., W. T. REYNOLDS, JR., G. J. SHIFLET and G. SPANOS, 1990: Met. Trans. A, 21A (1990), p1343.

AARONSON, H. I., and M. G. HALL, 1994: Metall. Mat. Trans. A, 25A (1994), p1797.

AARONSON, H. I., P. WANG, D. J. MICHEL, C. R. FENG and V. K. VASUDEVAN, 1994: in "Solid→Solid phase Transformations", ed. W. C. Johnson, J. M. Howe, D. E. Laughlin and W. A. Soffa, The Minerals, Metals & Materials Society (1994), p505.

ACKERT, R. J., and J. G. PARR, 1971: JISI, 209 (1971), p912.

ÅGREN, J., 1989: Acta Metall., 37, 1 (1989), p181.

AKSELSEN, O. M., J. K. SOLBERG and Ø. GRONG, 1988: Scand. J. Metallurgy, 17, 5 (1988), p194.

ANDREW, K. W., 1965: JISI, 203 (1965), p721.

ARAKI, T., M. ENOMOTO and K. SHIBATA, 1991: Mat. Trans. JIM, 32 (1991), p729.

ARAKI, T. et al eds., 1992: "Atlas of Bainitic Microstructure", ISIJ, Tokyo, V1 (1992), p4.

ARAKI, T., K. SHIBATA and H. NAKAJIMA, 1992: in "Gilbert R. Speich Symposium Proccedings on Fundamentals of Aging and Tempering in Bainitic and Martensitic Steel Products", Montreal, Quebec, Canada, 25-28 October 1992, p113.

ARAKI, T., K. SHIBATA and H. NAKAJIMA, 1994: Mat. Sci. Forum, V163-165 (1994), p75.

ARAKI, T. and K. SHIBATA, 1995: Mat. Sci. Forum, V189-190 (1995), p267.

BAIN, E. C., 1924: Trans AIME, 70 (1924), p25.

BARRETT, C. S., and T. B. MASSALSKI, 1966: "Structure of Metals", McGraw-Hill, New York (1966), p236.

BASH, P. W., J. BEVER and C. A. VERBRAAK, 1980: Scripta Metall., 14 (1980), p205.

BASTON, N., 1991: HND Thesis, Sheffield City Polytechnic (1991).

BEE, J. V., and R. W. K. HONEYCOMBE, 1978: Met. Trans. A, 9A (1978), p587.

BELL, T., and W. S. OWEN, 1967: JISI, 205 (1967), p428.

BENTLEY, J., E. A. KENIK, K. B. ALEXANDER, Z. L. WANG and A. T. FISHER, 1991: Electron Optics Bulletin, 130 (1991), p13.

BHADESHIA, H. K. D. H., and D. V. EDMONDS, 1979: Met. Trans. A, 10A (1979), p895.

BHADESHIA, H. K. D. H., and D. V. EDMONDS, 1980: Acta Metall., 28 (1980), p1265.

BHADESHIA, H. K. D. H., 1992: "Bainite in Steels", Institute of Materials, London (1992).

BHATTACHARYYA, S. K., J. H. PEREPEZKO and T. B. MASSALSKI, 1974: Acta Metall., 22 (1974), p879.

BIBBY, M. J., and J. G. PARR, 1964: JISI, 202 (1964), p100.

BILBY, B. A., and J. W. CHRISTIAN, 1961: JISI, 197 (1961), p122.

BISCHOFF, E., and M. RÜHLE, 1990: in "Microstructural and Microanalytical Characterization in Material Development and Quality Control", Berlin, Germany, 25-27, April, 1990, p299.

BODNER, R. L., and S. S. HANSEN, 1994: Met. Trans. A, 25A (1994), p665.

BOLTON, J. D., 1970: PhD Thesis, Sheffield City Polytechnic (1970).

BOLTON, J. D., E. R. PETTY and G. B. ALLEN, 1971: Met. Trans. A, 2 (1971), p2915.

BOWLES, J. S., and J. R. MACKENZIE, 1954: Acta Metall., 2 (1954), p129.

BORGENSTAM, A., and M. HILLERT, 1996: Met. Trans. A, 27A (1996), p1501.

BORGENSTAM, A., and M. HILLERT, 1997: Acta Metall., 45, 5 (1997), p2079.

BRANDES, E. A., and G. B. BROOK eds., 1992: "Smithells, Metals Reference Book", 7th Edition, Butterworth, Heinemann, Oxford (1992), p13-56.

BRAMHALL, M. D., 1989: PhD Thesis, Sheffield City Polytechnic (1989).

BREEDIS, J. F., and C. M. WAYMAN, 1962: Trans. AIME, 224 (1962), p1128.

BUNSHAH, R. F., and R. F. MEHL, 1953: Trans. AIME, 197 (1953), p1251.

CAWLEY, J., C. F. HARRIS and E. A. WILSON, 1994: in "Recent Research on Bainitic Microstructures and Transformation Behaviour of (Very) Low Carbon HSLA Steels", Bainite Research Committee, ISIJ, Tokyo (1994), p11.

CHADWICK, G. A., 1972: "Metallography of Phase Transformations", Butterworths, London (1972), p284.

CHRISTIAN, J. W., 1965: in "Physical Properties of Martensite and Bainite", The Iron and Steel Institute, London (1965), p1.

CHRISTIAN, J. W. and D. V. EDMONDS, 1984: in "Proceedings of the International Conference on Phase Transformations in Ferrous Alloys", ed. A. R. Marder and J. I. Goldstein, TMS-AIME, Warrendale, Pennyslvania (1984), p293.

CHRISTIAN, J. W., 1990: Met. Trans. A, 21A (1990), p799.

CHRISTIAN, J. W., 1994: Met. Trans. A, 25A (1994), p1821.

CLARK, H. M., and C. M. WAYMAN, 1970: in "Phase Transformations", ASM Metal Park, Ohio (1970), p59.

DAHMEN, U., 1987: Scripta Met., 21 (1987), p1029.

DAUTOVICH, D. P., and J. S. BOWLES, 1972: Acta Metall., 20 (1972), p1137.

DEARDO, A. J., 1995: ISIJ, 35, 8 (1995), p946.

DOHERTY, R. D., 1996: in "Physical Metallurgy Volume II", ed. R. W. Cahn and P. Haasen, Elsevier Science Publishers BV, Holland (1996), p1364

DOIG, P. and P. E. J. FLEWITT, 1988: in "EMAG'87 Analytical Electron Microscopy", ed. G. W. Lorimer, The Institute of Metals, London (1988), p229.

DUBÉ, C. A., 1948: PhD Thesis, Carnegie Institute of Technology (1948).

DUBROV, V. A., 1966: Fiz. Metal. Metalloved., 21, 4 (1966), p551.

DUWEZ, P., 1951: Trans. AIME, 191 (1951), p765.

EDMONDS, D. V., and R. C. COCHRANE, 1990: Met. Trans. A, 21A (1990), p1527.

EFSIC, E. J., and C. M. WAYMAN, 1967: Trans. AIME, 239 (1967), p873.

ENTIN, R. I., 1962: in "Decomposition of Austenite by diffusional Processes", ed. V. F. Zackay and H. I. Aaronson, Interscience, New York (1962), p295.

ENTWISLE, A. R., 1956: in "The Mechanism of Phase Transformations in Metals", The Institute of Metals, London (1956), p315.

FAST, J. D., 1950: Philips Tech. Rev., 11 (1950), p303.

FAULKNER, R. G., E. A. LITTLE and G. J. ADETUNJI, 1990: Mat. Charaterization, 25, 1 (1990), p83.

FLOREEN, S., H. W. HAYDEN, and T. M. DEVINE, 1971: Met. Trans., 2 (1971), p1403.

FURUHARA, T, and H. I. AARONSON, 1991: Acta Met. Mat., 39, 11 (1991), p2887.

FURUKIMI, O., A. NARUMOTO, Y. NAKANO, C. SHIGA and T. TANAKA, 1987: Trans. ISIJ, 27 (1987), p460.

GERBERICH, W. W., Y. T. CHEN, D. G. ATTERIDGE and T. JOHNSON, 1981: Acta Metall., 29 (1981), p1187.

GILBERT, A., and W. S. OWEN, 1962: Acta Met., 10 (1962), p45.

GOLDSTEIN, J. I., 1983: in "Phase Transformation in Ferrous Alloy, Proceedings of an International Conference", Philadelphia, PA, USA, 4-6 Oct 1983, p1.

GOMERSALL, D. W., and J. G. PARR, 1965: JISI, 203 (1965), p275.

GOODENOW, R. H., and R. F. HEHEMANN, 1965: Trans. Met. AIME, 233 (1965), p1777.

GOODHEW, P. J., and F. J. HUMPHREYS, 1988: "Electron Microscopy and Analysis", 2nd edition, Taylor and Francis, London (1988), p201.

GRENINGER, A. B., 1939: Trans. AIME, 133 (1939), p204.

GRENINGER, A. B., and A. R. TROIANO, 1940: Trans. AIME, 140 (1940), p307.

GRENINGER, A. B., 1942: Trans. ASM, 30 (1942), p1.

HABRAKEN, L. J., and M. ECONOMOPOULOS, 1967: in "Transformation and Hardenability in Steels", Climax Molybdenum, Michigan (1967), p69.

HALL, M. G., and H. I. AARONSON, 1994: Met. Trans. A, 25A (1994), p1923

HAYZELDEN, C., and B. CANTOR, 1985: Int. J. Rapid Solidification, 3 (1985), p237.

HEHEMANN, R. F., and A. R. TROIANO, 1956: Met. Prog., 70, 2 (1956), p97.

HEHEMANN, R.F., 1970: in "Phase Transformations", ASM, Metals Park, Ohio (1970) p379.

HEHEMANN, R. F., K. R. KINSMAN and H. I. AARONSON, 1972: Metall. Trans., 3A (1972), p1071.

HILLERT, M., 1962: in "Decomposition of Austenite by Diffusional Processes", Interscience, New York (1962) p197.

HILLERT, M., 1975: Met. Trans. A, 6A (1975), p5.

HILLERT, M., 1984: Met. Trans. A, 15A (1984), p411.

HILLERT, M, 1994: Met. Trans. A, 25A (1994), p1957.

HOLDEN, A., J. D. BOLTON, and E. R. PETTY, 1971: JISI, 209 (1971), p721.

HOWE, J. M., 1994: Met. Mat. Trans. A, 25A (1994), p1917.

HULTGREN, A., 1947: Trans. ASM, 39 (1947), p915.

HWANG, S. K., S. JIN and J. W. MORRIS, JR., 1975: Met. Trans. A, 6A (1975), p2015.

HWANG, S. K., and J. W. MORRIS, JR., 1979: Met. Trans. A, 10A (1979), p545.

HWANG, S. K., and J. W. MORRIS, JR., 1980: Met. Trans. A, 11A (1980), p1197.

JANA, S., and C. M. WAYMAN, 1970: Met. Trans., 1 (1970), p2825.

JIN, S., J. W. MORRIS, Jr. and V. F. ZACKAY, 1975: Met. Trans. A, 6A (1975), p141.

JIN, S., S. K. WANG and J. W. MORRIS, JR., 1975: Met. Trans. A, 6A (1975), p1721.

JOLLEY, W., 1968: Trans. TMS-AIME, 242 (1968), p306.

JONES, F. W., and W. I. PUMPHREY, 1949: JISI, 163 (1949), p121.

JÖNSSON, B., and J. ÅGREN, 1990: Acta Metall. Mater., 38, 3 (1990), p433.

JÖNSSON, B., 1990: J. Appl. Phys., 67, 3 (1990), p1307.

JUNG, Y. C., K. NAKAI, H. OTHSUBO and Y. OHMORI, 1994: ISIJ, 34 (1994), p43.

JUNG, Y. C., H. UENO and H. OTHSUBO, 1995: ISIJ, 35, 8 (1995), p1001.

KARLYN, D. A., J. W. CAHN and M. COHEN, 1969: Trans. TMS-AIME, 245 (1969), p197.

KATSUMATA, M., Y. NAMIMURA and T. INOUE, 1994: in "Recent Research on Bainitic Microstructures and Transformation Behaviour of (Very) Low Carbon HSLA Steels", Bainite Research Committee, ISIJ, Tokyo (1994), p41.

KAUFMAN, L., and M. COHEN, 1956: Trans. AIME, 206 (1956), p1393.

KAUFMAN, L., E. V. CLOUGHERTY and R. J. WEISS, 1963: Acta Metall., 11 (1963), p323.

KIM, K.J., and L. H. SCHWARTZ, 1978: Mat. Sci. Eng., 33 (1978), p5.

KIM, J. I., and J. W. MORRIS, JR., 1980: Met. Trans. A, 11A (1980), p1401.

KIM, J. I., and J. W. MORRIS, JR., 1981: Met. Trans. A, 12A (1981), p1957.

KIM, J. I., C. K. SYN and J. W. MORRIS, JR., 1983: Met. Trans. A, 14A (1983), p93.

KIM, J. I., H. J. KIM and J. W. MORRIS, JR., 1984: Met. Trans. A, 15A (1984), p2213.

KIMURA, H., 1994: ISIJ, 34, 3 (1994), p225.

KINSMAN, K. R., and H. I. AARONSON, 1967: in "Transformations and Hardenability in Steels", Climax Molybdenum, Michigan (1967), p33.

KINSMAN, K. R., and H. I. AARONSON, 1970: Metall. Trans. A, 1A (1970), p1485.

KINSMAN, K. R., E. EICHEN, and H. I. AARONSON, 1975: Met. Trans. A, 6a (1975), p303.

KINSMAN, K. R., R. H. RICHMAN and J. D. VERHOVEN, 1976: J. Mat. Sci., 11 (1976), p1487.

KITTL, J. E. AND T. B. MASSALSKI: Acta Metall., 15 (1967), p161.

KO, T., 1953: JISI, 175 (1953), p16.

KOISTINEN, D. P. and R. E. MARBURGER, 1959: Acta Metall., 7, 1 (1959), p59.

KRAUSS, G., and S. W. THOMPSON, 1995: ISIJ, 35, 8 (1995) p937.

KURDJUMOV, G. V., and G. SACHS, 1930: Z. Phys., 64 (1930), p325.

KUMAR, A. AND V. RAMAN, 1981: Acta Metall., 29 (1981), p1131.

LANGE, W. F. III, M ENOMOTO and H. I. AARONSON, 1988: Met. Trans. A, 19A (1988), p427.

LEE, B., S. MILLMAN, I. L. MACDOUGALL, S R. KEOWN and B. B. ARGENT, 1977: Met. Sci., 11 (1977), p261.

LEE, S., D. KWON and Y. K. LEE, 1995: Met. Trans. A, 26A (1995), p1093.

LESLIE, W. C., 1971: Met. Trans. 2 (1971), p1989.

MAKI, T., S. SHIMOOKA and I. TAMURA, 1971: Met. Trans., 2 (1971), p2944.

MAKI, T., 1990: Mat. Sci. Forum, V56-58 (1990), p157.

MAKI, T., 1994: in "Proceedings of Physical Metallurgy of IF Steels", ISIJ, Tokyo, 1994, p183.

MARDER, J. M., and A. R. MARDER, 1969: Trans. ASM, 62 (1969), p1.

MARSHALL, C. W., R. F. HEHEMANN and A. R. TROIANO, 1962: Trans. ASM, 55 (1962), p135.

MÅRTENSSON, H., 1972: Scand. J. of Metall., 1 (1972), p319.

MASSALSKI, T. B., 1958: Acta Met., 6 (1958), p243.

MASSALSKI, T. B., 1970: in "Phase Transformations", ASM, Metals Park, Ohio (1970), p433.

MASSALSKI, T. B., A. J. PERKINS and J. JAKLOVSKY, 1972: Met. Trans., 3 (1972), p687.

MASSALSKI, T. B., J. H. PEREPEZKO and J. JAKLOVSKY, 1975: Mat. Sci. Eng., 18 (1975), p193.

MASSALSKI, T. B., 1984: Met. Trans. A, 15A (1984), p421.

MASSALSKI, T. B., 1985: in "Metals Handbook 9th Edition", ASM, V9 (1985), p655.

MCEVILY, A. J., R. G. DAVIES, C. L. MAGEE and T. L. JOHNSTON, 1967: in "Transformations and Hardenability in Steels", Climax Molybdenum, Michigan (1967), p179.

MCEVILY, A. J., and C. L. MAGEE, 1968: in "Low Alloy Steels", London, The Iron and Steel Institute (1968), p111.

MENON, E. S. K., M. R.PLICHTA and H. I. AARONSON, 1983: Scripta Metall., 17 (1983), p1455.

MENON, E. S. K., and H. I. AARONSON, 1985: Mat. Sci. Forum, V3 (1985), p211.

MENON, E. S. K., M. R. PLICHTA and H. I. AARONSON, 1988: Acta Metall., 36 (1988), p321.

MIRZAYEV, D. A., O. P. MOROZOV and M. M. SHTEYNBERG, 1973: Fiz. Metal. Metalloved., 36, 3 (1973), p560.

MIRZAYEV, D. A., V. M. SCHASTLIVTSEV and S. YE. KARZUNOV, 1987: Phys. Met. Metall., 63, 4 (1987), p129.

MOISEYEV, A. N., L. I. IZYUMOVA, M. P. USIKOV and E. I. ESTRIN, 1981: Phys. Met. Metall., 51, 4 (1981), p137.

MOROZOV, O. P., D. A. MIRZAYEV and M. M. SHTEYNBERG, 1971: Phys. Met. Metall., 32 (1971), p170.

MOROZOV, O. P., D. A. MIRZAYEV and M. M. SHTEYNBERG, 1972: Phys. Met. Metall., 34 (1972), p114.

MOU, YIWEN, and H. I. AARONSON, 1994: Acta Metall. Mater., 42, 6, (1994), p2159.

NAYLOR, J. P., AND P. R. KRAHE, 1975: Met. Trans. A, 6A (1975), p594.

NASIM, M., 1979: PhD Thesis, Sheffield City Polytechnic (1979).

NILAN, T. G. ,1967: in "Transformation and Hardenability in Steels", Climax Molybdenum, Michigan (1967), p57.

NISHIYAMA, Z., 1934: Sci. Rep., Tohoku Univ., 23 (1934), p637.

NISHIYAMA, Z., 1978: "Martensitic Transformation", ed. M. E. Fine, M. Meshii and C. M. Wayman, Academic Press (1978).

OHMORI, Y., H. OTHSUBO, Y. C. JUNG, S. OKAGUCHI and H. OTHANI, 1994: Met. Mat. Trans. A, 25A (1994), p1981.

OKAMOTO, H. and M. OKA, 1990: Mat. Sci. Forum, V56-58 (1990), p287.

OKAMOTO, H., 1992: J. of Phase Equilibria, 13, 5 (1992), p543.

OSHIMA, R., S. SUGIMOTO, M., SUGIYAMA, T. HAMADA and F. E. FUJITA, 1985: Mat. Trans. JIM, 26 (1985), p523.

OSLON, G. B., H. K. D. H. BHADESHIA and M. COHEN, 1988: Acta. Metall., 22 (1989), p381.

OTHANI, H., S. OKAGUCHI, Y. FUJISHIRO, Y. OHMORI, 1990: Met. Trans. A, 21A, 4 (1990), p877.

OTSUKA, H., H. HAMADA, H. TANAHASHI and T. MARUYAMA, 1990: Mat. Sci. Forum", V56-58 (1990), p222.

OWEN, W. S., E. A. WILSON and T. BELL, 1964: in "High Strength Materials", ed. V. F. Zackay, New York, Wiley (1964), p167.

OWEN, W. S., and E. A. WILSON, 1965: in "Physical Properties of Martensite and Bainite", The Iron and Steel Institute, London (1965), p53.

PASCOVER, J. S., and S. V. RADCLIFFE, 1968: TMS-AIME, 242 (1968), p673.

PATTERSON, R. L., and C. M. WAYMAN, 1966: Acta Metall., 14 (1966), p347.

PEREPEZKO, J. H., 1984: Met. Trans. A, 15A (1984), p437.

PETTY, E. R. ed., 1970: "Martensite: Fundamentals and Technology", Longman, London (1970).

PICHARD, C., J. RIEU, and C. GOUX, 1976: Met. Trans. A, 7A (1976), p1811.

PICKERING, F. B., 1976: "The Basis of Quantitative Metallography", Monograph No.1, Institute of Metallurgical Technicians (1976).

PICKERING, F. B., 1978: "Physical Metallurgy and the Design of Steels", Applied Science Publishers, London (1978).

PLICHTA, M. R., and H. I. AARONSON, 1980: Acta. Metall. 28 (1980), p1041.

PLICHTA, M. R., W. A. T. CLACK and H. I. AARONSON, 1984: Metall. Trans. A, 15A (1984), p427.

PURDY, G. R., and M. HILLERT, 1984: Acta Metall., 32, 6 (1984), P823.

RAO, M. M., and P. G. WINCHELL, 1967: TMS-AIME, 239 (1967), p956.

RÄSÄNEN, E. O., 1969: PhD thesis, Technical University, Otaniemi-Helsinki (1969).

REES, W. P., AND B. E. HOPKINS, 1952: JISI, 172 (1952), p403.

RELLICK, J. R. AND C. J. MCMOHAN JR., 1970: Met. Trans., 1 (1970), p929.

REYNOLDS, W. T., Jr., F. Z. LI, C. K. SHUI and H. I. AARONSON, 1990: Met. Trans. A, 21A (1990), p1433.

RICKS, R. A., P. R. HOWELL, and R. W. K. HONEYCOMBE, 1979: Met. Trans. A, 10A (1979), p1049.

RICKS, R. A., J. V. BEE and P. R. HOWELL, 1981: Met. Trans. A, 12A (1981), p1587.

RICKS, R. A., P. D. SOUTHWICK and P. R. HOWELL: J. of Microscopy, 124 , 1 (1981), p23.

RIGSBEE, J. M. and H. I. AARONSON, 1979: Acta Metall., 27, 3 (1979), p365.

ROBERTS, M. J., 1970: Met. Trans, 1 (1970), p3287.

ROMIG, A. D., JR., and J. I. GOLDSTEIN, 1980: Met. Trans. A, 11A (1980), p1151.

SAGE, A. M., 1989: Metals and Materials, 5, 10 (1989), p584.

SANDVIK, B. P. J., H. O. MARTIKAINEN and V. K. LINDROOS, 1984: Scripta Metall., 18 (1984), p81.

SASAKI, G., AND M. J. YOKOTA, 1975: Met. Trans. A, 6A (1975), p586.

SATO, A., K. SOMA and T. MORI, 1982: Acta Metall., 30, 11 (1982), p1901.

SAUVEUR, A., and C. H. CHOU, 1929: Trans AIME, 84 (1929), p350.

SCHASTLIVTSEV, V. M., D.A. MIRZAYEV, S. E. KARZUNOV and I. L. YAKOVLEVA, 1995: ISIJ, 35, 8 (1995), p955.

SHIBATA, K., and K. ASAKURA, 1995: ISIJ, 35, 8 (1995), p982.

SKOGSMO, J. and A. ATRENS, 1994: Acta Metall. Mater., 42, 4 (1994), p1139.

SOMURA, T., R. OSHIMA and F. E. FUJITA, 1980: Scripta Metall., 14 (1980), p855.

SPANOS, G., H. S. FANG, D. S. SARMA and H. I. AARONSON, 1990: Metall. Trans. A, 21A, (1990), p1391.

SPEICH, G. R., 1985: in "Metals Handbook 9th Edition", ASM, V9 (1985), p668.

SWANSON, W. D., and J. G. PARR, 1964: JISI, 202 (1964), p104.

SWARTZENDRUBER, L. J., 1991: J. of Phase Equilibria, 12, 3 (1991), p288.

SYN, C. K., S. JIN and J. W. MORRIS, JR., 1976: Met. Trans. A, 7A (1976), p1827.

TAMURA, I., C. OUCHI, T. TANAKA and H. SEKINE, 1988: "Thermomechanical Processing of High Strength Low Alloy Steels", Butterworths (1988).

THOMPSON, S. W., D. J. COLVIN, and G. KRAUSS, 1988: Scripta. Metall., 22 (1988), p1069.

TITCHMARCH. J. M., 1997: School of Science / Materials Research Institute, research discission meeting, Sheffield Hallam University (1997).

TSUZAKI, K., K. FUJIWARA and T. MAKI, 1990: Mat. Trans. JIM, 32, 8 (1990), p667.

TSUZAKI, K., A. KODAI, and T. MAKI, 1994: Met. Trans. A, 25A (1994), p2009.

UMEMOTO, M., T. HYODO and I. TAMURA, 1984: Acta Metall., 32, 8 (1984), p1191.

VORLICEK, V., and P. E. J. FLEWITT, 1994: Acta. Metall. Mater., 42, 10 (1994), p3309.

WAKASA, K., and C. M. WAYMAN, 1981: Acta Metall., 29 (1981), p973, p991.

WALLBRIDGE, J. M., and J. G. PARR, 1966: JISI, 204 (1966), p119.

WANG, S. C., and J. R. YANG, 1992: Mat. Sci. Eng., A154, 1 (1992), p43.

WATANABE, M., and C. M. WAYMAN, 1971: Met. Trans., 2 (1971), p2229.

WATSON, J. D. and P. G. MCDOUGALL, 1973: Acta Met., 21 (1973) p961.

WAYMAN, C. M. and H. K. D. H. BHADESHIA, 1996: in "Physical Metallurgy Volume II", ed. R. W. Cahn and P. Haasen, Elsevier Science Publishers BV, Holland (1996), p1508.

WECHSLER, M. S., D. S. LIEBERMAN and T. A. READ, 1953: TRANS AIME, 197 (1953), P1503.

WILSON, E. A., 1965: PhD Thesis, University of Liverpool (1965).

WILSON, E. A., 1968: JISI, 206 (1968), p164.

WILSON, E. A., 1970: Scr. Metall., 3 (1970), p309.

WILSON, E. A., S. P. ALLEN and J. BUTLER, 1982: Met. Sci., 16 (1982), p539.

WILSON, E. A., 1984: Met. Sci., 18 (1984), p471.

WILSON, E. A., 1991: Mat. Sci. Tech., 7, (1991), p1089.

WILSON, E. A., 1994: ISIJ, 34 (1994), p615.

WILSON, E. A., 1995: Mat. Sci. Tech., 11, (1995), p1110.

WANG, S. C., and J. R. YANG, 1992: Mat. Sci. Eng., A154, 1 (1992), p43.

YANG, L., D. ZHU, J. ZHANG and J. CHEN, 1994: Acta Met. Sinica, 30, 8 (1994), pA344.

YEO, R. B. G., 1964: Trans. ASM, 57 (1964), p411.

YU, Z. Z., and P. C. CLAPP, 1989: Met. Trans. A, 20A (1989), p1601.

ZENER, C., 1946: Trans. AIME, 167 (1946), p513.

ZHAO, J. C., 1992: Mat. Sci. Tech., 8 (1992), p997.

ZHAO, J. C., and M. R. NOTIS, 1995: Mat. Sci. Eng., R15, 4-5 (1995), p135.